Study on hydrogel microspheres adsorbed at the air/water interface

Doctoral Dissertation
(Shinshu University)

by

Haruka Minato

Graduate School of Textile Science & Technology
March 2020

Table of Contents

Chapter 2

i. Introductory Remarks

Background

In the context of materials science, the term 'interface' usually refers to the boundary between two phases (e.g. liquid/liquid, liquid/solid, solid/solid, solid/gas, or gas/liquid), where individual phases separate due to the minimized Gibbs free energy. However, at interfaces that involve a fluid interface such as liquid/liquid or gas/liquid, the liquid or the gas phase can be stabilized by adsorbing materials such as surfactants, polymers, or colloids at the interface, which decreases the Gibbs free energy and results in the formation of a macroscopically mixed state between the different phases. Using such stabilizers, droplets and bubbles can be stabilized in a bulk liquid for a relatively long period of time despite the fact that the process resides in a non-equilibrium state that progresses toward the thermal equilibrium state. Since Langmuir's seminal contributions to the field of interfacial chemistry around 1920,[1] various types of stabilizers have been reported and developed. Ramsden and Pickering have described that colloidal particles can stabilize air/water and oil/water interfaces, and subsequently, oil/water emulsions have been termed 'Pickering emulsions'.[2,3] Here, colloidal particles with a diameter range from several nanometers to several tens of micrometers are dispersed in a solvent.

In the case of surfactants, the presence of both hydrophilic and hydrophobic parts is important for their adsorption onto the fluid interface. The adsorption energy of surfactants can be calculated by the balance between hydrophilicity and hydrophobicity using the *Hydrophilic-Lipophilic Balance* (HLB).[4,5] On the other hand, for colloidal particles with homogeneous chemical composition and properties on the surface, the wettability is the most crucial factor for a stable adsorption at the fluid interface.[6] In the case of the adsorption of colloidal particles at the air/water or oil/water interface, the adsorption energy of the colloidal particles is calculated using equation 1, from the contact angle, θ, which describes the wettability of the particles to oil or water:[6,7]

$$\Delta G = -\gamma \pi R^2 (1 \pm \cos\theta)^2 \qquad (1)$$

, where ΔG is the energy change upon adsorption of the colloidal particle onto the fluid interface, γ the interfacial tension, and R the radius of the colloidal particles. Equation 1 shows that θ is a crucial factor for particle-stabilized bubbles or emulsions, as well as for the HLB of surfactant-stabilized bubbles or emulsions. For example, the calculated adsorption energy of colloidal

particles is 4.0×10^5 k_BT under the conditions that cyclohexane/water interfacial tension, γ, is 51 mN/m,[8] R is 100 nm, and θ is 90 °, which is larger than that of common surfactants (10 ~ 20 k_BT).[9] This result indicates that once adsorbed onto the interface, it is difficult for the particles to desorb. Air/water and oil/water interfaces treated with colloidal particles are relatively stable, which is one of reason that bubbles and emulsions stabilized by particles have been attracting attention.

Other characteristics of colloidal particles as stabilizers have also received increased attention as they add further fascinating properties to their interfacial behavior. For instance, stimulus-responsive colloidal particles in foams can rapidly and on demand destroy, move, deform, or structurally change the foams using external stimuli[10] such as changes in temperature,[11-13] pH,[11,13-15] light,[12,16] magnetic fields,[17,18] or mechanical stress[19]. Moreover, a solvent stabilized by colloidal particles can be dispersed not only in other solvents but also in air, which is called 'dry liquid' or 'liquid marble'.[20-23] Liquid marble can also respond to external stimuli when stimulus-responsive particles are present.[20-23] Furthermore, compared to rigid colloidal particles, hydrogel microspheres (microgels), which are colloidal particles with three-dimensional polymer networks that swell in water, have also received increased attention as a soft material that may be able to stabilize fluid interfaces. Soft microgels can be better stabilizers than rigid particles as they deform at fluid interfaces. Additionally, microgels can, given their molecular architecture, respond to external stimuli such as changes in temperature,[24-26] pH,[26,27] light,[28-30] electric fields,[31] or to chemical reactions[32-41]. For example, typical temperature-responsive cross-linked poly(*N*-isopropyl acrylamide) (pNIPAm) microgels, which can be prepared with uniform size-distribution via precipitation polymerization,[24,25] exhibit a volume-phase-transition temperature (VPTT) of ~32 °C, due to the properties of pNIPAm.[42,43] At the VPTT, swollen microgels rapidly shrink with increasing temperature. Changes in the physicochemical properties of the microgels in response to external stimuli can feasibly be expected to lead to many applications in e.g. the food industry,[44-49] cosmetics,[50-52] and smart delivery systems.[53-57] Moreover, the size and structures of microgels can be changed upon adsorption at the interface due to their softness, which might change the interfacial properties such as the interfacial distortion and tensions, as well as the rheological properties. In order to better understand the mechanisms operative at such interfaces and to develop applications, intimate knowledge of the behavior of soft deformable microgels at fluid interfaces is of paramount importance.

Yet, theoretically and computationally describing the behavior of microgels at the fluid interface is challenging, given that the structure of the microgels depends on their environment. Accordingly, various types of techniques have been used to analyze the interfacial behavior of microgels at the fluid interface. In the case of the air/water interface, it was first reported in 1999 that pNIPAm microgels lower the surface tension of water, which was discovered using the pendant-drop method.[58] Although it had previously been reported that polymer chains of NIPAm adsorb onto the air/water interface,[59-62] it has been shown that the microgel morphology, which depends on the degree of cross-linking and the preparation method, influences the time required to reach a steady state.[58] Surface tension measurement techniques, such as the pendant-drop method, the Wilhelmy plate method, and the Langmuir Blodgett (LB) technique, have been used to investigate the interfacial behavior of microgels (e.g. adsorption and deformation) at the air/water interface.[63-65] Subsequently, the temperature responsiveness[63,64] and deformability[65] of microgels at the interface have been discussed based on surface-pressure values. However, the interfacial behavior of microgels has not yet been evaluated using direct visualization techniques. Recently, assemblies of microgels adsorbed at the air/water interface have been investigated by atomic force microscopy (AFM).[66-69] Here, the interfacial arrangement of microgels on a substrate that was lifted through the air/water interface was observed,[66-69] which revealed that the assembly structure depends on the compression at the air/water interface[66] and on the microgel softness,[67,68] although several other factors might also have to be considered. For example, the interaction between microgels and the substrate, the lifting rate of the substrate, and the drying process might influence the structure of the microgel assemblies. On the other hand, the group of Suzuki has examined the assembly mechanism and the structure of the microgel assemblies at the air/water interface by *in-situ* visualization using optical microscopy.[70-73] Moreover, the morphology of microgels adsorbed at the air/water interface has been examined[74] using neutron reflectivity[75,76] and molecular dynamics simulations.[69] However, an evaluation of the microgel morphology for a single particle by direct *in-situ* visualization remains difficult at the air/water interface due to the lower limits of the resolution of conventional microscopy techniques.

In the case of oil/water interfaces, further observation techniques such as cryogenic scanning electron microscopy (cryo-SEM),[77-81] cryogenic field emission scanning electron microscopy (cryo-FE-SEM),[82] confocal microscopy,[83,84] and transmission X-ray microscopy[85] have been employed. In a study of microgels adsorbed onto the oil/water interface, it has been

proposed that the microgels adsorbed onto the fluid interface adopt a fried-egg conformation[78] and a core-corona morphology,[79] albeit that it should be noted here that during cryo-SEM or cryo-FE-SEM, the samples were observed in the frozen instead of the liquid state. The direct *in-situ* observation of microgels adsorbed at the fluid interface by confocal microscopy[83,84] or transmission X-ray microscopy[85] showed that microgels predominantly adopt a spherical conformation at the interface.[83,85] However, these results are different from those obtained from cryo-SEM. As much experimental information related to the morphology of deformed microgels at the fluid interface has recently become available, the interfacial behavior of microgels has also been investigated theoretically.[81,83,84] For example, the adsorption energy of a single microgel at the interface (~10^6 k_BT) has been determined by Monteillet *et al.* using the following equation:[84]

$$\Delta G = \Pi_s \pi R^2 \qquad (2)$$

, where Π_s is the entropic surface pressure balanced by the internal osmotic pressure within the microgel. Style *et al.*[81] have applied Neumann's triangle construction[86] to the theoretical calculation of the deformation of microgels at the interface, which revealed that the deformation depends on the ratio of its size relative to the lengthscales of the elastocapillarity and the plastocapillarity, u_r. Subsequently, the adsorption energy was estimated using the following equation:

$$\Delta G = \gamma \pi R^2 (1 + u_r) \qquad (3)$$

Kwok *et al.* have reported that micron-sized microgels do not highly deform at the oil/water interface.[83] As a result, the adsorbed microgel is flattened at the interface. Thus, assuming a microgel with a radius of $(1 + \upsilon\varepsilon)R$, the following equation was proposed:

$$\Delta G = \gamma \pi R^2 (1 - |\cos\theta|)^2 (1 + \upsilon\varepsilon)^2 \qquad (4)$$

, where υ is the Poisson ratio and ε the strain of the uniform flattening deformation (for common materials, $\upsilon = 0.4$ was used).

Since the development of Pickering emulsions[78,80,82,83,87,88] and foams[89-92] stabilized by microgels, the interfacial behavior of microgels at fluid interfaces has been investigated using various observation techniques and theoretical analysis methods (**Table 1**). However, the details of the adsorption behavior, the deformation conformation, and the organization of the structure of microgels at the fluid interface remain unclear. Therefore, the author investigated in this study the interfacial behavior, i.e., the adsorption and deformation of microgels at the air/water interface using microgels whose size allow a direct *in-situ* observation with optical microscopy. Within the

remit of this thesis, the behavior of the microgels at the interface is discussed by systematically combining macroscopic/microscopic evaluation methods with previously established knowledge. In **Chapter 1**, the deformed structure of microgels adsorbed at the air/water interface was investigated, which proved to be difficult due to the limitations associated with the resolution of the microscopy technique and the size of the microgels. Consequently, larger, micron-sized microgels were prepared by a modified aqueous precipitation polymerization method, although the synthesis of such large particles proved to be non-trivial due to the fact that gravity effects strongly influence particle motion and colloidal stability.[93,94] The deformation dynamics of soft microgels were quantitatively investigated using microgels that can deform to a size of 20 μm upon adsorption at the air/water interface. In **Chapter 2**, the focus was placed on the effect of charge incorporated in microgels, which is one of the most important parameters in such particles, and the adsorption, deformation, and self-organization behavior of charged microgels were investigated.

Table 1. Evaluation method for understanding the microgel morphology at the fluid interface

Evaluation method			Air/water interface	Oil/water interface
Pendant-drop method			[58,95]	[97,98]
Wilhelmy plate method + LB			[63,64,65]	
		AFM	[66,67,68,69]	[96,102]
In-situ	Optical microscopy		[70,71,72,73,95]	
	Confocal microscopy			[83,84]
	X-ray microscopy			[85]
	Neutron reflectivity		[75,76]	
Ex-situ	Cryo-SEM/FESEM		[89]	[77,78,79,80,81,82]
Simulation			[69]	[99,100,101,102]

References

(1) Langmuir, I. The constitution and fundamental properties of solids and liquids. Part I. solids. *J. Am. Chem. Soc.* **1916**, *38*, 2221-2295.

(2) Ramsden, W. Separation of solids in the surface-layers of solutions and ‘suspensions’ (observations on surface-membranes, bubbles, emulsions, and mechanical coagulation). - Preliminary account. *Proc. R. Soc. London, Ser. A* **1903**, *72*, 156-164.

(3) Pickering S. U. CXCVI. Emulsions. *J. Chem. Soc.* **1907**, *91*, 2001-2021.

(4) Griffin, W. C. Classification of surface-active agents by "HLB". *J. Soc. Cosmet. Chem.* **1949**, *1*, 311-326.

(5) Griffin, W. C. Calculation of HLB values of non-ionic surfactants. *J. Soc. Cosmet. Chem.* **1954**, *5*, 249-256.

(6) Binks, B. P.; Horozov, T. S. *Colloidal Particles at Liquid Interfaces.* Cambridge University Press, Cambridge, U. K. **2006**

(7) Levine, S.; Bowen, B.D.; Partridge, S.J. Stabilization of emulsions by fine particles I. Partitioning of particles between continuous phase and oil/water interface. *Colloids Surf.,* **1989**, *38*, 325.

(8) Inraelachvili, J. N. *Intermolecular and surface forces*, 3rd ed.; Academic Press: Cambridge, MA, **2011**.

(9) Aveyard, R.; Clint, J, H.; Horozov, T. S. Aspects of the stabilisation of emulsions by solid particles: Effects of line tension and monolayer curvature energy. *Phys. Chem. Chem. Phys.* **2003**, *5*, 2398-2409.

(10) Fujii, S.; Nakamura, Y. Stimuli-responsive bubbles and foams stabilized with solid particles. *Langmuir* **2017**, 33, 7365-7379.

(11) Fujii, S.; Akiyama, K.; Nakayama, S.; Hamasaki, S.; Yusa, S.; Nakamura, Y. pH- and temperature-responsive aqueous foams stabilized by hairy latex particles. *Soft Matter* **2015**, *11*, 572-579.

(12) Salonen, A.; Langevin, D.; Perrin, P. Light and temperature bi-responsive emulsion foams. *Soft Matter* **2010**, *6*, 5308-5311.

(13) Sigolaeva, L. V.; Gladyr, S. Y.; Mergel, O.; Gelissen, A. P. H.; Noyong, M.; Simon, U.; Pergushov, D. V.; Kurochkin, I. N.; Plamper, F. A.; Richtering, W. Easy-preparable butyrylcholinesterase/microgel construct for facilitated organophosphate biosensing. *Anal. Chem.* **2017**, *89*, 6091-6098.

(14) Lin, Q.; Liu, K. H.; Cui, Z. G.; Pei, X. M.; Jiang, J. Z.; Song, B. L. pH-Responsive Pickering foams stabilized by silica nanoparticles in combination with trace amount of dodecyl dimethyl carboxyl betaine. *Colloid Surf. A: Physicochem. Eng. Asp.* **2018**, *544*, 44-52.

(15) Nakayama, S.; Hamasaki, S.; Ueno, K.; Mochizuki, M.; Yusa, S.; Nakamura, Y.; Fujii, S. Foams stabilized with solid particles carrying stimuli-responsive polymer hairs. *Soft Matter* **2016**, *12*, 4794-4804.

(16) Fameau, A. L.; Lamb, S.; Velev, O. D. Multi-stimuli responsive foams combining particles and s elf-assembling fatty acids. *Chem. Sci.* **2013**, *4*, 3874-3881.

(17) Lam, S.; Blanco, E.; Smoukov, S. K.; Velikov, K. P.; Velev, O. D. Magnetically responsive Pickering foams. *J. Am. Chem. Soc.* **2011**, *133*, 13856-13859.

(18) Blanco, E.; Lam, S.; Smoukov, S. K.; Velikov, K. P.; Khan, S. A.; Velev, O. D. Stability and viscoelasticity of magneto-Pickering foams. *Langmuir* **2013**, *29*, 10019-10027.

(19) Taccoen, N.; Lequeux, F.; Gunes, D. Z.; Baroud. C. N. Probing the mechanical strength of an armored bubble and Its implication to particle-stabilized foams. *Physical Review X* **2016**, *6*, 011010.

(20) Dupin, D.; Armes, S. P.; Fujii, S. Stimulus-responsive liquid marble. *J. Am. Chem. Soc.* **2009**, *131*, 5386-5387.

(21) Paven, M.; Mayama, H.; Sekido, T.; Butt, H. J.; Nakamura, Y.; Fujii, S. Light-driven delivery and release of materials using liquid marbles. *Adv. Funct. Mater.* **2016**, *26*, 3199-3206.

(22) Kozuka, S.; Banno, T.; Fujii, S.; Nakamura, Y.; Yusa, S. Disruption of liquid marbles induced by host-guest interaction. *Chemistry Letters* **2019**, *48*, 840-843.

(23) Shimogama, N.; Uda, M.; Oyama, K.; Hanochi, H.; Hirai, T.; Nakamura, Y.; Fujii, S. Hydrophobic poly(3,4-ethylenedioxythiophene) particles synthesized by aqueous oxidative coupling polymerization and their use as near-infrared-responsive liquid marble stabilizer. *Polymer Journal* **2019**, *51*, 761-770.

(24) Pelton, R. H.; Chibante, P. Preparation of aqueous latices with *N*-isopropylacrylamide. *Colloids Surf.* **1986**, *20*, 247–256.

(25) Pelton, R. Temperature-sensitive aqueous microgels. *Adv. Colloid Interface Sci.* **2000**, *85*, 1–33.

(26) Karg, M.; Pastoriza-Santos, I.; Rodriguez-González, B.; von Klitzing, R.; Wellert, S.; Hellweg, T. Temperature, pH, and Ionic Strength Induced Changes of the Swelling Behavior of PNIPAM-Poly(allylacetic acid) Copolymer Microgels. *Langmuir* **2008**, *24*, 6300-6306.

(27) Hoare, T.; Pelton, R. Highly pH and Temperature Responsive Microgels Functionalized with Vinylacetic Acid. *Macromolecules* **2004**, *37*, 2544-2550.

(28) Nayak, S.; Lyon, L. A. Photoinduced Phase Transitions in Poly(*N*-isopropylacrylamide) Microgels. *Chem. Mater.* **2004**, *16*, 2623-2627.

(29) Dai, S.; Ravi, P.; Tam, K. C. Thermo- and photo-responsive polymeric systems. *Soft Matter* **2009**, *5*, 2513-2533.

(30) Lu, D.; Zhu, M.; Wu, S.; Wang, W.; Liana, Q.; Saunders, B. R. Triply responsive coumarin-based microgels with remarkably large photo-switchable swelling. *Polym. Chem.* **2019**, *10*, 2516-2526.

(31) Colla, T.; Mohanty, P. S.; Nöjd, S.; Bialik, E.; Riede, A.; Schurtenberger, P.; Likos, C. N. Self-Assembly of Ionic Microgels Driven by an Alternating Electric Field: Theory, Simulations, and Experiments. *ACS Nano* **2018**, *12*, 4321-4337.

(32) Suzuki, D.; Sakai T.; Yoshida, R. Self-Flocculating/Self-Dispersing Oscillation of Microgels. *Angew. Chem. Int. Ed.* **2008**, *47*, 917-920, *Nature Materials* **2008**, *7*, 95.

(33) Suzuki, D.; Yoshida, R. Temporal Control of Self-Oscillation for Microgels by Crosslinking Network Structure. *Macromolecules* **2008**, *41*, 5830-5838.

(34) Suzuki, D.; Yoshida, R. Effect of Initial Substrate Concentration of the Belousov-Zhabotinsky Reaction on Self-Oscillation for Microgel System. *J. Phys. Chem. B* **2008**, *40*, 12618-12624.

(35) Suzuki, D.; Yoshida, R. Synthesis and Characterization of Submicron-sized, Self-oscillating Hydrogel Particles. *Trans. Mater. Res. Soc. Japan* **2009**, *34*, 465-467.

(36) Suzuki, D.; Taniguchi, H.; Yoshida, R. Autonomously Oscillating Viscosity in Microgel Dispersions. *J. Am. Chem. Soc.* **2009**, *131*, 12058-12059.

(37) Taniguchi, H.; Suzuki, D.; Yoshida, R. Characterization of Autonomously Oscillating Viscosity Induced by Swelling/Deswelling Oscillation of the Microgels. *J. Phys. Chem. B* **2010**, *114*, 2405-2410.

(38) Suzuki, D.; Yoshida, R. Self-Oscillating Core/shell Microgels: Effect of Cross-linked Nano-shell on Autonomous Oscillation of the Core. *Polym. J.* **2010**, *42*, 501-508.

(39) Suzuki, D.; Kobayashi, T.; Yoshida, R.; Hirai, T. Soft actuators of organized self-oscillating microgels. *Soft Matter* **2012**, *8*, 11447-11449.

(40) Matsui, S.; Kureha, T.; Nagase, Y.; Okeyoshi, K.; Yoshida, R.; Sato, T.; Suzuki, D. Small-Angle X-ray Scattering Study on Internal Microscopic Structures of Poly(N-isopropylacrylamide-co-tris(2,2-bipyridyl))ruthenium(II) Complex Microgels. *Langmuir* **2015**, *31*, 7228-7237.

(41) Matsui, S.; Inui, K.; Kumai, Y.; Yoshida, R.; Suzuki, D. Autonomously Oscillating Hydrogel Microspheres with High-Frequency Swelling/deswelling and Dispersing/flocculating Oscillations. *ACS Biomaterials Science & Engineering* **2019**, 5, 5615-5622.

(42) Heskins, M.; Guillet, J. E.; Solution Properties of Poly(*N*-isopropylacrylamide). *J. Macromol. Sci. Chem. A* **1986**, *2*, 1441-1455.

(43) Schild, H. G. Poly(*N*-isopropylacrylamide): experiment, theory and application. *Prog. Polym. Sci.* **1992**, *17*, 163-249.

(44) Kwok, M. H.; Sun, G.; Ngai, T. Microgel Particles at Interfaces: Phenomena, Principles, and Opportunities in Food Sciences. *Langmuir* **2019**, *35*, 4205-4217.

(45) Sarkar, A.; Zhang, S.; Holmes, M.; Ettelaie, R. Colloidal aspects of digestion of Pickering emulsions: Experiments and theoretical models of lipid digestion kinetics. *Adv. Colloid Int. Sci.* **2019**, *263*, 195-211.

(46) Xiao, J.; Li, Y.; Huang, Q. Recent advances on food-grade particles stabilized Pickering emulsions: Fabrication, characterization and research trends. *Trends Food Sci. Technol.* **2016**, *55*, 48-60.

(47) Shewan, H. M.; Stokes, J. R. Review of techniques to manufacture micro-hydrogel particles for the food industry and their applications. *J. Food Eng.* **2013**, *119*, 781-792.

(48) McClements, D. J. Recent progress in hydrogel delivery systems for improving nutraceutical bioavailability. *Food Hydrocolloids* **2017**, *68*, 238–245.

(49) Gu, L.; Su, Y.; Zhang, Z.; Zheng, B.; Zhang, R.; McClements, D. J.; Yang, Y. Modulation of Lipid Digestion Profiles Using Filled Egg White Protein Microgels. *J. Agric. Food Chem.* **2017**, *65*, 6919–6928.

(50) Tang, J.; Quinlan, P. J.; Tam, K. C. Stimuli-responsive Pickering emulsions: recent advances and potential applications. *Soft Matter* **2015**, *11*, 3512-3529.

(51) Zhang, H.; Tumarkin, E.; Sullan, R. M. A.; Walker, G. C.; Kumacheva, E. Exploring microfluidic routes to microgels of biological polymers *Macromol. Rapid Commun.* **2007**, *28*, 527-538.

(52) Kaneda, I.; Sogabe, A.; Nakajima, H. Water-swellable polyelectrolyte microgels polymerized in an inverse microemulsion using a nonionic surfactant. *J. Colloid Interface Sci.* **2004**, 275, 450–457.

(53) Seiffert, S. Small but Smart: Sensitive Microgel Capsules. *Angew. Chem. Int. Ed.* **2013**, *52*, 11462-11468.

(54) Das, M.; Mardyani, S.; Chan W. C. W.; Kumacheva, E. Biofunctionalized pH-Responsive Microgels for Cancer Cell Targeting: Rational Design. *Adv. Mater.* **2006**, *18*, 80-83.

(55) McClements, D. J. Recent developments in encapsulation and release of functional food ingredients: delivery by design Author links open overlay panel. Curr. Opin. Food Sci. **2018**, *23*, 80-84.

(56) Li, W.; Zhang, L. Y.; Ge, X. H.; Xu, B. Y.; Zhang, W. X.; Qu, L. L.; Choi, C. H.; Xu, J. H.; Zhang, A.; Lee, H. M.; Weitz, D. A. Microfluidic fabrication of microparticles for biomedical applications. *Chem. Soc. Rev.* **2018**, *47*, 5646-5683.

(57) Merkel, T. J.; Jones, S. W.; Herlihy, K. P.; Kersey, F. R.; Shields, A. R.; Napier, M.; Luft, J. C.; Wu, H.; Zamboni, W. C.; Wang, A. Z.; Bear, J. E.; DeSimone, J. M. Using mechanobiological mimicry of red blood cells to extend circulation times of hydrogel microparticles. *Proc. Natl. Acad. Sci. U. S. A.* **2011**, *108*, 586–591.

(58) Zhang, J.; Pelton, R. Poly(*N*-isopropylacrylamide) Microgels at the Air-Water Interface. *Langmuir* **1999**, *15*, 8032-8036.

(59) Kawaguchi, M.; Saito, W.; Kato, T. Poly(*N*-isopropylacrylamide) Films at the Air-Water Interface. *Macromolecules* **1994**, *27*, 5882-5884.

(60) Zhang, J.; Pelton, R. Poly(*N*-isopropylacrylamide) at the Air/Water Interface. *Langmuir* **1996**, *12*, 2611-2612.

(61) Kawaguchi, M.; Hirose, Y.; Kato, T. Effects of Temperature and Concentration on Surface Tension of Poly(*N*-isopropylacrylamide) Solutions. *Langmuir* **1996**, *12*, 3523-3526.

(62) Zhang, J.; Pelton, R. The dynamic behavior of poly(*N*-isopropylacrylamide) at the air/water interface. *Colloid Surf. A: Physicochem. Eng. Asp.* **1999**, *156*, 111-122.

(63) Nakahama, K.; Fujimoto, K. Thermosensitive Two-Dimensional Arrays of Hydrogel Particles. *Langmuir* **2002**, *18*, 10095-10099.

(64) Maldonado-Valderrama, J.; Del Castillo-Santaella, T.; Adroher-Benítez, I.; Moncho-Jordá, A.; Martín-Molina, A. Thermoresponsive microgels at the air–water interface: the impact of the swelling state on interfacial conformation. *Soft Matter* **2017**, *13*, 230-238.

(65) Deshmukh, O. S.; Maestro, A.; Duits, M. H. G.; van den Ende, D.; Stuart, M. C.; Mugele, F. Equation of state and adsorption dynamics of soft microgel particles at an air-water interface. *Soft Matter* **2014**, *10*, 7045–7050.

(66) Rey, M.; Fernández-Rodríguez, Á, M.; Steinacher, M.; Scheidegger, L.; Geisel, K.; Richtering, W.; Squires, T. M.; Isa, L. Isostructural solid-solid phase transition in monolayers of soft core-shell particles at fluid interfaces: structure and mechanics. *Soft Matter* **2016**, *12*, 3545-3557.

(67) Rey, M.; Hou, X.; Tang, J. S. J.; Vogel, N. Interfacial arrangement and phase transitions of PNiPAm microgels with different crosslinking densities. *Soft Matter* **2017**, *13*, 8717-8727.

(68) Picard, C.; Garrigue, P.; Tatry, M. C.; Lapeyre, V.; Ravaine, S.; Schmitt, V.; Ravaine, V. Organization of microgels at the air-water interface under compression: role of electrostatics and cross-linking density Christine. *Langmuir* **2017**, *33*, 7968-7981.

(69) Harrer, J.; Rey, M.; Ciarella, S.; Löwen, H.; Janssen, L. M. C.; Vogel, N. Stimuli-Responsive Behavior of PNiPAm Microgels under Interfacial Confinement. *Langmuir* **2019**, *35*, 32, 10512-10521.

(70) Suzuki, D.; Horigome, K. Binary Mixtures of Cationic and Anionic Microgels. *Langmuir* **2011**, *27*, 12368–12374.

(71) Horigome, K.; Suzuki, D. Drying Mechanism of Poly(N-isopropylacrylamide) Microgel Dispersions. *Langmuir* **2012**, *28*, 12962–12970.

(72) Suzuki, D.; Horigome, K. Assembly of Oppositely Charged Microgels at the Air/Water Interface. *J. Phys. Chem. B* **2013**, *117*, 9073–9082.

(73) Takizawa, M.; Sazuka, Y.; Horigome, K.; Sakurai, Y.; Matsui, S.; Minato, H.; Kureha, T.; Suzuki, D. Self-Organization of Soft Hydrogel Microspheres during the Evaporation of Aqueous Droplets. *Langmuir* **2018**, *34*, 4515-4525.

(74) Karg, M.; Pich, A.; Hellweg, T.; Hoare, T.; Lyon, L. A.; Crassous, J. J.; Suzuki, D.; Gumerov, R. A.; Schneider, S.; Potemkin, I. I.; Richtering, W. Nanogels and Microgels: From Model Colloids to Applications, Recent Developments, and Future Trends. *Langmuir* **2019**, *35*, 6231-6255.

(75) Zielińska, K.; Sun, H.; Campbell, R. A.; Zarbakhsh, A.; Resmini, M. Smart nanogels at the at the air/water interface: Q1 structural studies by neutron reflectivity. *Nanoscale* **2016**, *8*, 4951–4960.

(76) Zielińska, K.; Campbell, R.A.; Zarbakhsh, A.; Resmini, M. Adsorption versus aggregation of NIPAM nanogels: new insight into their behaviour at the air/water interface as a function of concentration. *Phys. Chem. Chem. Phys.* **2017**, *19*, 17173-17179.

(77) Brugger, B.; Rütten, S.; Phan, K.; Möller, M.; Richtering, W. The colloidal suprastructure of smart microgels at oil–water interfaces. *Angew. Chem., Int. Ed.* **2009**, *48*, 3978– 3981.

(78) Destribats, M.; Lapeyre, V.; Wolfs, M.; Sellier, E.; Leal-Calderon, F.; Ravaine, V.; Schmitt, V. Soft microgels as Pickering emulsion stabilisers: role of particle deformability. *Soft Matter* **2011**, *7*, 7689-7698.

(79) Geisel, K.; Isa, L.; Richtering, W. Unraveling the 3D Localization and Deformation of Responsive Microgels at Oil/Water Interfaces: A Step Forward in Understanding Soft Emulsion Stabilizers. *Langmuir* **2012**, *28*, 15770-15776.

(80) Destribats, M.; Lapeyre, V.; Sellier, E.; Leal-Calderon, F.; Ravaine, V.; Schmitt, V. Origin and control of adhesion between emulsion drops stabilized by thermally sensitive soft colloidal particles. *Langmuir* **2012**, *28*, 3744-3755.

(81) Style, R. W.; Isa, L.; Dufresne, E. R. Adsorption of soft particles at fluid interfaces. *Soft Matter* **2015**, *11*, 7412-7419.

(82) Schmidt, S.; Liu, T.; Ruetten, S.; Phan, K. H.; Moeller, M.; Richtering, W. Influence of Microgel Architecture and Oil Polarity on Stabilization of Emulsions by Stimuli-Sensitive Core-Shell Poly(*N*-isopropylacrylamide-*co*-methacrylic acid) Microgels: Mickering versus Pickering Behavior? *Langmuir* **2011**, *27*, 9801-9806.

(83) Kwok, M. H.; Ngai, T. A confocal microscopy study of micron-sized poly(*N*-isopropylacrylamide) microgel particles at the oil–water interface and anisotopic flattening of highly swollen microgel. *J. Colloid Interface Sci.* **2016**, *461*, 409-418.

(84) Monteillet, H.; Workamp, M.; Appel, J.; Kleijn, J. M.; Leermakers, F. A.; Sprakel, J. Ultrastrong Anchoring Yet Barrier-Free Adsorption of Composite Microgels at Liquid Interfaces. *Adv. Mater. Interfaces* **2014**, *1*, 1300121.

(85) Geisel, K.; Henzler, K.; Guttmann, P.; Richtering, W. New Insight into Microgel-Stabilized Emulsions Using Transmission X-ray Microscopy: Nonuniform Deformation and Arrangement of Microgels at Liquid Interfaces *Langmuir* **2015**, *31*, 83-89.

(86) Gennes, P. G.; Brochard-Wyart, F.; Quéré, D. *Capillarity and wetting phenomena: drops, bubbles, pearls, waves.* Springer **2003**

(87) Ngai, T.; Behrens, S. H.; Auweter, H. Novel emulsions stabilized by pH and temperature sensitive microgels. *Chem. Commun*. **2005**, 331–333.

(88) Richtering, W. Responsive Emulsions Stabilized by Stimuli-Sensitive Microgels: Emulsions with Special Non-Pickering Properties. *Langmuir* **2012**, *28*, 17218–17229.

(89) Buchcic, C.; Tromp, R. H.; Meinders, M. B. J.; Stuart, M. A. C. Harnessing the advantages of hard and soft colloids by the use of core–shell particles as interfacial stabilizers. *Soft Matter* **2017**, *13*, 1326-1334.

(90) Maestro, A.; Jones, D.; Candela, C. S. de Rojas.; Guzman, E.; Duits, M. H. G.; Cicuta, P. Maestro, A., et al. Tuning Interfacial Properties and Processes by Controlling the Rheology and Structure of Poly(*N*-isopropylacrylamide) Particles at Air/Water Interfaces. *Langmuir* **2018**, *34*, 7067-7076.

(91) Horiguchi, Y.; Kawakita, H.; Ohto, K.; Morisada, S. Temperature-responsive Pickering foams stabilized by poly(*N*-isopropylacrylamide) nanogels. *Adv. Powder Tech.* **2018**, *29*, 266-272.

(92) Wu, D.; Mihali, V.; Honciuc, A. pH-Responsive Pickering Foams Generated by Surfactant-Free Soft Hydrogel Particles. *Langmuir* **2019**, *35*, 212−221.

(93) Vanderhoff, J. W.; E1-Aasser, M. S.; Micale, F. J.; Sudol, E. D.; Tseng, C.M.; Silwanwicz, A.; Kornfeld, D. M.; Vicente, F. A. preparation of large-particle-size monodisperse latexes in space: Polymerization Kinetics and Process Development. *J. Dispersion Sci. Technol.* 1984, *5*, 231-246.

(94) Tsuchida, A.; Yoshimi, H.; Kiriyama, S.; Ohiwa, K.; Okubo, T. Interfacial polycondensation of nylon-6,6 in microgravity as studied by free-fall experiments. *Colloid Polym. Sci.* **2003**, *281*, 760-765.

(95) Cohin, Y.; Fisson, M.; Jourde, K.; Fuller, G. G.; Sanson, N.; Talini, L.; Monteux, C. Tracking the interfacial dynamics of PNiPAM soft microgels particles adsorbed at the air–water interface and in thin liquid films *Rheol Acta* **2013**, *52*, 445-454.

(96) Rauh, A.; Rey, M.; Barbera, L.; Zanini, M.; Karg, M.; Isa, L. Compression of hard core–soft shell nanoparticles at liquid–liquid interfaces: influence of the shell thickness. *Soft Matter* **2017**,*13*, 158-169.

(97) Li, Z.; Geisel, K.; Richtering, W.; Ngai, T. Poly(*N*-isopropylacrylamide) microgels at the oil–water interface: adsorption kinetics. *Soft Matter* **2013**, *9*, 9939-9946.

(98) Wu, Y.; Wiese, S.; Balaceanu, A.; Richtering, W.; Pich, A. Behavior of Temperature-Responsive Copolymer Microgels at the Oil/Water Interface. *Langmuir* **2014**, *30*, 7660−7669.

(99) Geisel, K.; Rudov, A. A.; Potemkin, I. I.; Richtering, W. Hollow and Core−Shell Microgels at Oil−Water Interfaces: Spreading of Soft Particles Reduces the Compressibility of the Monolayer. *Langmuir* **2015**, *31*, 13145−13154.

(100) Rumyantsev, A. M.; Gumerov, R. A.; Potemkin, I. I. A polymer microgel at a liquid–liquid interface: theory vs. computer simulations. *Soft Matter* **2016**, *12*, 6799-6811.

(101) Camerin, F.; Fernández-Rodríguez, M. Á.; Rovigatti, L.; Antonopoulou, M. N.; Gnan, N.; Ninarello, A.; Isa, L.; Zaccarelli, E. Microgels Adsorbed at Liquid−Liquid Interfaces: A Joint Numerical and Experimental Study. *ACS Nano* **2019**, *13*, 4548−4559.

(102) Bochenek, S.; Scotti, A.; Ogieglo, W.; Fernández-Rodríguez, M. Á.; Schulte, M. F.; Gumerov, R. A.; Bushuev, N. V.; Potemkin, I. I.; Wessling, M.; Isa, L.; Richtering, W. Effect of the 3D Swelling of Microgels on Their 2D Phase Behavior at the Liquid–Liquid Interface. *Langmuir* in press. DOI: 10.1021/acs.langmuir.9b02498

Chapter 1

"The deformation behavior of microgels at the air/water interface"

*Part of this work was published in "Haruka Minato, Masaki Murai, Takumi Watanabe, Shusuke Matsui, Masaya Takizawa, Takuma Kureha, Daisuke Suzuki, *Chemical Communication* **2018**, *54*, 932-935. DOI: 10.1039/C7CC09603H"

1-1. Introduction

The ‘‘softness’’ of colloidal particles is crucial for their functions in the human body; for instance, red blood cells (RBCs) carry oxygen/carbon dioxide in capillaries whose diameter is much smaller than that of RBCs. Unlike RBCs, soft microgels which can be synthesized artificially are colloidal particles of cross-linked polymeric networks with high contents of water (>90%) that deform or deswell under external stress. The ‘‘softness’’ of microgels plays a crucial role in many applications including coatings,[1] food,[2,3] cosmetics,[4] colloidal crystals/glasses,[5-9] drug delivery systems,[10] biomaterials,[11-13] catalysts,[14,15] and stabilizers for oil/water (emulsions) and air/water (foams) interfaces.[16-21]

In order to further develop these applications and create new applications for soft colloidal particles, understanding the interfacial behavior of microgels is highly important. pNIPAm microgels are representative thermo-responsive microgels;[22-27] they show surface activity and adsorb at the air/water interface, which was first studied using the pendant-drop method.[28] This surface tension technique has been frequently used to discuss the adsorption behavior of soft pNIPAm-based microgels at the air/water interface.[28-30] These studies demonstrate the importance of softness, i.e., the degree of cross-linking in microgels, on the adsorption at the air/water interface. Recently, detailed structural information of adsorbed microgels has been studied using neutron reflectivity measurements,[31,32] molecular dynamics simulation[33] and transmission X-ray microscopy at the oil/ water interface.[34] Although the understanding of the interfacial behavior of soft microgels has progressed, the direct visualization of the interfacial dynamic behavior of individual soft microgels has, to the best of the author's knowledge, not yet been reported. Therefore, details on the interfacial behavior of soft microgels at the air/water or oil/water interface remains unclear and a matter of debate.

In order to better understand the interfacial behavior of soft microgels, the author examined for the first time the deformation dynamics of individual large microgels (>6 μm) that were developed unexpectedly directly at the air/water interface by fluorescence microscopy using a high-speed camera. It should be noted that the group of Suzuki has recently reported that negatively charged softer colloidal particles show faster adsorption on positively charged solid substrates. This was demonstrated by high-speed atomic force microscopy (AFM), which allowed us to observe aqueous systems in real time (1 frame per s).[35] However, this technique cannot be applied to systems at the air/water or oil/water (i.e., liquid) interfaces.

Since the first pNIPAm microgels have been synthesized by precipitation polymerization,[22,23] the largest uniform pNIPAm-based microgels (4.7 μm, pH = 10) have been reported by the Ngai group.[36-37] These microgels were obtained from initially increasing gradually the temperature of the reaction solution,[38] and adding the comonomers in aqueous solution in a continuous manner. In this context, the author found that much larger microgels can be obtained when a small amount of the cross-linker BIS is added at the beginning of the polymerization. Using the obtained larger micron-sized microgels, the author investigated the deformation behavior of microgels upon the adsorption at the air/water interface.

1-2. Experimental Details

1-2-1. Materials

N-isopropyl acrylamide (NIPAm, 98%), glycidyl methacrylate (GMA, 95%), *N*,*N*'-methylenebis(acrylamide) (BIS, 97%), 2,2'-azobis(2-methylpropinamidine) dihydrochloride (V-50, 95%), potassium peroxodisulfate (KPS, 95%), sodium chloride (NaCl, 99.5%), Rhodamine 6G (R6G), and 3-mercaptopropane sulfonic acid (MPSA) were purchased from Wako Pure Chemical Industries and used as received. Acrylic acid (AAc, 99%) was purchased from Sigma Aldrich and used as received. The $Ru(bpy)_3$ monomer (4-vinyl-4'-methyl-2,2'-bipyridine)bis(2,2'bipyridine)ruthenium(II)bis(hexafluorophosphate) was synthesized according to a previously reported procedure.[39] Distilled and ion-exchanged (EYELA, SA-2100E1) water was used in all experiments.

1-2-2. Preparation of Micron-sized Microgels

Poly(NIPAm-*co*-AAc) core–shell hydrogel microspheres (pNA microgels) (size > 6 μm) were prepared via a modified aqueous precipitation polymerization technique (**Scheme 1-1**). The polymerization was performed in a three-necked round-bottom flask (200 mL) equipped with a mechanical stirrer, a condenser, and a nitrogen gas inlet. Typically, the NIPAm monomer (0.6 g), AAc comonomer (63.2 μL), and cross-linker BIS (0.0098 g) were dissolved in deionized water (55 mL). The monomer solution was heated to 40 °C under a stream of nitrogen and constant stirring (250 rpm). The solution was sparged with nitrogen for a period of at least 30 min in order to remove any dissolved oxygen. Subsequently, the free-radical polymerization was initiated with KPS (0.055 g) dissolved in deionized water (1 mL). Immediately after the initiation, the temperature was increased from 40 °C to 60 °C using a temperature gradient of 1 °C/3 min. Thereafter, a mixture of NIPAm monomer (3.5 g), AAc comonomer (875 μL), cross-linker BIS (pNA(1.4): 0.0927 g or pNA(2.7): 0.1855 g), and NaCl (0.0204 g, 10 mM) dissolved in deionized water (35 mL) was added to the reaction mixture at a feeding rate of 0.1 mL/min using a syringe pump. After 5 h, the feeding was stopped, and the reaction was stirred for 2 h at 60 °C, after which the microgel dispersion was cooled in an ice bath to stop the polymerization. The obtained microgels were purified twice by centrifugation/redispersion in water using a relative centrifugal force (RCF) of 20,000 g to remove unreacted reagents and other impurities. Similar to the synthesis of pNA microgels, pure pNIPAm microgels (both positively and negatively charged), poly(NIPAm-*co*-GMA) microgels, and poly(NIPAm-*co*-Ru(bpy)$_3$) were prepared via this modified aqueous precipitation polymerization. **Table 1-1** summarizes the details for the polymerization and **Figure 1-1** shows the optical microscopy images and chemical composition of these microgels. Poly(NIPAm-*co*-acrylic acid) microgels denoted as pNA(*X*), where *X* indicates the BIS concentration (mol%) in the shell.

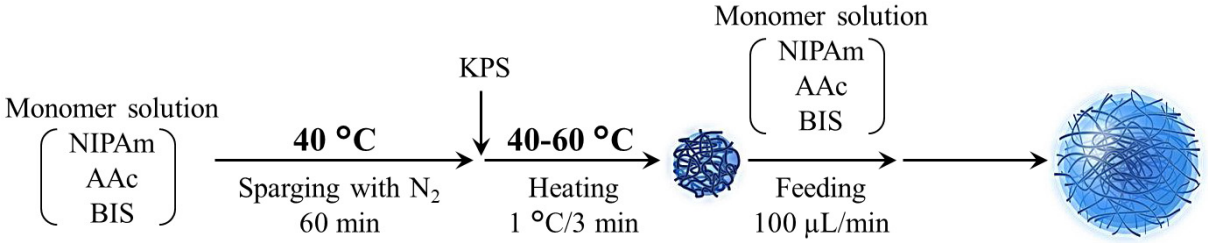

Scheme 1-1. pNA core–shell microgels prepared via a modified aqueous precipitation polymerization.

Table 1-1. Chemical composition of the pNIPAm-based microgels developed in this study

Code	Core monomer			Shell monomer					Temp. (°C)	Initiator	
	NIPAm (mol%)	BIS (mol%)	AAc (mol%)	NIPAm (mol%)	AAc (mol%)	GMA (mol%)	$Ru(bpy)_3$ (mol%)	BIS (mol%)		KPS (mM)	V-50 (mM)
pNA(1.4)	84	1	15	69.7	28.9	-	-	1.4	40→60	3.6	-
pNA(2.7)	84	1	15	68.8	28.5	-	-	2.7	40→60	3.6	-
pN/KPS	99	1	-	99	-	-	-	1	35→60	3.6	-
pN/V-50	99	1	-	99	-	-	-	1	40→60	-	3.6
pNG	99	1	-	69	-	27	-	4	40→60	-	3.6
pNG-MPSA*	-	-	-	-	-	-	-	-	-	-	-
pNRu	99.9	0.1	-	94.7	-	-	3.7	1.6	40→60	-	3.6

*pNG-MPSA microgels were prepared from pNG microgels according to a previous report.[40] Briefly, a mixture of pNG microgels (0.5 g), MPSA (ten times the amount of epoxy groups in the pNG microgels), and water (45 g) was poured in a 100-mL glass vial with stirring at room temperature, and the pH was adjusted to 11 with 1 M NaOH. The reaction was continued for 24 h. The obtained pNG–MPSA microgels were purified twice by centrifugation/redispersion in water using a RCF of 20,000g to remove impurities.

1-2-3. Characterization of the Microgels

Microgels in aqueous solution were observed with an optical microscope (BX51 or BX53, Olympus) equipped with a fluorescence system (ramp: U-RFL-T, excitation: 460-495 nm, emission: 510 nm) and a digital camera (ImageX Earth Type A-5.0M Ver. 3.0.4, Kikuchi-Optical Co., Ltd.) or high-speed camera (AX50 2SA, Photron). Note that the images shown in **Figure 1-7** were observed with an optical microscope (Axio Scope. A1, Zeiss) equipped with a fluorescence system (ramp: HBO-100, excitation: 450-490 nm, emission: 510 nm) and a digital camera (ImageX Earth Type S-2.0M Ver. 3.1.3, KikuchiOptical Co., Ltd.). These fluorescence systems were used

to excite the fluorescent dye Rhodamine 6G (R6G). The microgels were transferred into rectangular Vitrotube borosilicate capillaries (0.1 × 2.0 mm) by capillary action. In order to observe the microgels in detail, colloidal crystals of the microgels were obtained through a thermal annealing process at a concentration close to the critical concentration.

1-2-4. Dye Labeling Experiments

After labeling the obtained pNIPAm-based microgels with ~0.0001 wt% R6G at a microgel concentration of ~0.003 wt%, the samples were purified via centrifugation/redispersion in water using a RCF of 20,000 g to remove any excess R6G. The samples were observed by fluorescence microscopy.

1-2-5. Calculation of the Critical Concentration

The intrinsic viscosity ([η]) of each microgel at 25 °C was evaluated from the viscosity of sufficiently diluted dispersions measured with an Ubbelohde viscometer. As it is customary when dealing with microgels, the apparent volume fraction of the microgels (ϕ_{eff}; $\phi_{eff} \equiv c[\eta]/2.5$) was employed as a simple measure of the degree of packing, although ϕ_{eff} deviates from the real volume fraction in the concentrated regime where the microgels undergo deformation, deswelling, and interpenetration. The critical concentration, C^*, was a concentration of $\phi_{eff} = 1$.[41]

1-3. Results and Discussion

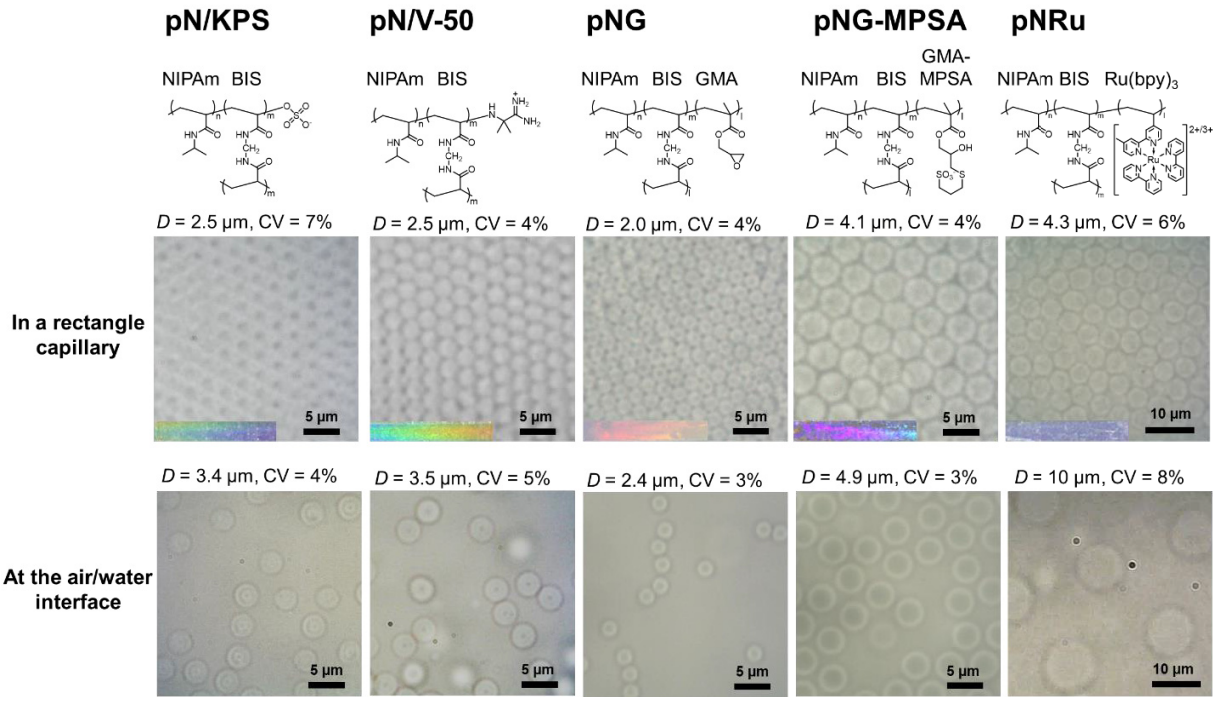

Figure 1-1. Optical microscopy images of different microgels. Inset photographs show colloidal crystals composed of each microgel. The microgels were observed in a rectangle capillary at high concentration (left column) and at the air/water interface (right column) of the dispersion droplets (N = 30). From these images, it is clear that these microgels are uniform, and that the applied synthetic method should be applicable to various pNIPAm-based microgels.

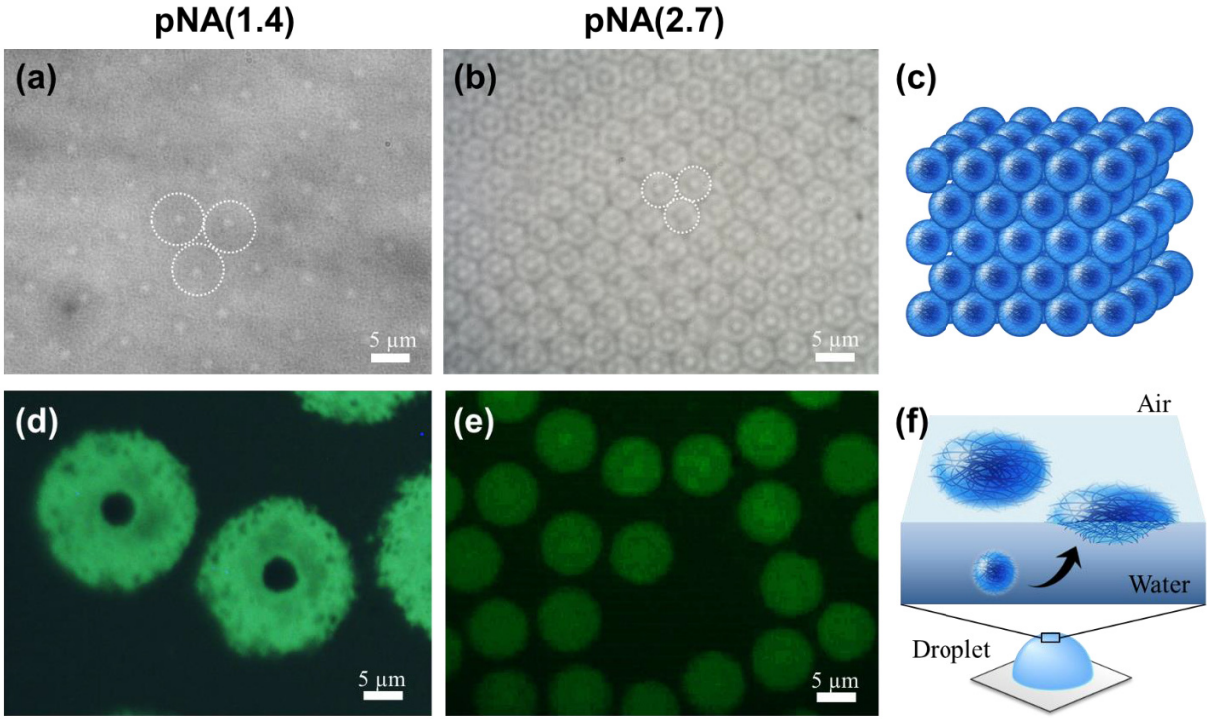

Figure 1-2. Optical microscopy images of (a) pNA(1.4) and (b) pNA(2.7) microgels packed in a rectangle capillary at the critical concentration (C^*, $\phi_{\mathrm{eff}} = 1.0$). The white dotted lines indicate the surface of individual microgels. (c) Scheme of hexagonal close-packed crystal structures. Fluorescence microscopy images of the same (d) pNA(1.4) and (e) pNA(2.7) microgels adsorbed at the air/water interface of a dispersion droplet. (f) Scheme of adsorbed microgels at the air/water interface. These samples were observed at room temperature.

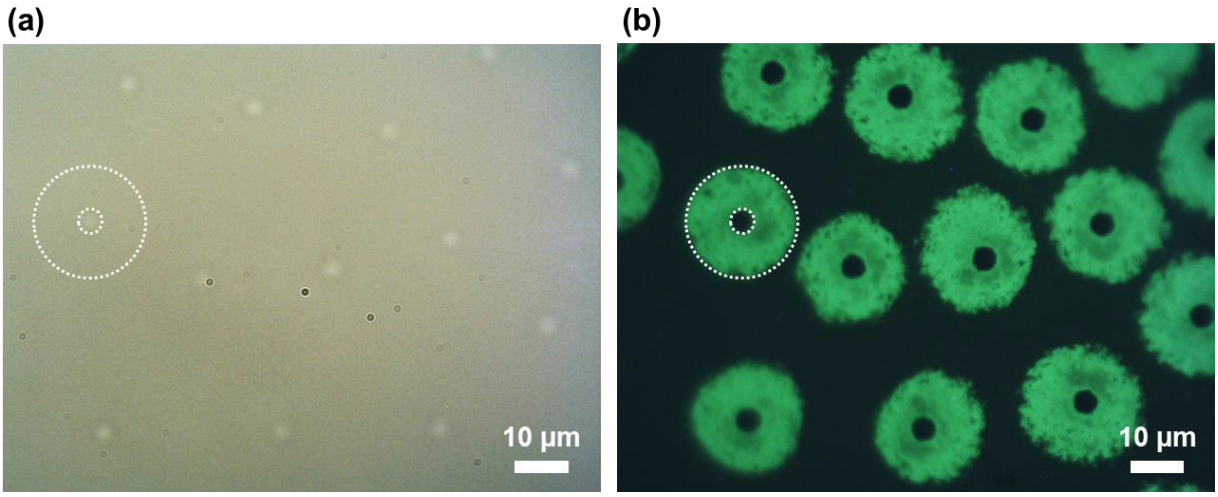

Figure 1-3. (a) Optical and (b) fluorescence microscopy images of the same pNA microgels after labelling with R6G dye molecules. The same area was observed at the air/water interface of the dispersion droplet at pH = 7 and 25 °C. The white dotted lines indicate the core part and the surface of an individual microgel.

The author confirmed that the modified precipitation polymerization method can also be applied to pure BIS-cross-linked pNIPAm microgels (both negatively and positively charged), pNIPAm-based microgels copolymerized with charged acrylic acid or reactive glycidyl methacrylate monomers (which in turn may incorporate various functional molecules),[40] and p(NIPAm-*co*-tris(2,2'-bipyridyl)) ruthenium(II) complex microgels, which exhibit autonomous swelling/deswelling and flocculating/dispersing oscillation[42-51] (**Table 1-1** and **Figure 1-1**). In the present study, the author selected poly(NIPAm-*co*-acrylic acid) microgels, henceforth denoted as pNA(*X*), where *X* indicates the BIS concentration (mol%) in the shell, for further studies, as their diameter was the largest among all the aforementioned microgels. The detail mechanism of the modified precipitation polymerization will be discussed elsewhere.

Figure 1-2(a) shows pNA(1.4) microgels packed in a rectangle capillary as observed by optical microscopy (6.3 μm, pH = 7, 25 °C). Here, the microgels were examined at the critical concentration (*C**, ϕ_{eff} = 1.0), where polymer chains on the microgels begin to contact each other. It should be noted that the shells of the microgels are almost transparent, as they have been highly expanded by water; however, the pNA microgels are indeed closely packed as no random movement was observed. Subsequently, the deformation of the pNA(1.4) microgels was examined at the air/water interface of a dispersion droplet deposited on a glass substrate at pH = 7 and 25 °C (**Figure 1-2(d)**). To visualize all the microgels, fluorescent R6G was adsorbed on the pNA microgels by electrostatic attraction with the acrylic acid moieties. As a result, highly deformed microgels were visualized at the air/water interface, whose diameter increased to 20 μm (CV = 9%, *N* = 50), which is more than three times that of the spherical microgels. In the fluorescence microscopy images, core (dark part)–shell (green fluorescence part) microgels were observed. By optical microscopy, only the cores could be visualized, and a size of 4 μm was calculated (**Figure 1-3**), indicating that the polymer density in the shell is too low to visualize due to the limited resolution of the optical microscope. The highly spread thin shell was only visible upon adding the fluorescent dye.

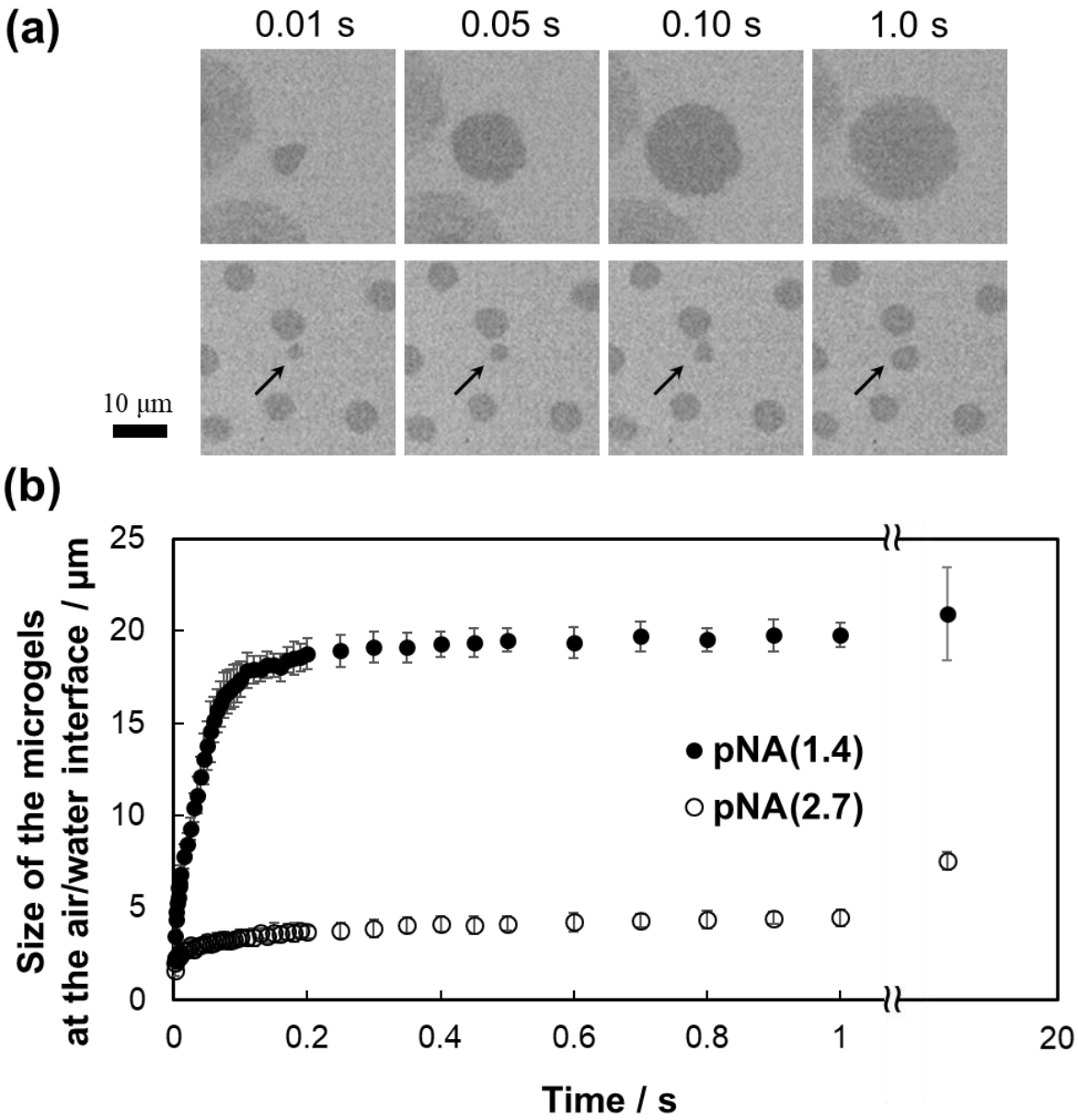

Figure 1-4. (a) pNA(1.4) and pNA(2.7) microgels upon adsorption at the air/water interfaces visualized by fluorescence microscopy equipped with a high-speed camera at pH = 3 and 25 °C. It should be noted that these images were recorded in grey scale. (b) Time evolution of the size of pNA(1.4) and pNA(2.7) microgels upon adsorption at the air/water interface (N = 10).

To gain insight into how microgels are deformed at the air/water interface, the exact moment of the adsorption of the microgels was monitored by fluorescence microscopy using a high-speed camera (**Figure 1-4**). For the pNA(1.4) microgels shown in **Figure 1-4**, the size of the microgels spread radially at the interface became 17 μm within 0.1 s. Subsequently, the size gradually increased to ~20 μm within 1 s, where it reached an equilibrium. To evaluate the impact of the microgel softness on the deformation kinetics, pNA microgels with a higher BIS concentrations in the shell were prepared (pNA(2.7); **Table 1-1** and **Figure 1-2(b)(e)**). The author confirmed that the deformation of the stiffer pNA(2.7) microgels at the interface was fast, similar to that of the softer pNA(1.4) microgels, although the highly cross-linked pNA(2.7) microgels were only slightly deformed at the air/water interface (**Figure 1-4(b)**). The degree of deformation is defined as D_{ads}/D_{C^*}, where D_{ads} represents the size of the microgels adsorbed at the interface and D_{C^*} represents the diameter of the microgels packed in a rectangle capillary at C^* (**Figure 1-2(a)(b)**). In this case, D_{ads}/D_{C^*} was 3.2 for pNA(1.4) and 1.9 for pNA(2.7) in the equilibrium state. In the previous work,[35] Suzuki et al. were unable to quantify the kinetics of deformation of the microgels at the solid/water interface due to the lack of time resolution of the high-speed AFM (1 frame per s); nevertheless, it was possible to observe the deformation of all the tested microgels at these interfaces.[35] However, in the present study, it was able to confirm for the first time that the deformation kinetics at the air/water interface is so fast that the softness or cross-link density of the microgels does not exert a significant impact.

In order to understand the deformation in more detail, the deformation dynamics were analyzed using time-lapse images. Pseudo-first-order and the pseudo-second-order equations were applied to analyze the deformation kinetics.[52] These kinetic models can be expressed in linear form as follows:

$$\log(D_e - D_t) = \log(D_e) - (k_1/2.303)\, t \quad (1\text{-}1)$$

$$(t/D_t) = 1/k_2 {D_e}^2 + (1/D_e)t \quad (1\text{-}2)$$

where D_e and D_t (μm) represent the size of microgels adsorbed at the air/water interface at equilibrium and at arbitrary time t (s), respectively. k_1 (s^{-1}) is the rate constant of the pseudo-first-order model, while k_2 (μm μm^{-1} s^{-1}) is the rate constant of the pseudo-second-order model.

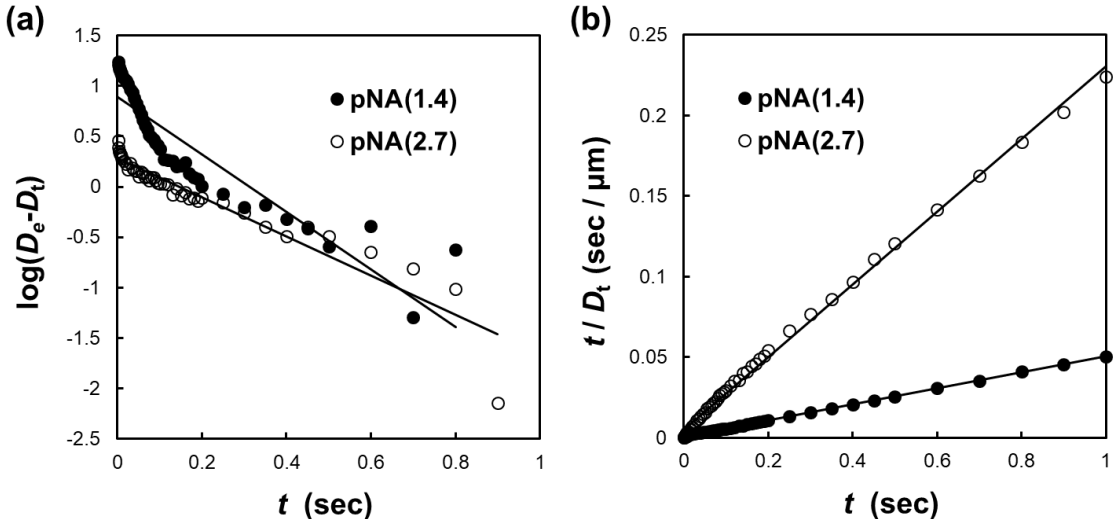

Figure 1-5. Plots of (a) pseudo-first-order eqn (1) and (b) pseudo-second-order kinetic (eqn (2)) for the deformation of pNA(1.4) and pNA(2.7) microgels at the air/water interface; recorded with a fluorescence microscope equipped with a high-speed camera.

Table 1-2. Deformation kinetic parameters at pNA(1.4) and pNA(2.7) microgels

Microgels	Plot parameters			Calculated parameter
	k_2 (sec^{-1})	D_e (μm)	R^2	D_{ads}/D_{C^*}
pNA(1.4)	2.74	20.1	0.9995	3.2
pNA(2.7)	10.4	4.43	0.9968	1.9

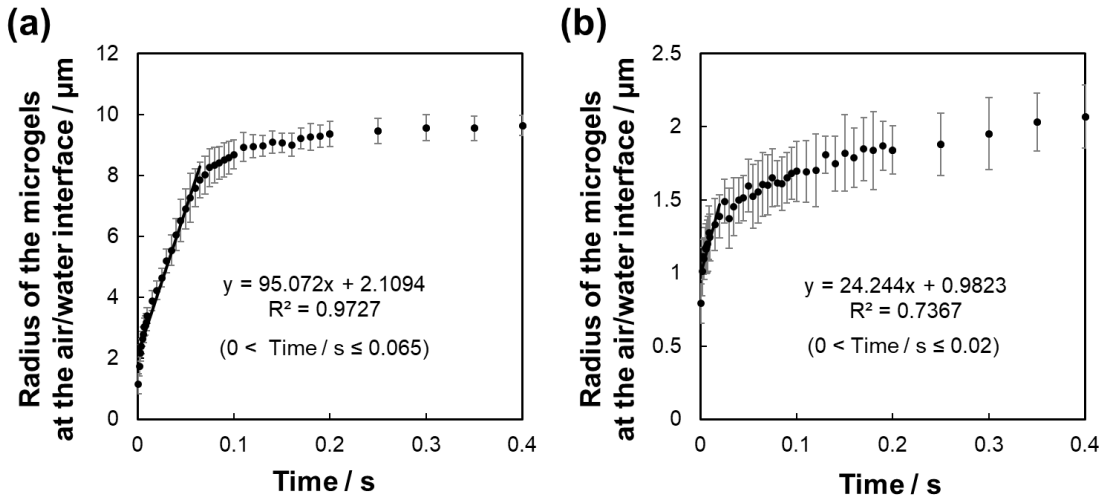

Figure 1-6. Radius of (a) pNA(1.4) and (b) pNA(2.7) microgels as a function of time at the air/water interface, which were calculated from the diameter (**Figure 1-4**).

Figure 1-5 shows the plots of pseudo-first-order and the pseudo-second-order kinetics for the deformation of pNA(1.4) and pNA(2.7) microgels. The correlation coefficient (R^2) of the pseudo-second-order model was ~1, and that of the pseudo-first-order model was not, indicating a good fit of the pseudo-second-order model for these microgels (**Table 1-2**). It suggests that one part of the deformation dynamics should be explained by a two-stage deformation speed; during the first stage, the microgels rapidly deform at the air/water interface, which is caused by a collision of the microgels at the air/water interface. During the second stage, the surface-active polymer chains on the microgel gradually spread to stabilize the interface thermodynamically. Here, the deformation rate of the microgels during the first stage was calculated from the fitted line (**Figure 1-6**), affording deformation rates (v) of 95 μm s-^{1} and 24 μm s^{-1} for pNA(1.4) and pNA(2.7), respectively. Although the initial deformation rate, v, of these microgels was significantly different, it seems that the deformation of the microgels is completed very quickly, i.e., within a few seconds regardless of the degree of cross-linking (i.e., irrespective of the softness).

Finally, the time-dependent deformation of pNA(1.4) microgels at the air/water interface in a dilute microgel dispersion (~0.003 wt%) was monitored during drying (**Figure 1-7**). In the previous studies,[53-55] the structure of the adsorbed microgels at the air/water interface could not be determined due to limitations of the resolution. In this study, however, given that the thin shell of the microgels can be visualized, the author could confirm for the first time that the adsorbed and highly deformed microgels gradually engage in contact with each other (**Figure 1-7(a)(b)**), before the size of the microgels largely decreases with decreasing interfacial area upon drying. The degree of deformation of the pNA(1.4) microgels decreased with time from D_{ads}/D_{C^*} = 3.2 (1 min) to 3.0 (36 min) and 2.4 (42 min).

It is also noteworthy that the method reported herein for the synthesis of large microgels may also be applicable to other microgels, such as autonomously oscillating microgels,[42-51] although the detailed mechanism of the polymerization should be clarified experimentally. This investigation on the interfacial behavior of large microgels may thus open new research avenues in the areas of fundamental colloidal chemistry and applied materials chemistry.

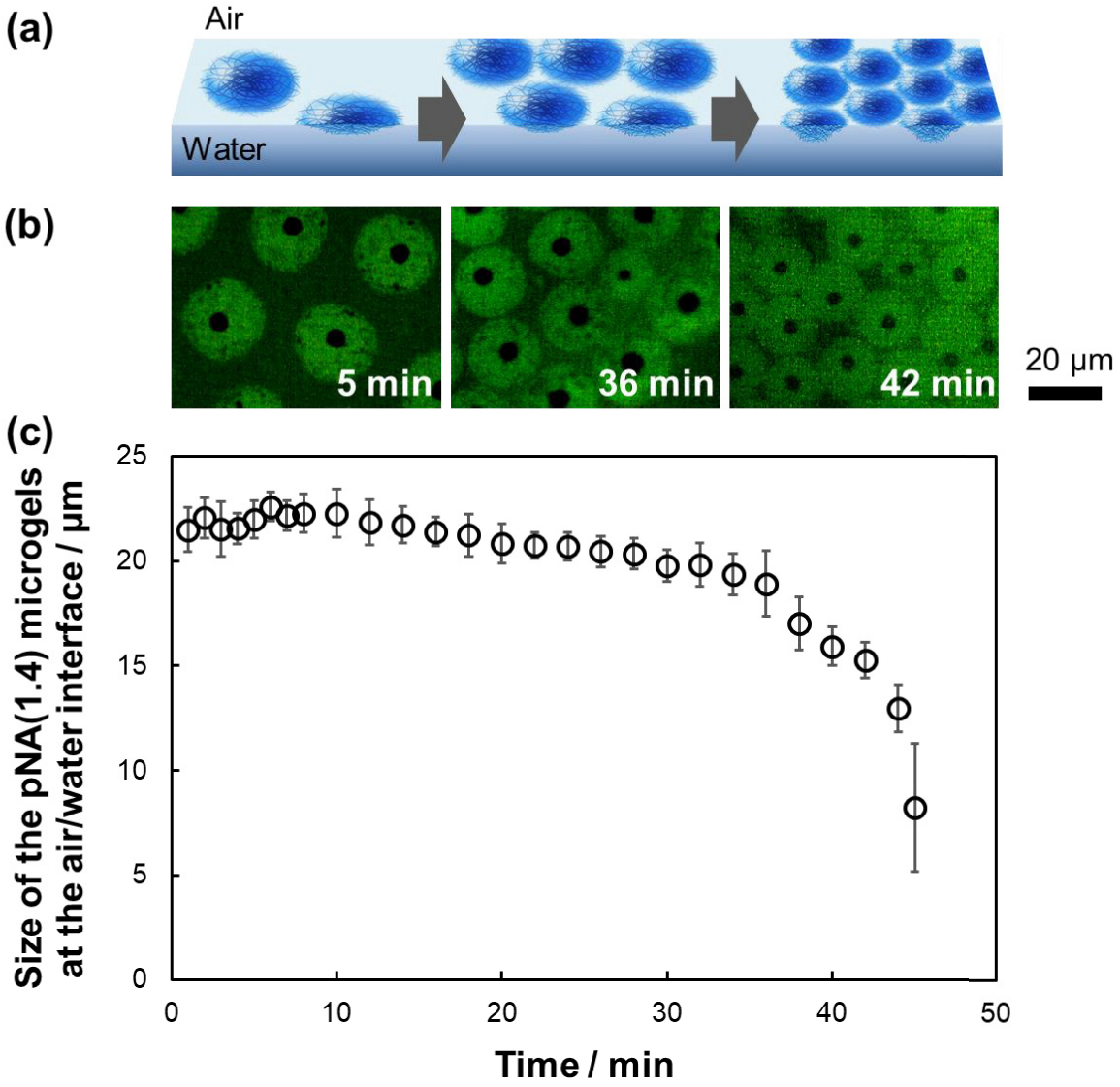

Figure 1-7. (a) Scheme, (b) fluorescence microscopy images and (c) size of pNA(1.4) microgels at the air/water interface of dilute microgel droplets as a function of time during evaporation of the solvent ($N = 30$).

1-4. Conclusions

The deformation kinetics of soft pNIPAm-based microgels upon adsorption at the air/water interface was quantified for the first time using large pNIPAm-based microgels synthesized by a modified aqueous precipitation polymerization technique. The deformation process of the microgels upon adsorption at the interface was visualized and analyzed directly. The microgels adsorbed and deformed very quickly at the air/water interface, and the deformation kinetics could be feasibly explained using a pseudo-second-order model. Additionally, the highly deformed microgels adsorbed at the interface finally engaged in contact with each other, before gradually deforming during drying. Moreover, the method to produce such large microgels was also successfully applied to other functional microgels. Therefore, these new findings for the evaluation of the ‘‘softness’’ of microgels at the air/water interface may promote the development of new applications related to the interfacial behavior of microgels.

1.5. References

(1) Li, W.; Hu, L.; Zhu, J.; Li, D.; Luan, Y.; Xu, W.; Serpe, M. J. Comparison of the Responsivity of Solution-Suspended and Surface-Bound Poly(*N*-isopropylacrylamide)-Based Microgels for Sensing Applications. *ACS Appl. Mater. Interfaces*, **2017**, *9*, 26539–26548.

(2) McClements, D. J. Recent progress in hydrogel delivery systems for improving nutraceutical bioavailability. *Food Hydrocolloids* **2017**, *68*, 238–245.

(3) Gu, L.; Su, Y.; Zhang, Z.; Zheng, B.; Zhang, R.; McClements, D. J.; Yang, Y. Modulation of Lipid Digestion Profiles Using Filled Egg White Protein Microgels. *J. Agric. Food Chem.* **2017**, *65*, 6919–6928.

(4) Kaneda, I.; Sogabe, A.; Nakajima, H. Water-swellable polyelectrolyte microgels polymerized in an inverse microemulsion using a nonionic surfactant. *J. Colloid Interface Sci.* **2004**, 275, 450–457.

(5) Lyon, L. A.; Debord, J. D.; Debord, S. B.; Jones, C. D.; McGrath, J. G.; Serpe, M. J. Microgel Colloidal Crystals. *J. Phys. Chem. B* **2004**, *108*, 19099–19108.

(6) Hellweg, T.; Dewhurst, C. D.; Brückner, E.; Kratz, K.; Eimer, W. Colloidal crystals made of poly(*N*-isopropylacrylamide) microgel particles. *Colloid Polym. Sci.* **2000**, *278*, 972–978.

(7) Mattsson, J.; Wyss, H. M.; Fernandez-Nieves, A.; Miyazaki, K.; Hu, Z.; Reichman, D. R.; Weitz, D. A. Soft colloids make strong glasses. *Nature* **2009**, 462, 83–86.

(8) Okubo, T.; Suzuki, D.; Yamagata, T.; Katsuno, A.; Sakurai, M.; Kimura H.; Tsuchida, A. Colloidal crystallization of thermo-sensitive gel spheres of poly (*N*-isopropyl acrylamide). *Colloid Polym. Sci.* **2011**, *289*, 291–299.

(9) Urayama, K.; Saeki, T.; Cong, S.; Uratani, S.; Takigawa, T.; Murai, M.; Suzuki, D. A simple feature of yielding behavior of highly dense suspensions of soft micro-hydrogel particles. *Soft Matter* **2014**, *10*, 9486–9495.

(10) Merkel, T. J.; Jones, S. W.; Herlihy, K. P.; Kersey, F. R.; Shields, A. R.; Napier, M.; Luft, J. C.; Wu, H.; Zamboni, W. C.; Wang, A. Z.; Bear, J. E.; DeSimone, J. M. Using mechanobiological mimicry of red blood cells to extend circulation times of hydrogel microparticles. *Proc. Natl. Acad. Sci. U. S. A.* **2011**, *108*, 586–591.

(11) Nakamoto, M.; Nonaka, T.; Shea, K. J.; Miura, Y.; Hoshino, Y. Design of Synthetic Polymer Nanoparticles That Facilitate Resolubilization and Refolding of Aggregated Positively Charged Lysozyme. *J. Am. Chem. Soc.* **2016**, *138*, 4282–4285.

(12) Gau, E.; Mate, D. M.; Zou, Z.; Oppermann, A.; Töpel, A.; Jakob, F.; Wöll, D.; Schwaneberg, U.; Pich, A. Sortase-Mediated Surface Functionalization of Stimuli-Responsive Microgels. *Biomacromolecules* **2017**, *18*, 2789–2798.

(13) Nuhn, L.; Tomcin, S.; Miyata, K.; Mailänder, V.; Landfester, K.; Kataoka, K.; Zentel, R. *Biomacromolecules* **2014**, *15*, 4111–4121.

(14) Ballauff, M.; Lu, Y. "Smart" nanoparticles: Preparation, characterization and applications. *Polymer* **2007**, *48*, 1815–1823.

(15) Lu, Y.; Ballauff, M. Spherical polyelectrolyte brushes as nanoreactors for the generation of metallic and oxidic nanoparticles: Synthesis and application in catalysis. *Prog. Polym. Sci.* **2016**, *59*, 86–104.

(16) Ngai, T.; Behrens, S. H.; Auweter, H. Novel emulsions stabilized by pH and temperature sensitive microgels. *Chem. Commun*. **2005**, 331–333.

(17) Fujii, S.; Read, E. S.; Binks, B. P.; Armes, S. P. Stimulus-Responsive Emulsifiers Based on Nanocomposite Microgel Particles. *Adv. Mater.* **2005**, *17*, 1014–1018.

(18) Suzuki, D.; Tsuji, S.; Kawaguchi, H. Janus Microgels Prepared by Surfactant-Free Pickering Emulsion-Based Modification and Their Self-Assembly. *J. Am. Chem. Soc.* **2007**, *129*, 8088–8089.

(19) Richtering, W. Responsive Emulsions Stabilized by Stimuli-Sensitive Microgels: Emulsions with Special Non-Pickering Properties. *Langmuir* **2012**, *28*, 17218–17229.

(20) Destribats, M.; Lapeyre, V.; Wolfs, M.; Sellier, E.; Leal-Calderon, F.; Ravaine, V.; Schmitt, V. Soft microgels as Pickering emulsion stabilisers: role of particle deformability. *Soft Matter* **2011**, *7*, 7689–7698.

(21) Kwok, M. H.; Ngai, T. A confocal microscopy study of micron-sized poly (*N*-isopropylacrylamide) microgel particles at the oil–water interface and anisotopic flattening of highly swollen microgel. *J. Colloid Interface Sci.* **2016**, *461*, 409–418.

(22) Pelton, R. H.; Chibante, P. Preparation of Aqueous Latices with *N*-Isopropylacrylamide. *Colloids Surf.* **1986**, *20*, 247–256.

(23) Pelton, R. Temperature-sensitive aqueous microgels. *Adv. Colloid Interface Sci.* **2000**, *85*, 1–33.

(24) Saunders, B. R.; Vincent, B. Microgel particles as model colloids: theory, properties and applications. *Adv. Colloid Interface Sci.* **1999**, *80*, 1–25.

(25) Nayak, S.; Lyon, L. A. Soft Nanotechnology with Soft Nanoparticles. *Angew. Chem., Int. Ed.* **2005**, *44*, 7686–7708.

(26) Plamper, F. A.; Richtering, W. Functional Microgels and Microgel Systems. *Acc. Chem. Res.* **2017**, *50*, 131–140.

(27) Suzuki, D.; Horigome, K.: Kureha, T.; Matsui, S.; Watanabe, T. Polymeric hydrogel microspheres: design, synthesis, characterization, assembly and applications. *Polym. J.* **2017**, *49*, 695–702.

(28) Zhang, J.; Pelton, R. Poly(*N*-isopropylacrylamide) Microgels at the Air-Water Interface. *Langmuir* **1999**, *15*, 8032–8036.

(29) Deshmukh, O. S.; Maestro, A.; Duits, M. H. G.; van den Ende, D.; Stuart, M. C.; Mugele, F. Equation of state and adsorption dynamics of soft microgel particles at an air-water interface. *Soft Matter* **2014**, *10*, 7045–7050.

(30) Keal, L.; Lapeyre, V.; Ravaine, V.; Schmitt, V.; Monteux, C. Drainage dynamics of thin liquid foam films containing soft PNiPAM microgels: influence of the cross-linking density and concentration. *Soft Matter* **2017**, *13*, 170–180.

(31) Zielińska, K.; Sun, H.; Campbell, R. A.; Zarbakhsh, A.; Resmini, M. Smart nanogels at the at the air/water interface: Q1 structural studies by neutron reflectivity. *Nanoscale* **2016**, *8*, 4951–4960.

(32) Zielińska, K.; Campbell, R. A.; Zarbakhsh, A.; Resmini, M. Adsorption versus aggregation of NIPAM nanogels: new insight into their behaviour at the air/water interface as a function of concentration. *Phys. Chem. Chem. Phys.* **2017**, *19*, 17173–17179.

(33) Harrer, J.; Rey, M.; Ciarella, S.; Löwen, H.; Janssen, L. M. C.; Vogel, N. Stimuli-Responsive Behavior of PNiPAm Microgels under Interfacial Confinement. *Langmuir* **2019**, *35*, 10512–10521.

(34) Geisel, K.; Henzler, K.; Guttmann, P.; Richtering, W. New Insight into Microgel-Stabilized Emulsions Using Transmission X-ray Microscopy: Nonuniform Deformation and Arrangement of Microgels at Liquid Interfaces. *Langmuir* **2015**, *31*, 83–89.

(35) Matsui, S.; Kureha, T.; Hiroshige, S.; Shibata, M.; Uchihashi, T.; Suzuki, D. Fast Adsorption of Soft Hydrogel Microspheres on Solid Surfaces in Aqueous Solution. *Angew. Chem. Int. Ed.* **2017**, *56*, 12146–12149.

(36) Li, Z.; Kwok, M. H.; Ngai, T. Preparation of Responsive Micrometer-Sized Microgel Particles with a Highly Functionalized Shell. *Macromol. Rapid Commun.* **2012**, *33*, 419–425.

(37) Kwok, M. H.; Li, Z.; Ngai, T. Controlling the Synthesis and Characterization of Micrometer-Sized PNIPAM Microgels with Tailored Morphologies. *Langmuir* **2013**, *29*, 9581–9591.

(38) Meng, Z.; Smith M. H.; Lyon, L. A. Temperature-programmed synthesis of micron-sized multi-responsive microgels. *Colloid Polym. Sci.* **2009**, *287*, 277–285.

(39) Ghosh P. K.; Spiro, T. G. Photoelectrochemistry of Tris(bipyridyl)ruthenium(II) Covalently Attached to *n*-Type SnO_2. *J. Am. Chem. Soc.* **1980**, *102*, 5543–5549.

(40) Suzuki, D.; Kawaguchi, H. Stimuli-sensitive core/shell template particles for immobilizing inorganic nanoparticles in the core. *Colloid Polym. Sci*. **2006**, *284*, 1443–1451.

(41) Urayama, K.; Saeki, T.; Cong, S.; Uratani, S.; Takigawa, T.; Murai, M.; Suzuki, D. A simple feature of yielding behavior of highly dense suspensions of soft micro-hydrogel particles. *Soft Matter* **2014**, *10*, 9486–9495.

(42) Suzuki, D.; Sakai T.; Yoshida, R. Self-Flocculating/Self-Dispersing Oscillation of Microgels. *Angew. Chem. Int. Ed.* **2008**, *47*, 917–920, *Nature Materials* **2008**, *7*, 95.

(43) Suzuki, D.; Yoshida, R. Temporal Control of Self-Oscillation for Microgels by Crosslinking Network Structure. *Macromolecules* **2008**, *41*, 5830–5838.

(44) Suzuki, D.; Yoshida, R. Effect of Initial Substrate Concentration of the Belousov-Zhabotinsky Reaction on Self-Oscillation for Microgel System. *J. Phys. Chem. B* **2008**, *40*, 12618–12624.

(45) Suzuki, D.; Yoshida, R. Synthesis and Characterization of Submicron-sized, Self-oscillating Hydrogel Particles. *Trans. Mater. Res. Soc. Japan* **2009**, *34*, 465–467.

(46) Suzuki, D.; Taniguchi, H.; Yoshida, R. Autonomously Oscillating Viscosity in Microgel Dispersions. *J. Am. Chem. Soc.* **2009**, *131*, 12058–12059.

(47) Taniguchi, H.; Suzuki, D.; Yoshida, R. Characterization of Autonomously Oscillating Viscosity Induced by Swelling/Deswelling Oscillation of the Microgels. *J. Phys. Chem. B* **2010**, *114*, 2405–2410.

(48) Suzuki, D.; Yoshida, R. Self-Oscillating Core/shell Microgels: Effect of Cross-linked Nano-shell on Autonomous Oscillation of the Core. *Polym. J.* **2010**, *42*, 501–508.

(49) Suzuki, D.; Kobayashi, T.; Yoshida, R.; Hirai, T. Soft actuators of organized self-oscillating microgels. *Soft Matter* **2012**, *8*, 11447–11449.

(50) Matsui, S.; Kureha, T.; Nagase, Y.; Okeyoshi, K.; Yoshida, R.; Sato, T.; Suzuki, D. Small-Angle X-ray Scattering Study on Internal Microscopic Structures of Poly(*N*-isopropylacrylamide-co-tris(2,2-bipyridyl))ruthenium(II) Complex Microgels. *Langmuir* **2015**, *31*, 7228–7237.

(51) Matsui, S.; Inui, K.; Kumai, Y.; Yoshida, R.; Suzuki, D. Autonomously Oscillating Hydrogel Microspheres with High-Frequency Swelling/deswelling and Dispersing/flocculating Oscillations. *ACS Biomaterials Science & Engineering* **2019**, 5, 5615-5622..

(52) Ghaedi, M.; Ansari, A.; Habibi, M. H.; Asghari, A. R.; Removal of malachite green from aqueous solution by zinc oxide nanoparticle loaded on activated carbon: Kinetics and isotherm study. *J. Ind. Eng. Chem.* **2014**, *20*, 17–28.

(53) Suzuki, D.; Horigome, K. Binary Mixtures of Cationic and Anionic Microgels. *Langmuir* **2011**, *27*, 12368–12374.

(54) Horigome, K.; Suzuki, D. Drying Mechanism of Poly(N-isopropylacrylamide) Microgel Dispersions. *Langmuir* **2012**, *28*, 12962–12970.

(55) Suzuki, D.; Horigome, K. Assembly of Oppositely Charged Microgels at the Air/Water Interface. *J. Phys. Chem. B* **2013**, *117*, 9073–9082.

Chapter 2

"The adsorption behavior of microgels at the air/water interface"

*Part of this work was published in "Haruka Minato, Masaya Takizawa, Seina Hiroshige, Daisuke Suzuki, *Langmuir* **2019**, *35*, 10412-10423. DOI: 10.1021/acs.langmuir.9b01933"
Reprinted with permission from Copyright (2019) American Chemical Society.

2-1. Introduction

Microgels have attracted much attention due to a wide range of potential applications in e.g. chemical or bio-sensors,[1-5] selective separations,[6-8] stabilizers for emulsions,[9-13] autonomous materials,[14,15] and drug-delivery systems,[16-18] as aforementioned. The high utility of microgels can be mostly attributed to their fascinating physicochemical properties such as softness (degree of crosslinking), which can be tuned by applying external stimuli. In a series of fundamental studies, thermo-responsive poly(*N*-isopropyl acrylamide) (pNIPAm) microgels (or derivatives thereof) have been widely used as they can be synthesized in uniform size by aqueous free radical precipitation polymerization.[19,20] So far, many functionalized microgels that can respond to stimuli such as changes in ionic strength or pH value, chemical reactions, light, and the presence/absence of biomolecules have been reported.[14,15,20-25] Among these functionalizations, the copolymerization with appropriately designed monomers is the most widely used and conventional approach due to the simplicity of the procedure. For instance, pH-responsive microgels are obtained from copolymerizations with e.g., acrylic or methacrylic acid monomers.[21] Furthermore, autonomously oscillating microgels, which show periodic swelling/deswelling and assembling/disassembling oscillations, are obtained from copolymerizations with charged catalysts such as ruthenium complexes in order to be able to respond to cyclic redox reactions.[14,15]

From a materials science point of view, the assembly of such microgels is important to obtain thin films or hierarchical bulk gels that show additional functionality. For instance, films of microgels copolymerized with amine groups[26,27] show faster and increased absorption and desorption of CO_2 than those of dispersions or bulk gels.[28,29] Microgels copolymerized with phenylboronic acid groups respond to glucose, which is expected to find applications in color-changing sensors.[23,30]

So far, many methods for microgel assemblies, including dip- and spin-coating, have been reported.[31-37] The group of Suzuki has been investigating the self-organization of microgels during the evaporation of aqueous sessile droplets in order to generate thin microgel films.[36-39] The author has previously discovered that soft and surface-active microgels based on e.g. pNIPAm spontaneously adsorb on the air/water interface of the droplet when sessile droplets are evaporated.[36,40] Subsequently, the adsorbed microgels are slowly arranged at the interface, and finally the arranged microgel monolayers are transferred onto the solid substrate,[36] which stands in sharp contrast to rigid microspheres made of e.g. polystyrene or silica.[41] To clarify the details of the formation mechanism, understanding the behavior of microgels at the air/water interface (e.g. adsorption, interpenetration, and deformation) is crucial. During the drying process, the size of the microgels is not crucial because the microgels are moved to the air/water interface by convection flow; however, the softness (degree of crosslinking) of the individual microgels is very important: the softer the microgels are, the faster the microgels adsorb at the air/water interface.[38] It has also been clarified that individual microgels are substantially deformed immediately upon attaching to the air/water interface, which was observed directly with an optical microscope equipped with a high-speed camera.[42]

The author hypothesized that if the aforementioned charged (or functionalized) microgels could be combined with the method, a variety of functionalized thin films of polyelectrolytes could potentially be obtained in an operationally simple and low-cost fashion within a short period of time, which would be useful for all applications that these microgel assemblies have already found. In this study, the author initially investigated the effect of charged groups immobilized in the microgels on the self-organization during the evaporation of aqueous sessile droplets. Especially, the impact of the charged groups in the microgels on their adsorption, interpenetration, and deformation behavior at the air/water interface was systematically investigated using a series of dispersions of charged microgels. The author is convinced that the results on the behavior of microgels at the air/water interface will contribute to the development of further applications for e.g. microgel-stabilized foams and emulsions, where the understanding of the behavior of functional microgels on the air/water interface is of paramount importance.

2-2. Experimental Details

2-2-1. Materials

N-isopropyl acrylamide (NIPAm, purity 98%), *N*,*N*'-methylenebis(acrylamide) (BIS, 97%), potassium peroxodisulfate (KPS, 95%), 2,2'-azobis(2-methylpropinamidine) dihydrochloride (V-50, 95%), rhodamine 6G (R6G), disodium hydrogenphosphate (99%), citric acid (98%), hydrochloric acid (HCl), hydroxide solution (NaOH), and sodium chloride (NaCl, 99.5%) were purchased from FUJIFILM Wako Pure Chemical Corporation (Japan) and used as received. Acrylic acid (AAc, 99%) was purchased from Sigma Aldrich and used as received. The monomer (4-vinyl-4'-methyl-2,2'-bipyridine)bis(2,2'bipyridine)ruthenium(II)bis (hexafluorophosphate) ($Ru(bpy)_3$) was synthesized according to a previously reported procedure.[43] Water for all reactions, including the preparation of solutions and the purification of polymers, was initially distilled and subsequently subjected to ion exchange (EYELA, SA-2100E1). Glass substrates (Neo Micro Cover Glass, Matsunami Glass Ind., Ltd.) were used after cleaning using 1) detergent in water, and 2) pure water.

2-2-2. Preparation of Charged Microgels

Negatively charged microgels were prepared by aqueous free radical precipitation copolymerization of NIPAm and AAc.[11] The copolymerizations were performed in a three-necked round-bottom flask equipped with a mechanical stirrer, a condenser, and a nitrogen gas inlet. The initial total concentration of each monomer for the microgels was 150 mM. Initially, the monomer solutions were prepared and dissolved in water in the three-necked round-bottom flask and heated to 70 °C under a stream of nitrogen and constant stirring (250 rpm). The solutions were allowed to stabilize for at least 30 min prior to initiating the polymerization in order to remove any dissolved oxygen. Subsequently, the free-radical polymerizations were initiated with KPS (2 mM) dissolved in water. The solutions were stirred for 4 h, and after completion of the polymerization, the obtained dispersions were cooled to room temperature. The microgels were purified via two cycles of centrifugation/redispersion in water using a relative centrifugal force (RCF) of 70000 G for ~90 min (Avanti J-26S XP, Beckman Coulter Inc.), followed by dialysis using cellulose tubing (36/32, Viskase Companies, Inc.) in water for around 1 week, whereby the water was changed daily. Henceforth, the obtained p(NIPAm-*co*-AAc) microgels will be denoted as NA*X*, whereby *X* represents the amount of charged AAc monomer (mol%). The pNIPAm microgels (henceforth

denoted as N) were prepared by temperature-programmed precipitation polymerization to increase their size, which is necessary for evaluating the individual microgels with an optical microscope.[38] After initiation of the polymerization, the temperature of the reaction solution was gradually increased from 45 to 70 °C (1 °C/3 min). The solution was stirred for 6 h, and the obtained dispersion was cooled to room temperature. The microgels were purified via two cycles of centrifugation/redispersion in water using an RCF of 70000 G for ~45 min (Avanti J-26S XP, Beckman Coulter Inc.), followed by dialysis using cellulose tubing in water for 3 days, whereby the water was changed daily.

2-2-3. Preparation of Charged Core/Shell Microgels

To check the potential influence of the pNIPAm shell that contains the charged core on the self-organization, core/shell microgels (henceforth referred to as CS) were prepared by seeded precipitation polymerization in the presence of charged microgels.[44] The polymerization was performed in a three-necked round-bottom flask (50 mL) equipped with a mechanical stirrer, a condenser, and a nitrogen gas inlet. Initially, the flask was charged with water (18.23 g), which was heated to 70 °C under a stream of nitrogen and constant stirring (250 rpm). The water was allowed to stabilize for 30 min prior to initiating the polymerization in order to remove any dissolved oxygen. Subsequently, seed microgels (NA5, 2.08 wt%, 5.77 g) and KPS (0.016 g) dissolved in water (1 mL) were added into the system to start the polymerization. After 5 min, the core NA5 microgels had shrank sufficiently, and a mixture of NIPAm monomer (99 mol%, 0.6720 g) and cross-linker BIS (1 mol%, 0.0096 g) dissolved in water (5 mL), which had been heated to 70 °C under a stream of nitrogen, was added to the reaction mixture. The solution was stirred for 4 h, and after completion of the polymerization, the obtained dispersions were cooled to room temperature. The microgels were purified via several cycles of centrifugation/redispersion in water to remove unreacted reagents and other impurities using an RCF of 70000 G for ~30 min (Avanti J-26S XP, Beckman Coulter Inc.).

2-2-4. Preparation of Micron-sized, Fluorescent, and Charged Microgels

To investigate the deformation of individual microgels upon adsorption at the air/water interface, micron-sized, fluorescent, and charged poly(NIPAm-*co*-Ru(bpy)$_3$) microgels (NRu microgels) were prepared via a modified aqueous precipitation polymerization technique that the

author has previously reported.[42] The polymerization was performed in a three-necked round-bottom flask (300 mL) equipped with a mechanical stirrer, a condenser, and a nitrogen gas inlet. Initially, the NIPAm monomer (0.6 g) and cross-linker BIS (0.0008 g) were dissolved in deionized water (55 mL). The monomer solution was heated to 40 °C under a stream of nitrogen and constant stirring (250 rpm). After sparging with nitrogen for a period of at least 30 min, the free-radical polymerization was initiated with V-50 (0.055 g) dissolved in water (1 mL). Immediately after the initiation, the temperature was gradually increased from 40 °C to 60 °C (1 °C/3 min). Thereafter, a mixture of NIPAm (1.0 g), $Ru(bpy)_3$ comonomer (0.135 g), cross-linker BIS (0.053 g), and NaCl (0.1753 g, 30 mM) dissolved in deionized water (100 mL) was added to the reaction mixture at a feeding rate of 0.8 mL/min using a syringe pump. After adding 90 mL of the mixture, the reaction was stirred for 2 h at 60 °C. Finally, the obtained microgel dispersion was cooled to stop the polymerization. The microgels were purified twice by centrifugation/redispersion in water to remove unreacted reagents and other impurities, followed by dialysis in water for around 1 week. It should be noted here that the obtained NRu microgels showed absorption peaks at 288 and 457 nm, and a fluorescence emission peak at 602 nm upon photoirradiation at 457 nm (**Figure 2-1**).

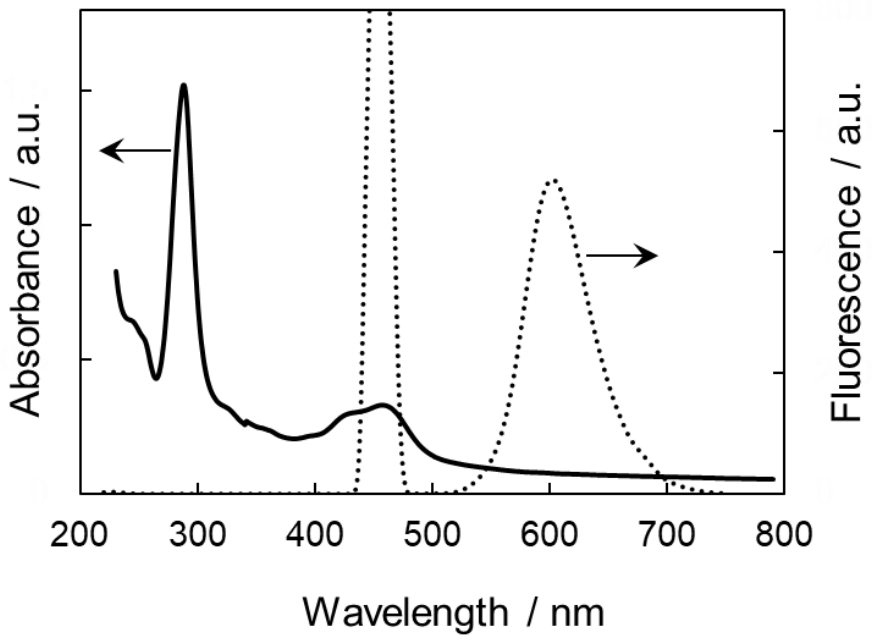

Figure 2-1. Absorption (solid line) and emission (dotted line) spectra of the NRu microgels in aqueous solution at 25 °C. The fluorescence emission peak at ~457 nm was detected due to measuring upon photoirradiation at 457 nm.

2-2-5. Characterization of the Microgels

The microgels were examined with an optical microscope (BX51, Olympus) equipped with a digital camera (ImageX Earth Type S-2.0 M Ver.3.0.5, Kikuchi-Optical Co., Ltd.). All microgel diameters were determined by measuring the center-to-center distance between neighboring microgels in order to calculate relatively accurate microgel diameters under low-contrast conditions. For the calculations, the author used the ImageJ software (1.49v, Wayne Rasband, National Institutes of Health) ($N = 50$) on optical microscopy images of colloidal crystals formed in glass capillaries. Colloidal crystals were prepared by transferring microgel dispersions into rectangular Vitrotube borosilicate capillaries (0.1 × 2.0 mm) using the capillary force. The microgels concentration was tuned to the critical concentration, C^* (g/mL), where the apparent volume fraction (Φ_{eff}, $\Phi_{eff} = [\eta]C/2.5$) equals 1.[42,45] Here, Φ_{eff} was calculated from the intrinsic viscosity, while $[\eta]$ (mL/g) was measured at 25 °C using an Ubbelohde viscometer. It should be noted that Φ_{eff} is used as a simple measure for the degree of packing, even though Φ_{eff} deviates from the real volume fraction in the concentrated regime where the microgels can deform, deswell and/or interpenetrate.[45]

The amount of acrylic acid introduced in the microgels was determined by conductometric titrations. The microgel dispersions were adjusted to pH ≈ 11 with a 1 M NaOH solution. The titrations were performed using standardized HCl solutions (0.1 or 0.01 M).

The electrophoretic mobility (EPM) of the microgels was evaluated using a Zetasizer Nano ZS instrument (Malvern Panalytical). The average EPM was calculated from three individual measurements. These measurements were conducted at a microgel concentration of 0.001 wt% at 25 °C in pure water. For the NA5 and NRu microgels, the EPM measurements were conducted at a microgel concentration of 0.001 wt% at 25 °C in a 1 mM NaCl solution in order to investigate the effect of the presence of NaCl.

The surface tension of the microgel dispersions was determined using the Wilhelmy plate method with a surface tensiometer (Automatic Surface Tensiometer Model CBVP-Z, Kyowa Interface Science Co., Ltd.) and a Pt plate at 25 °C, 24 h after placing each solution or dispersion (5 mL) in a glass dish. Average surface tension values were calculated from three individual measurements.

The amount of $Ru(bpy)_3$ monomer introduced in the microgels was estimated using UV−vis spectrophotometry measurements (V-630iRM, JASCO) at an absorbance of 458 nm, which is the wavelength of the maximum absorbance for $[Ru(bpy)_3]^{2+}$.

The absorption and emission spectra of NRu microgels were evaluated at 25 °C in pure water using a UV−vis spectrophotometer (V-630iRM, JASCO) and fluorescence spectrophotometer (FP-6300, JASCO), respectively.

2-2-6. Characterization of the Drying Phenomena

As a macroscopic evaluation, the shape of the sessile droplets during drying and the resulting dried structures were evaluated with a digital camera (Canon, EOS kiss ×4). The dispersions (30 μL) were dried on glass substrates (Neo Micro Cover Glass, Matsunami Glass Ind., Ltd.) at 25 ± 2 °C (**Figure 2-3(a)**). These substrates were used after cleaning with 1) detergent in water, and 2) pure water. The homogeneity of the distribution of the microgels in the films was compared by evaluating the grayscale, which was calculated using the "plot profile (ImageJ software)" of a straight line drawn on the observed optical microscopy images at the center of each film. In the optical microscopy observations, the images are darkened in the presence of packed microgels.

As a microscopic evaluation, the air/water interface at the center and the edge of the sessile droplet (1 μL) was observed at 25 ± 2 °C with an optical microscope (BX51, Olympus) equipped with a digital camera (ImageX Earth Type S-2.0 M Ver.3.0.5, Kikuchi-Optical Co., Ltd.). The number of microgels adsorbed at the air/water interface was calculated based on the optical microscopy movies. The pH value of the dispersions was controlled using McIlvaine buffers composed of 50 mM disodium hydrogenphosphate and 25 mM citric acid, or using simple electrolytes such as HCl, NaOH, and NaCl. Here, the concentration of the microgel dispersions was calculated based on the weight of the microgels after drying. The concentrations of dispersions were decreased or increased by diluting (with water) or centrifuging the dispersions, respectively.

2-2-7. Evaluation of the Mean-squared Displacements

To quantify the motion of microgels at the air/water interface, the microgel positions in an image time series recorded by optical microscopy were analyzed using the mean-squared displacement (MSD) as a function of the lag time (τ).[46,47] The particle-tracking data were obtained

by tracking the position of the microgels in a movie of ~ 6 s (30 frame s^{-1}) using the 'Pointing Cell Tracking' tool of the ImageJ software. The MSD of microgels adsorbed at the interface is given by:

$$\mathrm{MSD}(\tau) = \langle \left(r_i(t+\tau) - r_i(t) \right)^2 \rangle_{i,t} \quad (2\text{-}1)$$

where $r_i(t)$ is the position vector of *i*th particle at time *t*, and $\langle \quad \rangle_{i,t}$ indicates the average over the data of the microgels. In the liquid regime, where the particle motion is expected to be purely diffusive, the MSD should be proportional to the lag time, τ:

$$\mathrm{MSD}(\tau) = 2dD\tau \quad (2\text{-}2)$$

where *d* is the dimensionality of the displacement vectors and *D* is the self-diffusion coefficient. The movie of the microgels adsorbed at the air/water interface only provides their movement in two dimensions and therefore $d = 2$ for the obtained optical microscopy movies.[47]

2-2-8. Deformation Analysis of Individual Charged Microgels

The deformation of microgels at the air/water interface of droplets was observed with an optical microscope (BX53, Olympus) equipped with a fluorescence system (ramp: U-RFL-T, wavelength: 451-485 nm and 541-565 nm) and a high-speed camera (monochrome AX50 2SA, Photron). It should be noted here that the deformation was observed for only a few minutes after the dispersion droplet was deposited onto the glass substrate in order to ignore the influence of the increasing salt concentration as a result of the drying of the water.

2-3. Results and Discussion

2-3-1. Synthesis and Characterization of the Polyelectrolyte Microgels

Firstly, charged (or polyelectrolyte) microgels were synthesized by a conventional free radical precipitation polymerization with NIPAm and AAc, where the feed ratio of AAc was changed (NA*X* microgels, $1 \leq X \leq 50$ mol%). The size of all (~1 μm) was uniform, which was confirmed by optical microscopy images for a concentration of *C** for these microgels (**Table 2-1, Figure 2-2(a)~(f)**). The number of carboxyl groups incorporated in the microgels increased with increasing the proportion of the AAc fed during the polymerization (**Table 2-1**), and thus, the EPM, which is an indicator of the surface-charge density, showed negative values for all NA microgels. It has been reported that relatively uniform charge distribution in microgels is realized for poly(NIPAm-*co*-AAc) microgels prepared by precipitation polymerization, as the reactivity ratios

of NIPAm and AAc are similar (r_1 = 0.57 and r_2 = 0.32).[48-50] Thus, the author assumed that the amount of carboxyl groups would increase both on the surface and within the microgels. Indeed, the EPM values gradually decreased upon increasing the incorporated amount of AAc (**Table 2-1**), indicating that the surface-charge density originates from the carboxyl group increased. Additionally, the intrinsic viscosity [η], which is an indicator of the degree of swelling, increased with the amount of incorporated AAc (**Table 2-1**), indicating that the amount of carboxyl groups increased within the microgels and on the surface.

Next, core/shell structures were formed by adding AAc-free pNIPAm hydrogel shell onto NA5 microgels by seeded precipitation polymerization in order to investigate the effect of the charge distribution of the microgels on the drying behavior (**Figure 2-2(g)**).[44,51] After forming the shell, the amount of carboxyl groups in the microgels decreased to approximately 50% (core NA5 microgels: 0.42 mmol/g; CS microgels: 0.24 mmol/g), indicating that a shell of similar weight was formed on the core microgel (NA5). In addition, the EPM value of the CS microgels approached to that of AAc-free N microgels (EPM: -1.26×10^{-8} m^2/Vs (N microgels), -2.08×10^{-8} m^2/Vs (core NA5 microgels), and -1.24×10^{-8} m^2/Vs (CS microgels)), suggesting that the core was completely covered with the shell. In addition, the [η] value of the CS microgels was considerably lower than that of the core NA5 microgels, indicating that the shell restricts the swelling of the core, which has already been reported.[51]

Table 2-1. Chemical composition and characteristics of the negatively charged microgels

Code	NIPAm (mol%)	BIS (mol%)	AAc (mol%)	Diameter (nm)	-COOH content (mmol/g)	EPM (10^{-8} m^2/Vs)	[η] (mL/g)
[a]N	99	1	-	939 ± 68	N.D.	-1.26 ± 0.07	59.7
NA1	98	1	1	745 ± 75	0.11	-1.90 ± 0.03	79.7
NA5	94	1	5	1167 ± 50	0.42	-2.08 ± 0.18	166
NA10	89	1	10	1178 ± 104	1.18	-2.24 ± 0.03	163
NA20	79	1	20	1251 ± 61	2.22	-2.81 ± 0.06	322
NA50	49	1	50	1549 ± 108	5.18	-2.84 ± 0.14	482
[b]CS	99	1	-	1082 ± 73	0.24	-1.24 ± 0.05	41.0

[a]Reproduced with permission from reference 38. Copyright (2018) American Chemical Society.
[b]Core/shell (CS) microgels were prepared by seeded precipitation polymerization using NA5 microgels as seeds.

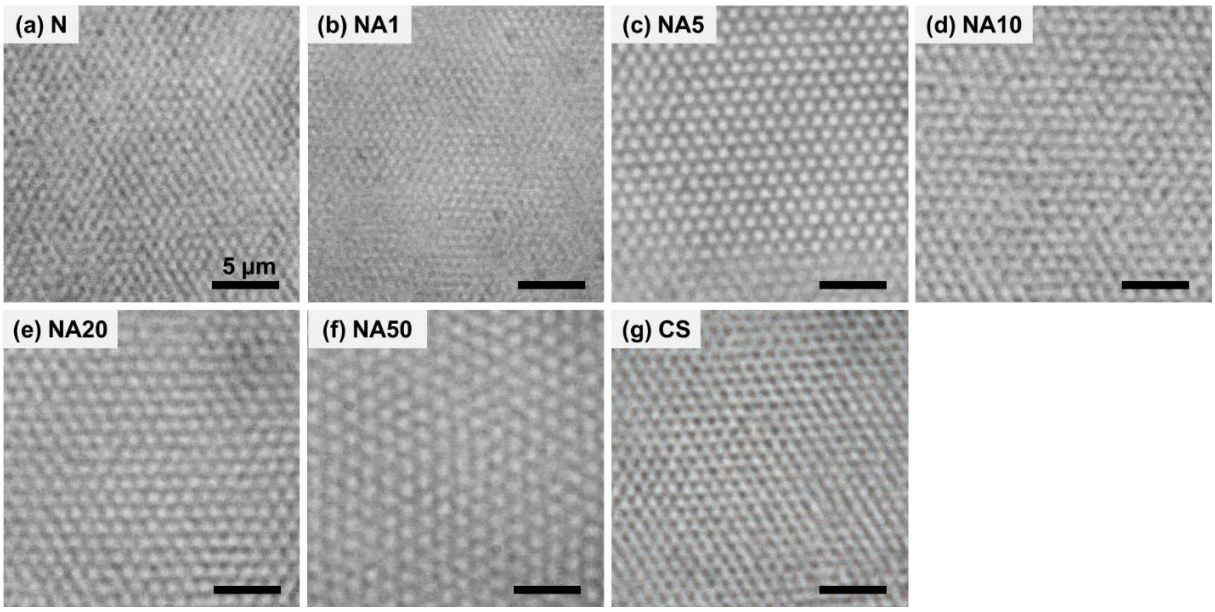

Figure 2-2. Optical microscopy images of colloidal crystals of (a)~(f) NAX ($1 \leq X \leq 50$) and (g) CS microgels at the critical concentration, C^*. From these images, the diameters of the microgels were calculated, and these are listed in **Table 2-1**.

2-3-2. Macroscopic Evaluation of Drying Microgel Sessile Droplets

As schematically illustrated in **Figure 2-3(a)** and reported in the previous study,[36,38] the self-organization of microgels was investigated at very low (~0.001 wt%) microgel concentrations, where soft and surface-active microgels are regularly arranged at the air/water interface, and the resulting films on the solid substrate exhibit iridescent structural colors. Therefore, in this study, the author initially checked the dependence of the microgel concentration on the drying phenomenon. **Figure 2-3(b)** shows the result for N microgels (without AAc groups), i.e., the same ones used in the previous study.[38] Similar to the previous study, homogeneous monolayer films with iridescent structural colors were obtained at low microgel concentrations (0.001, 0.005 wt%). Upon increasing the concentration, a white dot appeared near the center of the dried films (≥ 0.01 wt%). As shown in **Figure 2-3(c)**, the microgels were more concentrated in the white dot (region I) than in region II (microgel size: 353 ± 91 nm (region I); 598 ± 71 nm (region II); N = 50). The white dot was formed at that position, where water was present up to complete evaporation of the droplet (**Figure 2-4(b)**) due to the transportation of excess microgels present in the bulk solution to this position by the convention flow. Furthermore, ring-like stains were observed for higher microgel concentrations (≥ 0.1 wt%, **Figure 2-3(b)(d)**). These data indicate that excess microgels,

i.e., N microgels dispersed within the droplets, are moved to the edge of the droplet by convection flow to form ring-like stains (**Figure 2-3(b)(d)**, **Figure 2-4(c)**) or concentrated near the center of the droplet (**Figure 2-3(c)**, **Figure 2-4(b)**), although these phenomena were not observed for lower microgel concentrations.

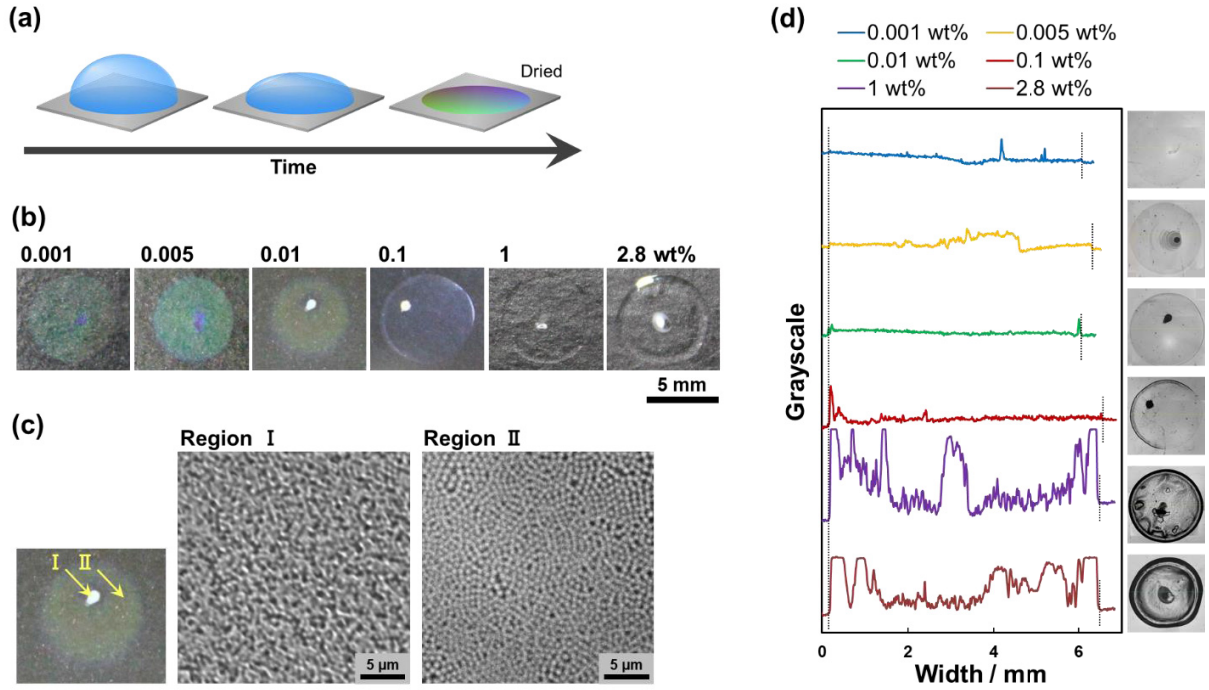

Figure 2-3. (a) Schematic illustration of the drying phenomenon of microgel sessile droplets. (b) Photographs of dried thin films containing N microgels formed after 30 μL of microgel droplets were dried at room temperature (~25 °C, ~70 % humidity) on glass substrates at different microgel concentrations. (c) Optical microscopy images of the thin films dried at 0.01 wt%. Two of the images show an enlarged view of region I and II. (d) Plot profile of each thin film dried at different concentrations. The dotted black line shows the boundary between the film and the substrate.

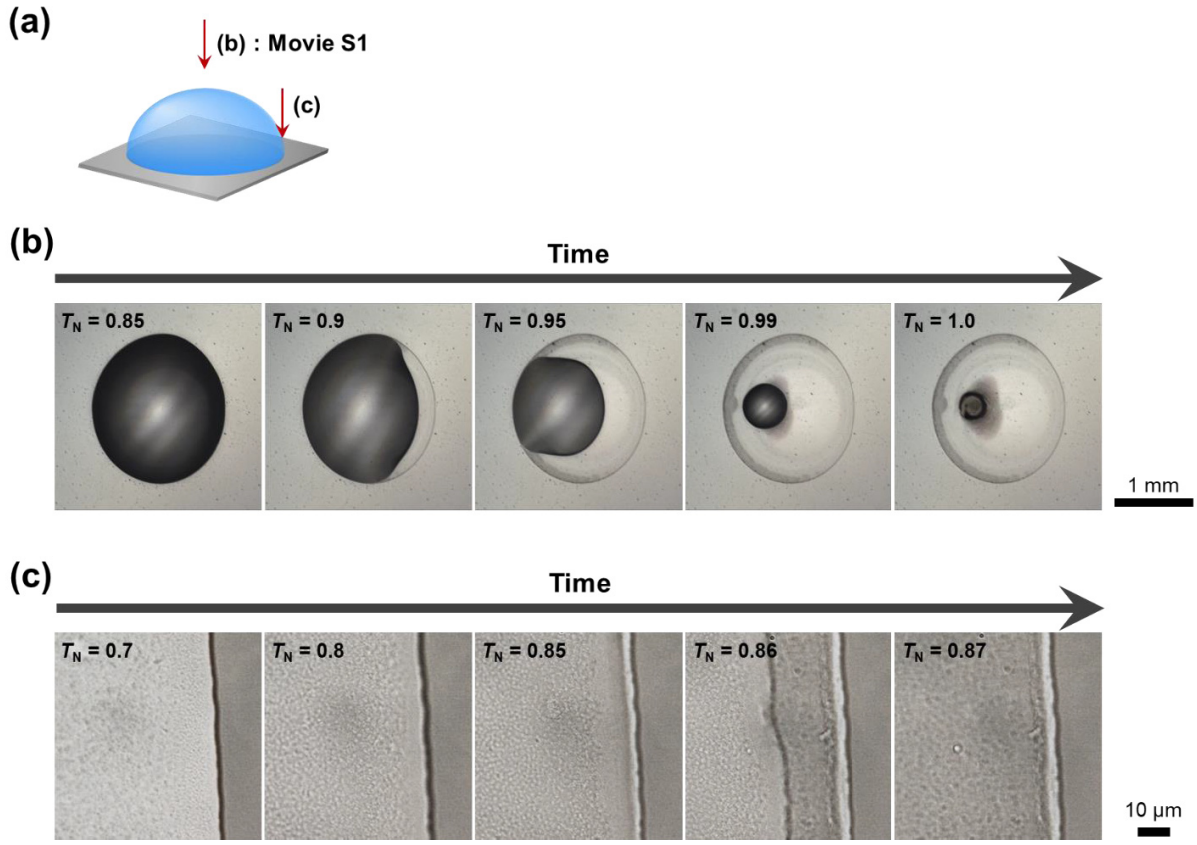

Figure 2-4. (a) Schematic illustration of the observation of sessile droplets by optical microscopy. (b), (c) Optical microscopy images of the sessile droplets containing N microgel dispersions (1 μL) as a function of the normalized time, T_N. The droplets (0.1 wt%) were dried at room temperature (~25 °C, ~30 % humidity). (b: **Movie S1**) The entire and (c) the edge of the droplets on the glass substrate were observed. (b) The sessile droplets were observed by reflected-light optical microscopy.

In contrast, homogeneous monolayer films showing iridescent colors could not be obtained for NA5 polyelectrolyte microgels, not even at low concentrations (0.001 wt% and 0.005 wt% in **Figure 2-5(a)**). The appearance of white dots (**Figure 2-5(b)**) and ring-like stains (**Figure 2-5(c)**), was, as mentioned above, dependent of the concentration, albeit in a slightly different manner. It should be noted here that the homogeneous monolayer films could not be obtained for any of the negatively charged NAX microgels ($1 \leq X \leq 20$ mol%) at low concentrations (**Figure 2-6(a)~(c)**). In the case of the NA50 microgels, the resulting films could not be visualized and the boundary between films and the glass substrate could not be recognized as the NA50 microgels were highly swollen by water. However, homogeneous thin films showing iridescent colors could

be obtained in the case of CS microgels, which contain a pNIPAm shell layer on a NA5 core, dried at low concentrations (0.001 wt% in **Figure 2-6(d)**). These results suggest that charged groups attached near the surface of the microgels affect the individual microgel motion within the sessile droplets.

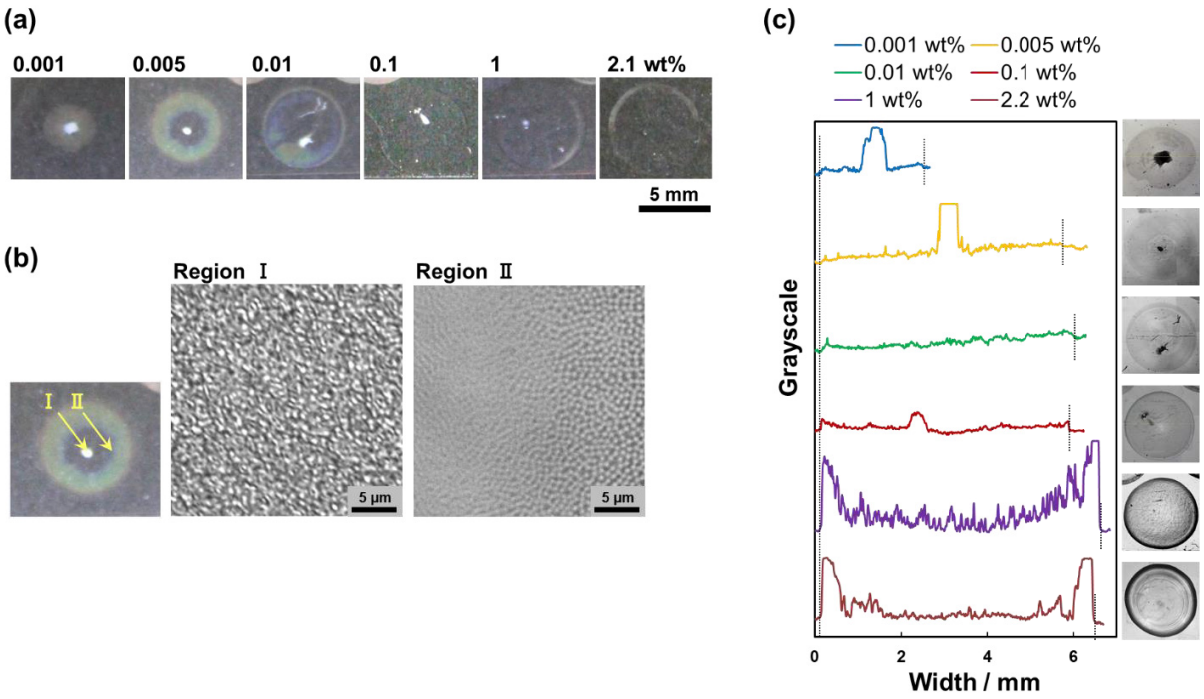

Figure 2-5. (a) Photographs of dried thin films containing NA5 microgels. 30 μL of droplets were dried at room temperature (~25 °C, ~70 % humidity) on glass substrates at different NA5 microgel concentrations. (b) Optical microscopy images of a thin film dried at 0.005 wt%. Two of the images show an enlarged view of region I and II. (c) Plot profile of each thin film dried at different concentrations. The dotted black line shows the boundary between the film and the substrate.

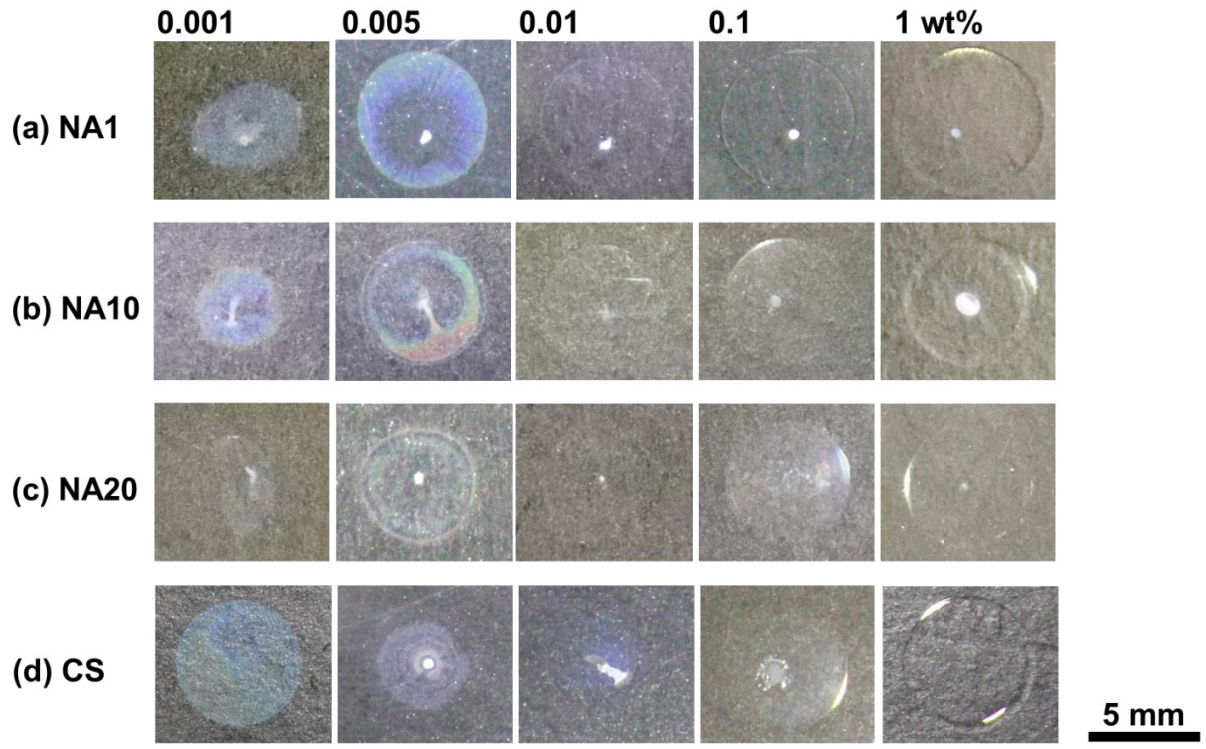

Figure 2-6. Photographs of the dried thin films containing (a) NA1, (b) NA10, (c) NA20, and (d) CS microgels formed after the microgel droplets (30 μL) were dried at room temperature (~25 °C, ~40 % humidity) on glass substrates at different microgel concentrations (0.001-1 wt%).

2-3-3. Evaluation of Individual Polyelectrolyte Microgel Movements at the Air/Water Interface.

Then, the author microscopically investigated the drying process of the sessile droplets. First, the center of the droplet was monitored by optical microscopy (**Figure 2-7(a)**). At the early stage (T_N~0.05; the normalized time, $T_N = T/ T_{dried}$, where T and T_{dried} denote the arbitrary time and the time for complete drying, respectively.), as reported in the previous work,[38] control N microgels were immediately adsorbed and arranged with intervals at the air/water interface after dropping a dispersion (1 μL) on a glass substrate (**Figure 2-7(b)**). Then, the adsorbed amount, N (or normalized amount, $N_N = N/ N_{dried}$, where N_{dried} denotes the adsorbed amount per unit of interfacial area when the droplet is completely dry.) at the interface increased until completely drying, as the adsorbed and highly deformed microgels at the interface were increasingly compressed given that the total surface area of the sessile droplets decreased due to evaporation of water (**Figure 2-7(c)(d)**).[38,42] Finally, the ordered structures formed at the interface were transferred onto the

substrate without any structural disruption (**Figure 2-7(b): N**).[38] In the case of the NA5 microgels, on the other hand, the microgels did not adsorb on the air/water interface at the early stage of drying (**Figure 2-7(b): NA5**, T_N~0.05). However, as time proceeded (T_N~0.25), the microgels gradually adsorbed on and arranged at the interface (**Figure 2-7(b)(c)(d)**). Here, in contrast to the N microgels, there was no interval between the NA5 microgels (e.g., the images taken at T_N~0.70, 0.80, 0.95). In the N microgel case, there are low density polymers on the shell of the deformed microgels in the interval between the microgels,[42] which might be due to the suppression of the deformation of charged microgels at the air/water interface. It should be noted here that similar results were reported when charged microgels are observed at the oil/water interface.[13,52] Additionally, NA5 microgels are thermally fluctuated at the interface (*vide infra*). Furthermore, different from N microgels, the arranged structures of the NA5 microgels formed at the interface were not transferred without disrupting the structures when the water was completely evaporated (**Figure 2-7(b): NA5**, T_N~1). Similar behavior to that of the NA5 microgels was observed in the case of the NA1, NA10, and NA20 microgels (**Figure 2-7(c)(d)**), indicating that the charged groups immobilized in the microgels lower the adsorption rate of the microgels at the air/water interface, and affect each characteristic process of the drying behavior of the microgel dispersions.

To clarify the reason why the thin films of charged microgels are inhomogeneous, the drying behavior of the edge of the sessile droplets containing microgels was monitored (**Figure 2-8**). In the case of the control N microgels, no microgels were seen due to a large curvature at the early stage (**Figure 2-8(a):** T_N~0.1, 0.2). As time proceeded (T_N~0.5), the microgels adsorbed at the air/water interface both at the center and at the edge of the same sessile droplet, suggesting that N microgels regularly pack over the whole area of the air/water interface. Upon drying, the arranged structure of the N microgels gradually transferred from the edge without disruption (**Figure 2-8(a):** T_N~0.6, 0.7). On the other hand, NA5 microgels gradually adsorbed to the interface at the edge and at the center of the sessile droplet (**Figure 2-8(b)**). While NA5 microgels continued to adsorb at the interface at the edge, the adsorbed NA5 microgels were carried from the edge to the center on the interface of the droplet by convection flow, even upon drying (**Figure 2-8(b):** e.g., T_N~0.5, 0.7, 0.8). Due to this drying behavior, NA5 microgels were uniformly arranged at the edge of the thin film on the substrate after drying. Getting closer to the center of the droplet, the impact of the convection flow on the microgel arrangement lowered, and the adsorbed NA5 microgels were disordered when they were transferred onto the glass substrate (**Figure 2-8(c)**).

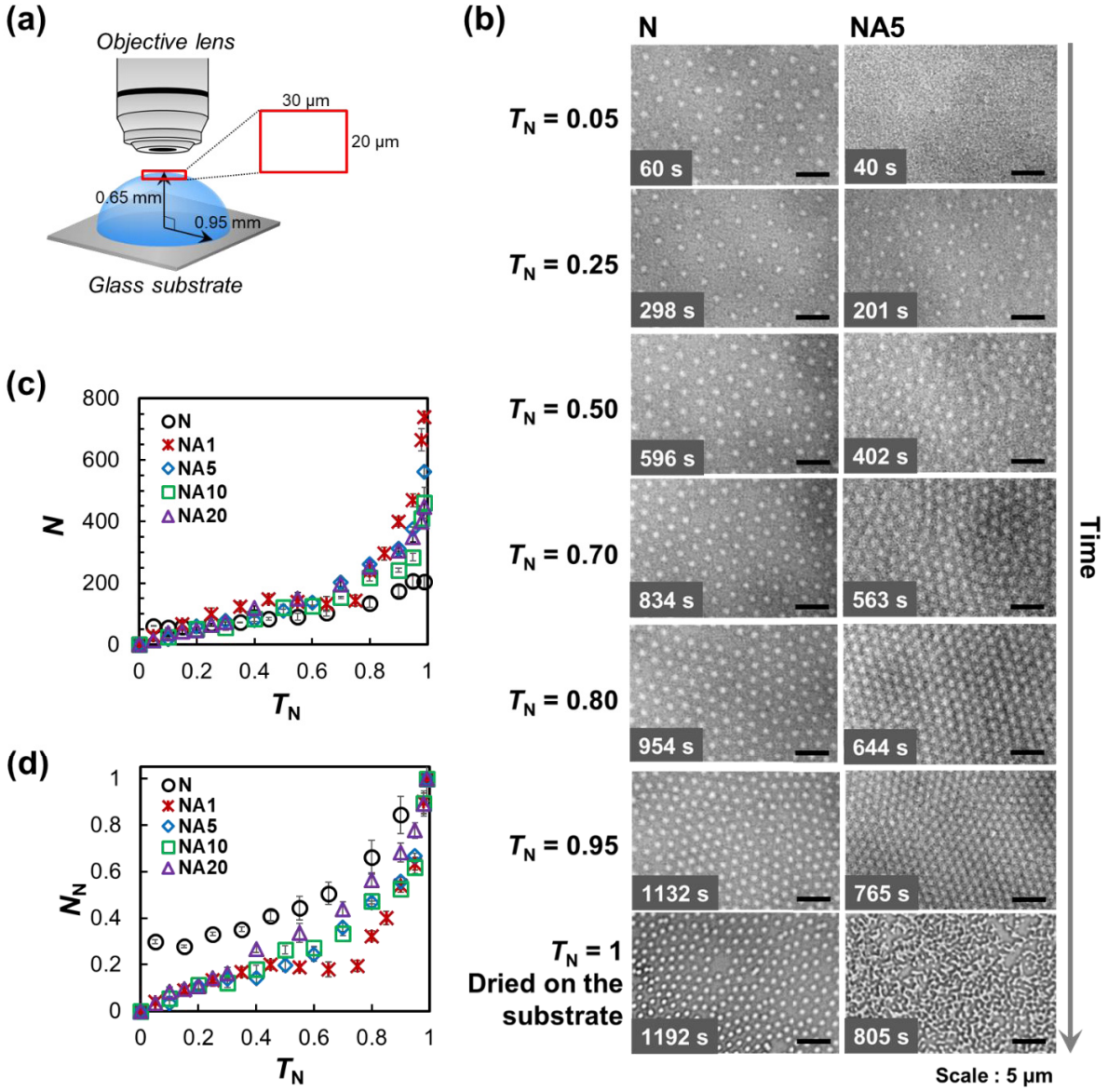

Figure 2-7. (a) Schematic illustration of the microscopic observation of the sessile droplets. The air/water interface at the center of the droplets was observed with an optical microscope. (b) Optical microscopy images of N and NA5 microgels at the air/water interface of each droplet on glass substrates as a function of the normalized time, T_N. It should be noted here that the NA50 microgels could not be observed due to their low contrast. (c) Adsorbed amount, N, and (d) normalized adsorbed amount, N_N, for each microgel as a function of T_N. The droplets were dried at room temperature (~25 °C, ~40 % humidity) at concentrations of 0.003 wt% (N) or 0.005 wt% (NA1, NA5, NA10, and NA20).

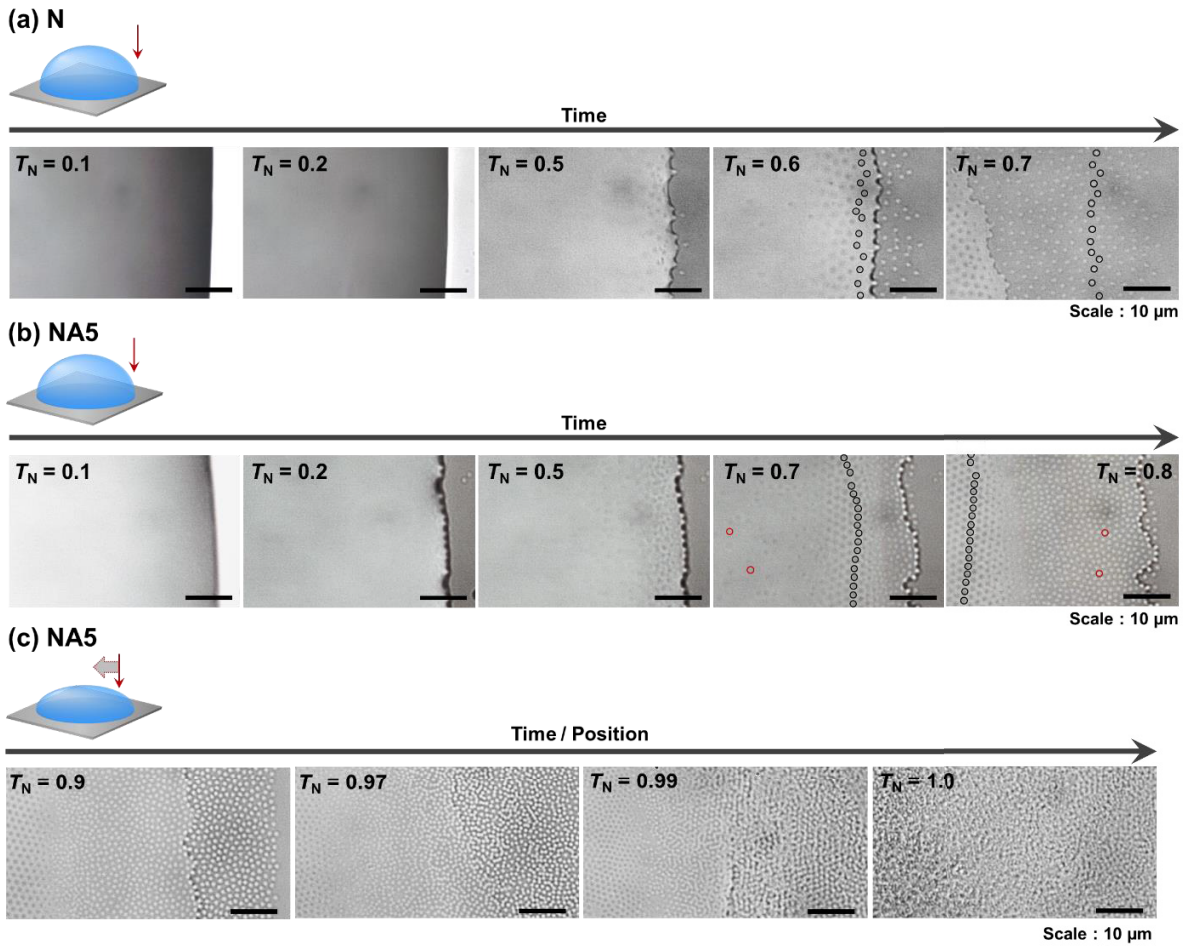

Figure 2-8. The drying process of dispersions including N or NA5 microgels was observed (a: N) (b: NA5) at the edge without moving the observation position and (c: NA5) from the edge to the center with moving the observation position of the droplet during the evaporation. The droplet of the 1 μL NA5 microgel dispersion was dried at room temperature (~25 °C, ~30 % humidity) at 0.005 wt% on the glass substrate. Marked microgels indicate the position of the particles before and after the passage of time.

As has been described above, the microgels fluctuate at the air/water interface. Therefore, the author subsequently examined the dynamic motion of the N microgels and polyelectrolyte microgels at the interface. The trajectory of the microgels was tracked as shown in **Figure 2-9** and **Figure 2-10**, which indicates that from the early stage of drying, individual N microgels are hardly moving at the interface (**Figure 2-9(a)**). On the other hand, individual NA5 microgels are moving considerably in two dimensions (**Figure 2-9(b)**), even though they are adsorbed at the air/water

interface. These movements were quantitatively evaluated, and the results are shown as MSD plots (**Figure 2-9**) using **eq.2-1**. For the N microgels, the slope of the MSD plots and the self-diffusion values calculated from **eq.2-2** were close to 0 for each T_N (**Figure 2-9(a)**, **Table 2-2**), indicating that the microgel movements are highly restricted at the air/water interface, even at the early stage of the drying process (T_N~0.25). On the other hand, the diffusivity of the NA5 microgels was significantly higher than that of the N microgels (**Figure 2-9(b)**, **Table 2-2**), and their self-diffusion coefficients were much larger than those of N microgels at T_N~0.25 (**Table 2-2**). As time proceeded, the self-diffusion coefficient values of the NA5 microgels gradually decreased with increasing packing density of the microgels at the air/water interface (**Table 2-2**). It should be noted here that at T_N~0.85, each NA5 microgel moved in the same direction (**Figure 2-9(b)**: T_N~0.85), which is due to the microgels moving at the interface from the edge of the droplet during evaporation (**Figure 2-8(b)**). Although the value approximated 0 at T_N~0.85, the NA5 microgel movements were not completely restricted, which might be a reason why the arranged structures of the NA5 microgels were not transferred onto the substrate without disrupting during evaporation.

The fact that charged microgels at the air/water interface are relatively mobile is different to the behavior of the previous work on colloidal crystals packed charged microgels, where movement is highly restricted due to different osmotic pressure between the inside and the outside of the microgels.[53,54] The difference may be due to the repulsive interactions between charged microgels at the air/water interface. In the previous work,[38] the author confirmed that N microgels arranged at the air/water interface are highly deformed, and that neighboring microgels are highly interpenetrated. Therefore, the arranged structures of the N microgels can be transferred onto the solid substrate without disruption. Therefore, in addition to high crystallinity induced by osmotic pressure, it seems feasible to conclude that charged NA5 microgels adsorbed at the interface are not highly interpenetrated with each other most likely due to repulsive interactions between the NA microgels, or between the NA microgels and the air/water interface. It is worthwhile noting that the NA microgels (e.g., NA20 microgels: 39.6 mNJ/m at 1.0 wt%) and the N microgels can lower the surface tension, suggesting that it is difficult to evaluate the microscopic movements of microgels exclusively by surface-tension measurements.

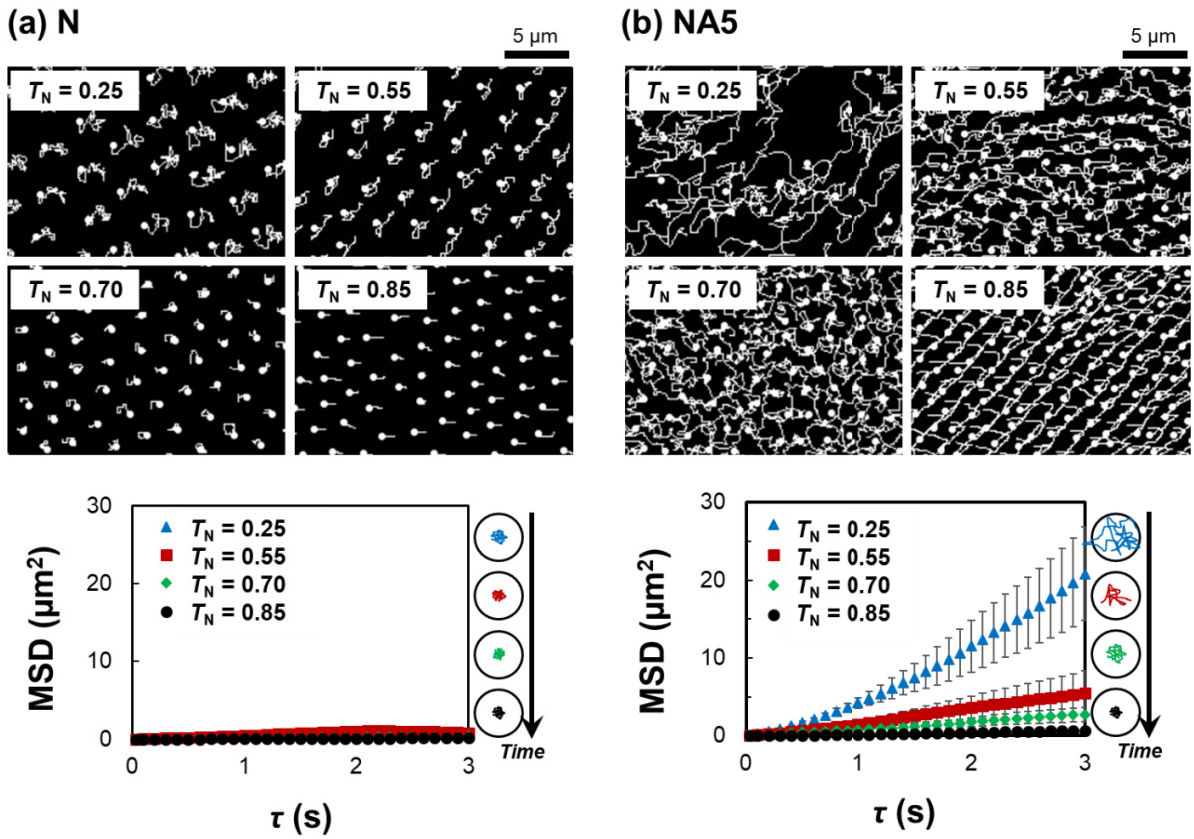

Figure 2-9. Particle-trajectory images and MSD plots of (a) N and (b) NA5 microgels adsorbed at the air/water interface of the sessile droplets at T_N = 0.25, 0.55, 0.70, and 0.85. The droplets were dried at room temperature (~25 °C, ~40 % humidity) at 0.003 wt% (N) and 0.005 wt% (NA5) on a glass substrate.

Table 2-2. For the N and NA5 microgels, self-diffusion coefficients were calculated from the MSD plots at T_N = 0.25, 0.55, 0.70, and 0.85.

Microgel	T_N	Slope (μm² s^{-1})	R^2	D (μm² s^{-1})
N	0.25	0.300	0.8793	0.0750
	0.55	0.415	0.8186	0.104
	0.70	0.112	0.9987	0.0279
	0.85	0.0535	0.9281	0.0134
NA5	0.25	6.03	0.9525	1.51
	0.55	1.78	0.9913	0.445
	0.70	0.887	0.9852	0.222
	0.85	0.213	0.9701	0.0532

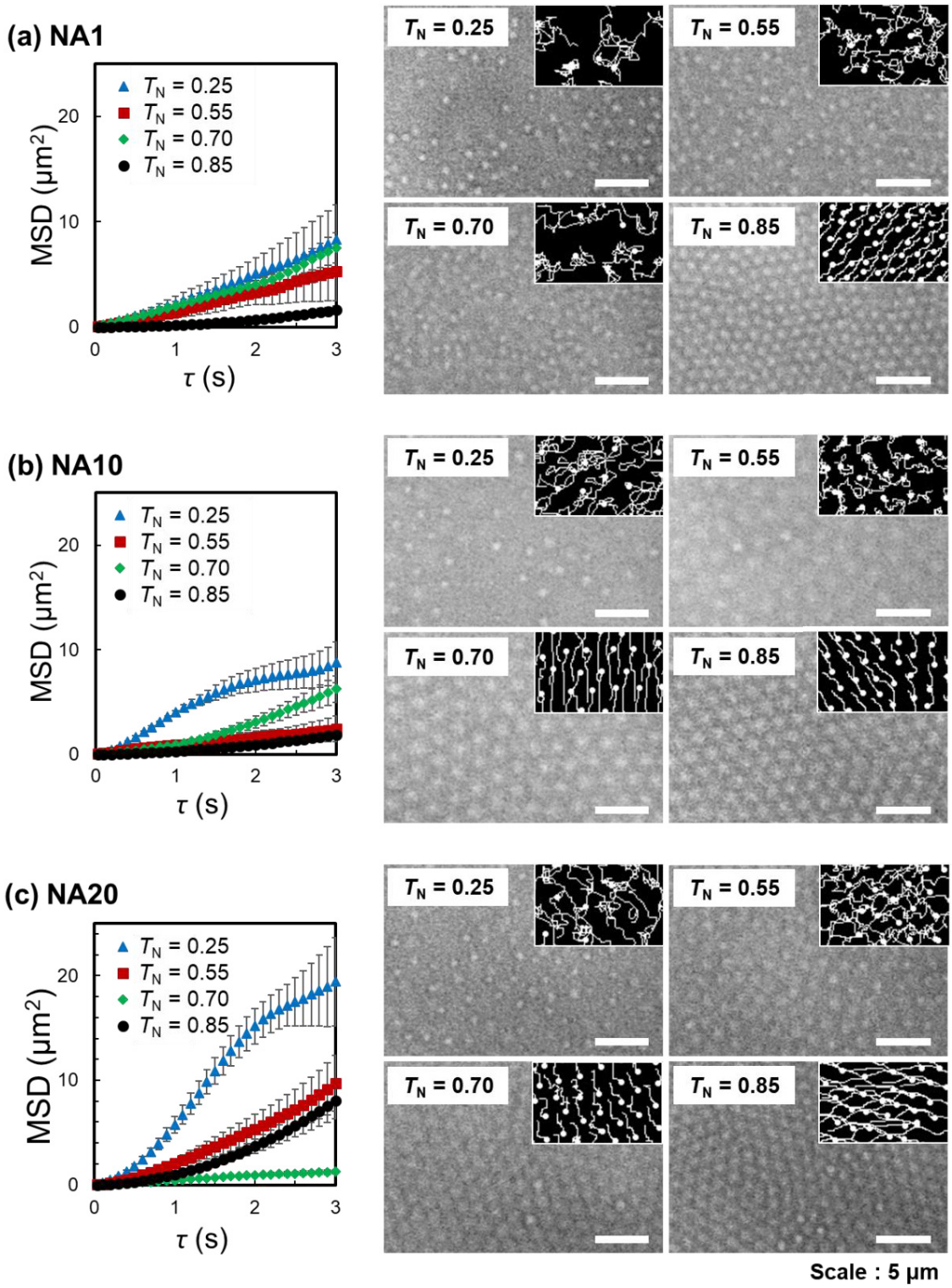

Figure 2-10. Particle-trajectory images and MSD plots of (a) NA1, (b) NA10, and (c) NA20 microgels adsorbed at the air/water interface of the sessile droplets at T_N = 0.25, 0.55, 0.70, and 0.85.

2-3-4. Effect of the pH value, the Ionic Strength, and the Charge Distribution in Microgels on the Polyelectrolyte Microgels at the Air/water Interface

The aforementioned results indicate an energy barrier when polyelectrolyte microgels approach the air/water interface. According to a previous report,[55] there are both attractive, i.e., van der Waals interactions, and repulsive interactions, i.e., an image-charge effect[56] and electric double layer interactions between colloidal particles and an interface. In this study, the author wanted to clarify the effect of charges immobilized on microgels on the interfacial phenomenon; therefore, the author initially observed NA5 microgels at the air/water interface at pH = 3 and pH = 7, where carboxyl groups in the NA microgels are protonated and deprotonated, respectively. However, the results obtained at pH = 3 and pH = 7 were, unexpectedly, almost identical (**Figure 2-11**). Even though, different from McIlvaine buffers, simple electrolyte was used for adjusting the pH values, the adsorption behavior was similar on the drying process of the microgels at pH ~ 3, pH ~ 7, and pH ~ 10 (**Figure 2-12**).

Thus, as another potential factor, the effect of the ionic strength in the sessile droplets on the static and dynamic adsorption behavior of the microgels at the air/water interface was investigated at the different concentrations of NaCl (**Figure 2-13, 2-14**). As expected, the adsorption numbers of the charge-screened NA5 microgels at the interface increased with increasing NaCl concentration (**Figure 2-13**). Moreover, the self-diffusion coefficient values calculated from the MSD plots of the charge-screened NA5 microgels also decreased with increasing NaCl concentration, and the value approached 0 when the droplet contained 1 mM NaCl at the initial state (**Figure 2-14, Table 2-3**), indicating that the individual mobility of the charge-screened microgels is restricted in the presence of NaCl (-2.08×10^{-8} m^2/Vs in pure water; -1.68×10^{-8} m^2/Vs in 1 mM NaCl). In this case, the electrostatic repulsive interactions both between the polyelectrolyte microgels, and between the microgels and the interface should decrease with increasing ionic strength as the electric double layer $(1/\kappa)$ of the particles is defined as $\kappa \propto \sqrt{n}$, where n is the salt concentration. Thus, the thickness of the electric double layer of the polyelectrolyte microgels decreases with increasing salt concentrations. In addition, the image-charge effect, which is also an electrostatic repulsive interaction, decreased in the presence of NaCl.[55] Hence, the presence of NaCl lowers not only the energy barrier between the microgels and the air/water interface, but also the repulsive interactions between the microgels adsorbed at the interface. These results confirm that a slight increase in ionic strength (~1 mM NaCl) affects the

interfacial behavior of polyelectrolyte NA5 microgels; therefore, the effect of pH value on the microgel adsorption behavior was not observed as the buffer solutions contain substantially higher concentrations of ions than those used in the NaCl tests.

Next, different from the conditions when NaCl was not added, the arranged structures of the charge-screened microgels at the air/water interface were transferred onto the substrates without significant disruptions after drying (**Figure 2-13(a)**; [NaCl] = 1 mM; T_N~1), suggesting that the adsorbed polyelectrolyte microgels at the interface are highly interpenetrated with each other due to weaker repulsive interactions between the microgels. Although the resulting microgel-monolayer film included salt as an additive, the salt could be easily removed by washing with pure water, which afforded a homogeneous monolayer film showing iridescent colors (**Figure 2-15)**. Furthermore, the negatively charged polyelectrolyte microgels could also be charge-screened in the presence of cationic dyes such as Rhodamine 6G (R6G), which interact electrostatically with charged carboxyl groups in the microgels.[57] After drying the dispersion of the polyelectrolyte microgels charge-screened with R6G, almost homogeneous monolayer films were obtained (**Figure 2-16**). These results indicate that charge-screened polyelectrolyte microgels show self-organization during drying of sessile droplets and create homogeneous monolayer films similar to the control N microgels as previously reported by the group of Suzuki.[38]

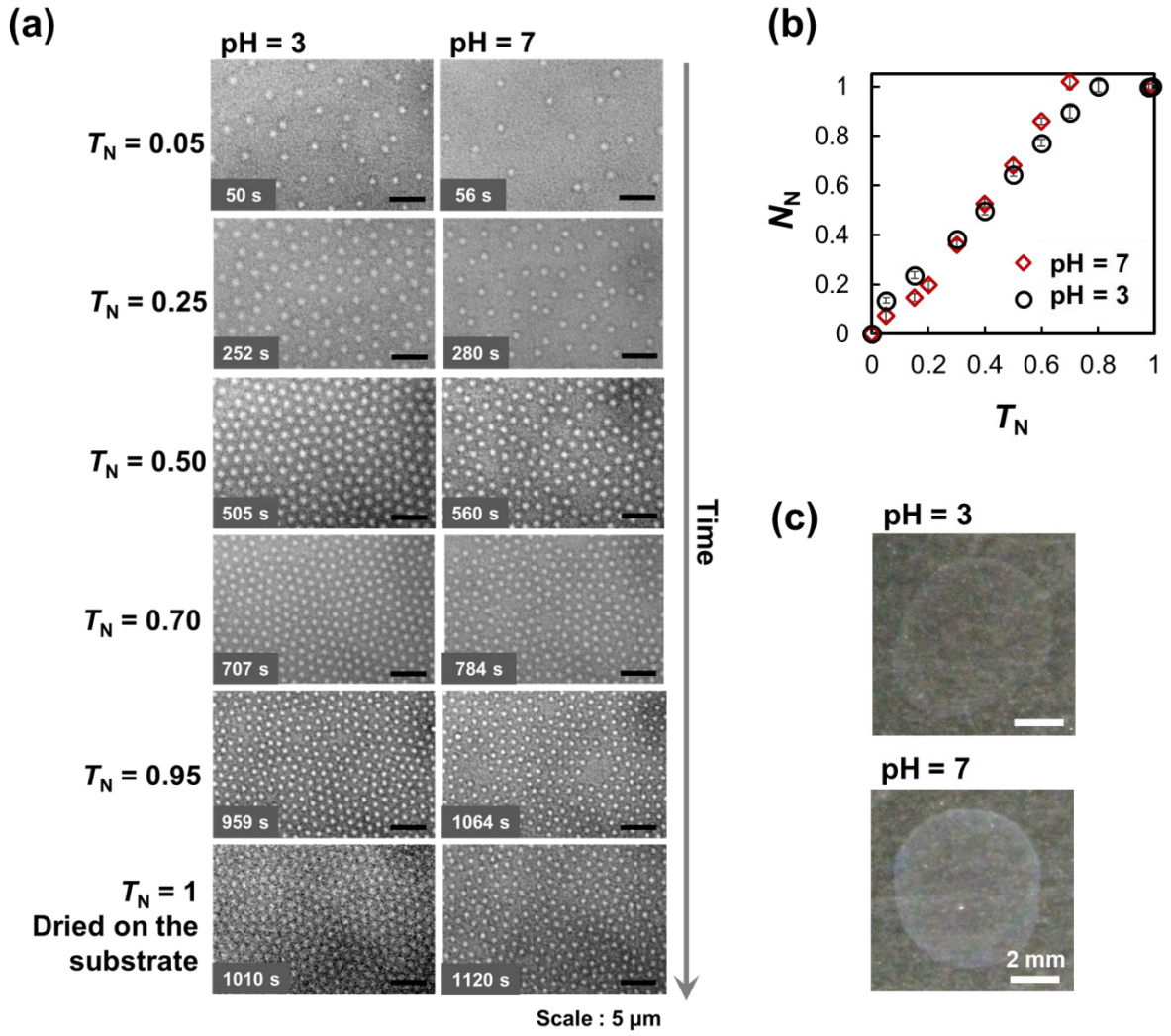

Figure 2-11. (a) Optical microscopy images of NA5 microgels at the air/water interface as a function of T_N. (b) Normalized adsorbed amount, N_N, for each charged microgel as a function of T_N. (c) Photographs of thin films of microgel dispersions after drying on glass substrate. The droplet was dried at room temperature (~25 °C; ~60 % humidity) at 0.005 wt% at pH = 3 or pH = 7. McIlvaine buffers, composed of 50 mM disodium hydrogen phosphate and 25 mM citric acid, were used.

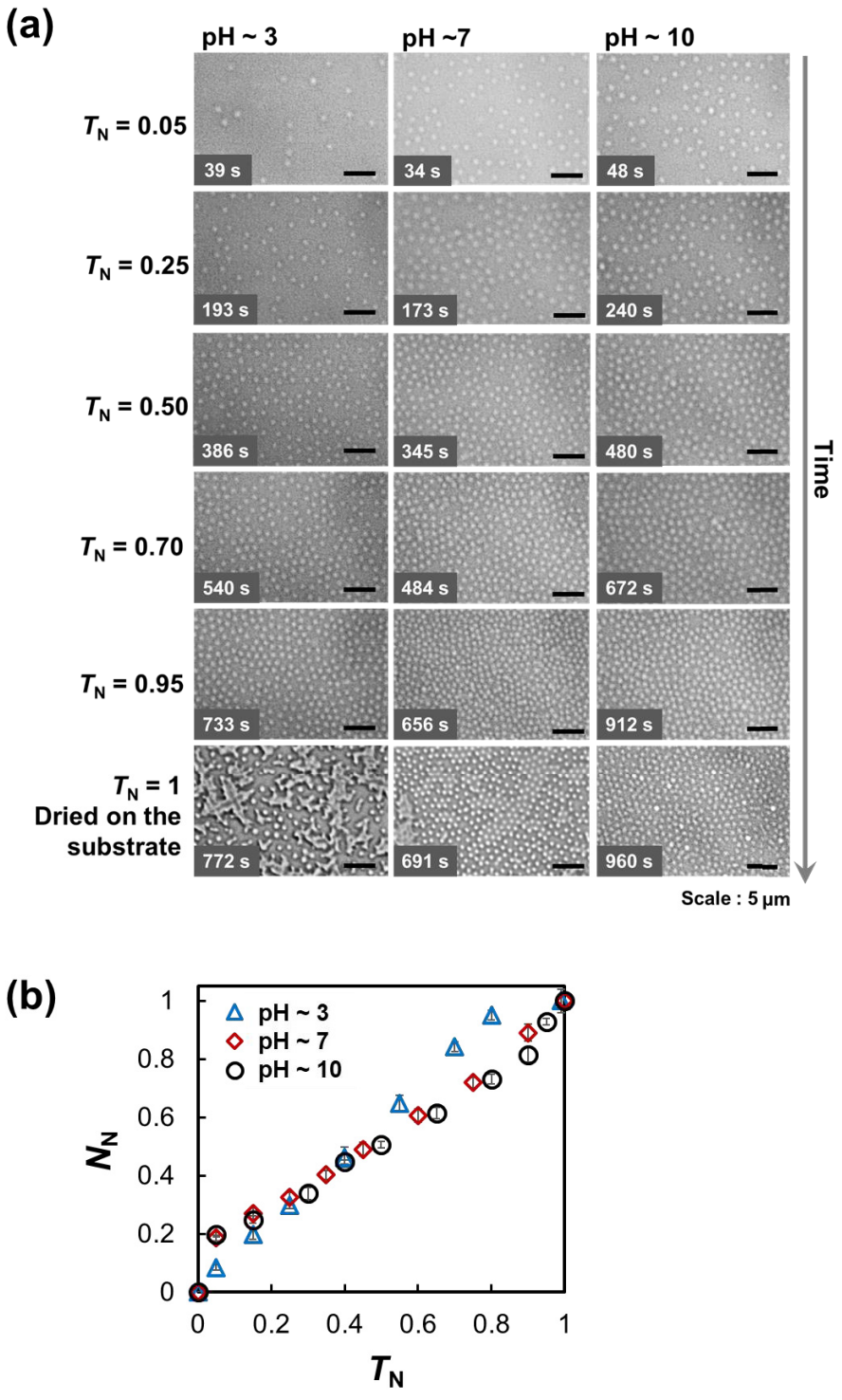

Figure 2-12. (a) Optical microscopy images of NA5 microgels at the air/water interface as a function of T_N. (b) Normalized adsorbed amount, N_N, for each charged microgel as a function of T_N. The droplet was dried at room temperature (~25 °C; ~60 % humidity) at 0.005 wt% at pH ~ 3, pH ~7, and pH ~ 10 in 10 mM simple electrolytes (HCl, NaOH, and NaCl).

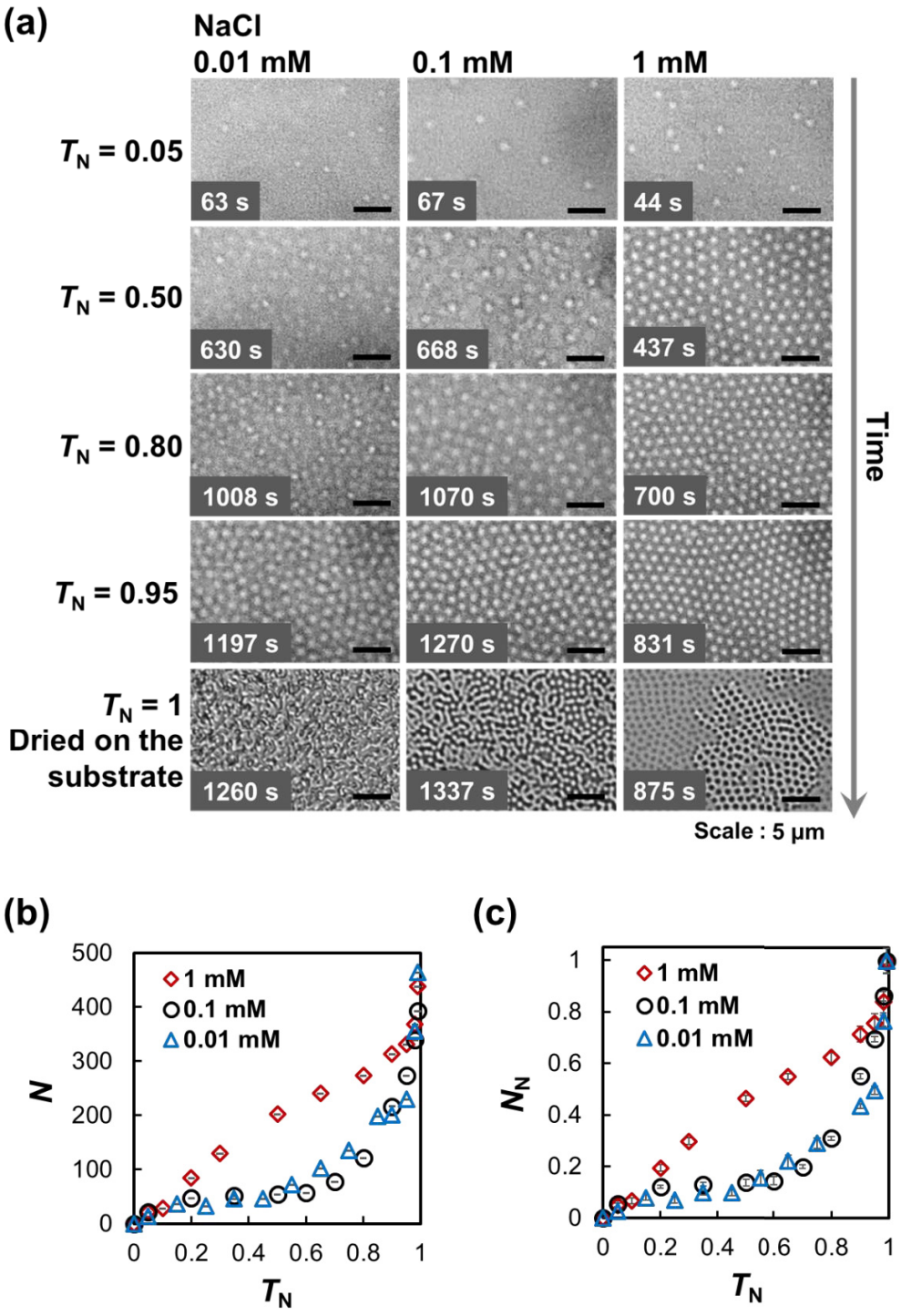

Figure 2-13. Impact of the ionic strength in NA5 microgel dispersions on the adsorption behavior at the air/water interface. (a) Optical microscopy images of NA5 microgels at the air/water interface of each droplet as a function of T_N at [NaCl] = 0.01, 0.1 and 1 mM. The adsorbed amount of (b) N and (c) N_N for each charged microgel as a function of T_N. The droplets were dried at room temperature (~25 °C, ~60 % humidity) at 0.005 wt% on glass substrates.

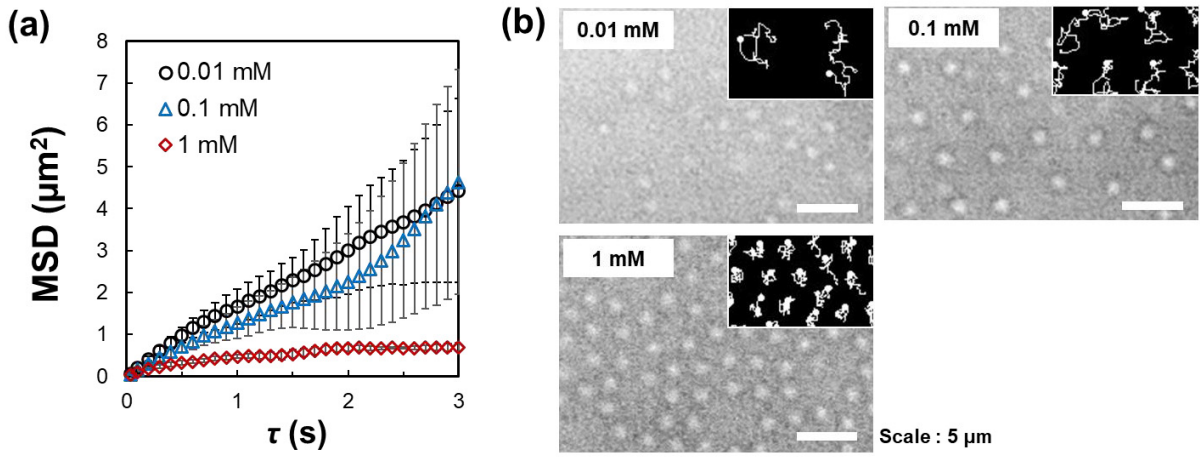

Figure 2-14. (a) Plots of MSD as a function of the lag time, τ, and (b) optical microscopy images with particle-trajectory images of the NA5 microgels at different NaCl concentrations at T_N~0.25 (insets). The sessile droplets were dried at room temperature (~25 °C, ~40 % humidity) at 0.005 wt% on a glass substrate.

Table 2-3. Self-diffusion coefficients for NA5 microgels, caluculated from the MSD plots at T_N = 0.25, 0.55, 0.70 and 0.85 at different NaCl concentrations.

NaCl (mM)	T_N	Slope (μm² s⁻¹)	R^2	D (μm² s⁻¹)
0.01	0.25	1.50	0.9905	0.376
	0.55	1.13	0.9786	0.284
	0.70	0.742	0.8994	0.185
	0.85	0.652	0.8620	0.163
0.1	0.25	1.31	0.9569	0.327
	0.55	1.16	0.9867	0.290
	0.70	0.851	0.9483	0.213
	0.85	0.163	0.9333	0.0407
1	0.25	0.299	0.5679	0.0749
	0.55	0.0160	0.9817	0.00400
	0.70	0.0403	0.9289	0.0101
	0.85	0.142	0.9088	0.0355

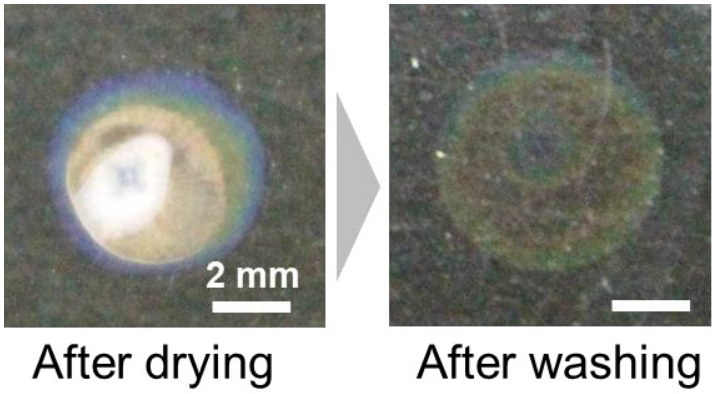

Figure 2-15. Photographs of the dried structures of the dispersion of NA5 microgels charge-screened at [NaCl] = 1 mM before and after washing with pure water.

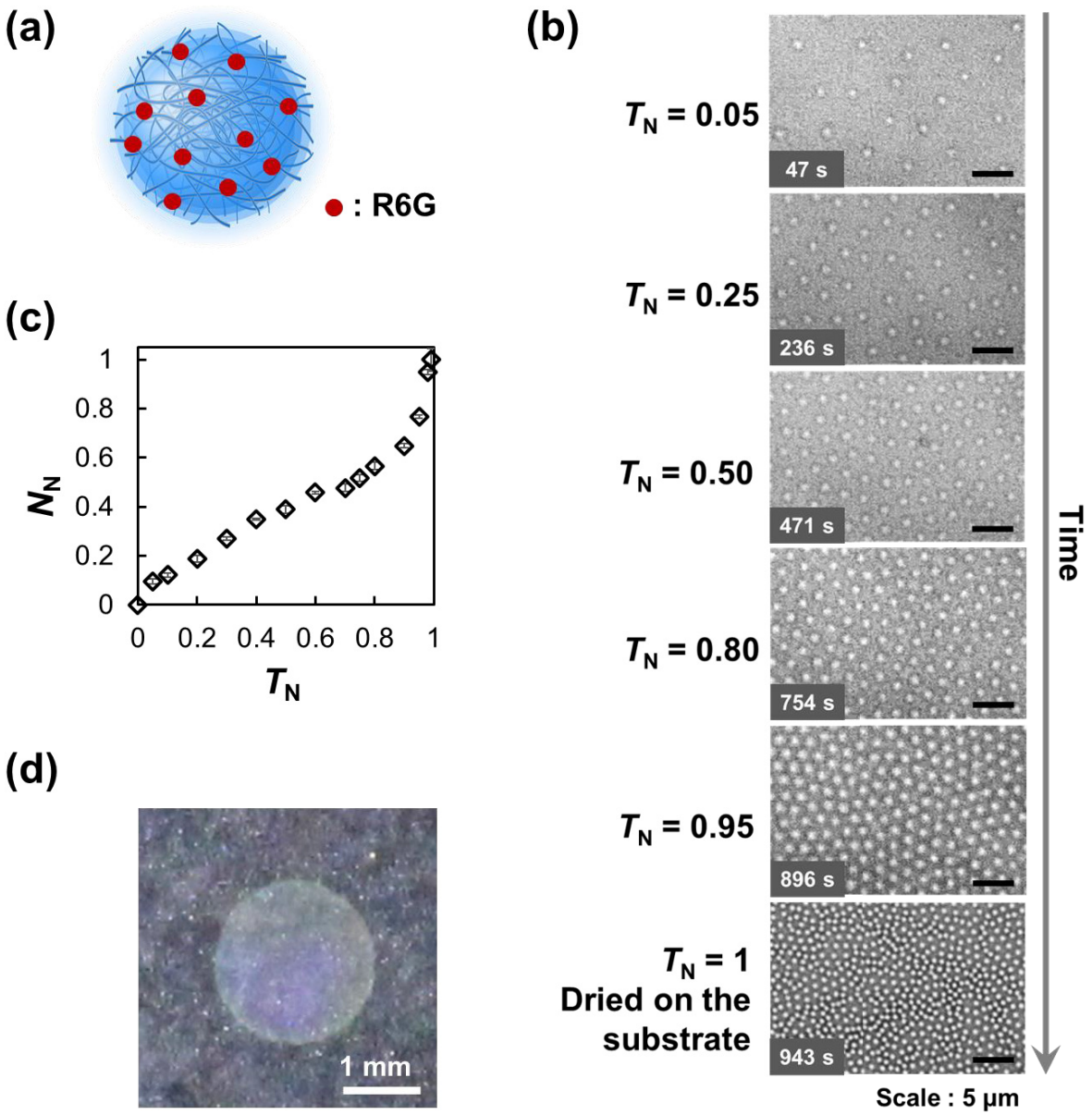

Figure 2-16. (a) Schematic illustration of the microgels in the presence of the cationic dye R6G. (b) Optical microscopy images of NA10 microgels in the presence of R6G at the air/water interface of the sessile droplet on glass substrates as a function of T_N. (c) Normalized adsorbed amount, N_N, for each charged microgel as a function of T_N. (d) Photographs of a thin film of microgel dispersions on glass substrates after drying. The droplets were dried at room temperature (~25 °C, ~60 % humidity) at 0.005 wt%. It should be noted here that the excess of R6G was removed by purifying via two cycles of centrifugation/redispersion in water after adding a sufficient amount of R6G (commensurate to the amount of carboxy groups) to these microgels.

Next, the author investigated the effect of the charge distribution in the microgels on the interfacial behavior using core/shell (CS) microgels, where the polyelectrolyte NA5 microgels are covered with AAc-free pNIPAm hydrogel shells. The CS microgels adsorbed on the air/water interface during the early stage (T_N~0.05) of the drying process (**Figure 2-17(a)(b)**). Subsequently, the normalized adsorbed amount, N_N, did not change from T_N~0.1 to T_N~0.4 (**Figure 2-17(b)**), before N_N increased gradually because the microgels were compressed with each other due to the decrease of the interfacial area upon evaporation, which is similar to the control N micorgels.[38] Moreover, the MSD plots show that the movement of the CS microgels adsorbed at the interface is also restricted (**Figure 2-17(c)**), which is also similar to the behavior of the control N microgels.[38] These results indicate that charge groups located near the surface of the polyelectrolyte microgels are crucial to control the interfacial behavior of the microgels.

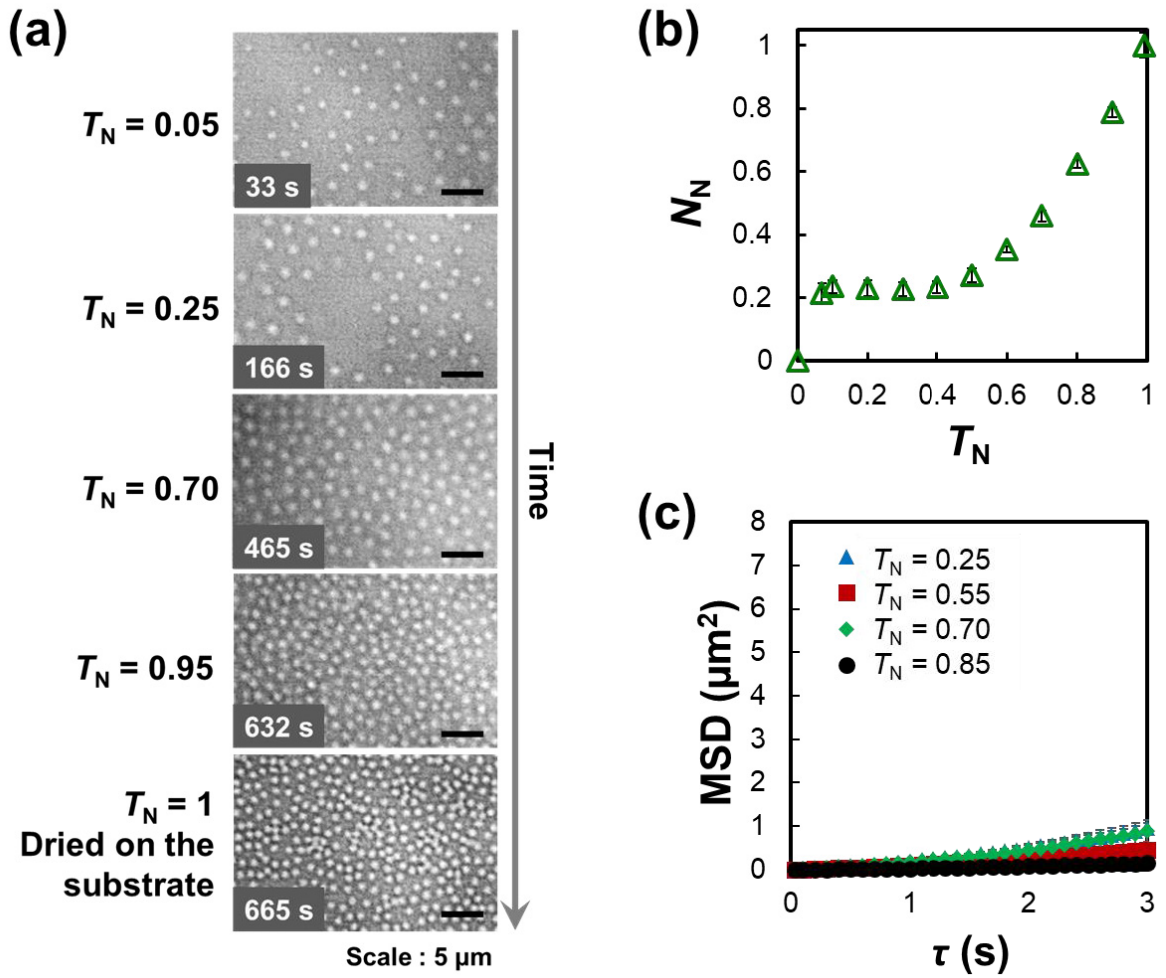

Figure 2-17. (a) Optical microscopy images of the CS microgels at the air/water interface of the droplets on glass substrates as a function of T_N. (b) Normalized adsorbed amount, N_N, for each charged microgel as a function of T_N. (c) The plots of MSD as a function of the lag time, τ, of the CS microgels. The droplets were dried at room temperature (~25 °C, ~60 % humidity) at a concentration of 0.005 wt%.

2-3-5. Analysis of the Adsorption Behavior of Polyelectrolyte Microgels at the Air/water Interface

In order to understand the adsorption process of polyelectrolyte microgels at the air/water interface (T_N < ~0.5), the following pseudo-first-order equation[58] and pseudo-second-order equation[38,58] were applied to the experimental data:

$$\ln(N_e - N_t) = \ln N_e - K_1 t \quad (2\text{-}3)$$

$$\frac{t}{N_t} = \frac{t}{N_e} + \frac{1}{K_2 N_e^2} \quad (2\text{-}4)$$

where N_e and N_t are the adsorbed amount at equilibrium (T_N = 1.0) and at the time t (s), while K_1 (s^{-1}) and K_2 (s^{-1}) represent the adsorption rate constant of the pseudo-first-order model and the pseudo-second-order model, respectively. The resulting correlation coefficients, R^2, of the pseudo-first-order model fitting (**eq. 2-3**) were higher ($R^2 \geq 0.95$) for all polyelectrolyte microgels (NA1, NA5, NA10, NA20) than those of the pseudo-second model fitting (**eq. 2-4**, **Figure 2-18**, **Table 2-4**), which is the opposite of the trend observed for the control N microgels[38] and the CS microgels, where the shell does not contain AAc-incorporated hydrogels. The similar values of the adsorption rate constant K_1 quantitatively indicates that the adsorption kinetics do not depend on the amount of charged AAc groups immobilized in the microgels (1~20 mol%) (**Table 2-4**).

Table 2-4. The parameters for the adsorption kinetics of the N, NA1, NA5, NA10, NA20, and CS microgels at the air/water interface.

Microgel	Pseudo-first order		Pseudo-second order	
	R^2	K_1 (s^{-1})	R^2	K_2 (s^{-1})
N	0.6627	-	0.9693	1.6×10^{-4}
NA1	0.9891	0.0006	0.9544	8.7×10^{-6}
NA5	0.9551	0.0005	0.0080	-
NA10	0.9517	0.0007	0.0711	-
NA20	0.9484	0.0008	0.1490	-
CS	0.4435	-	0.9787	7.6×10^{-4}

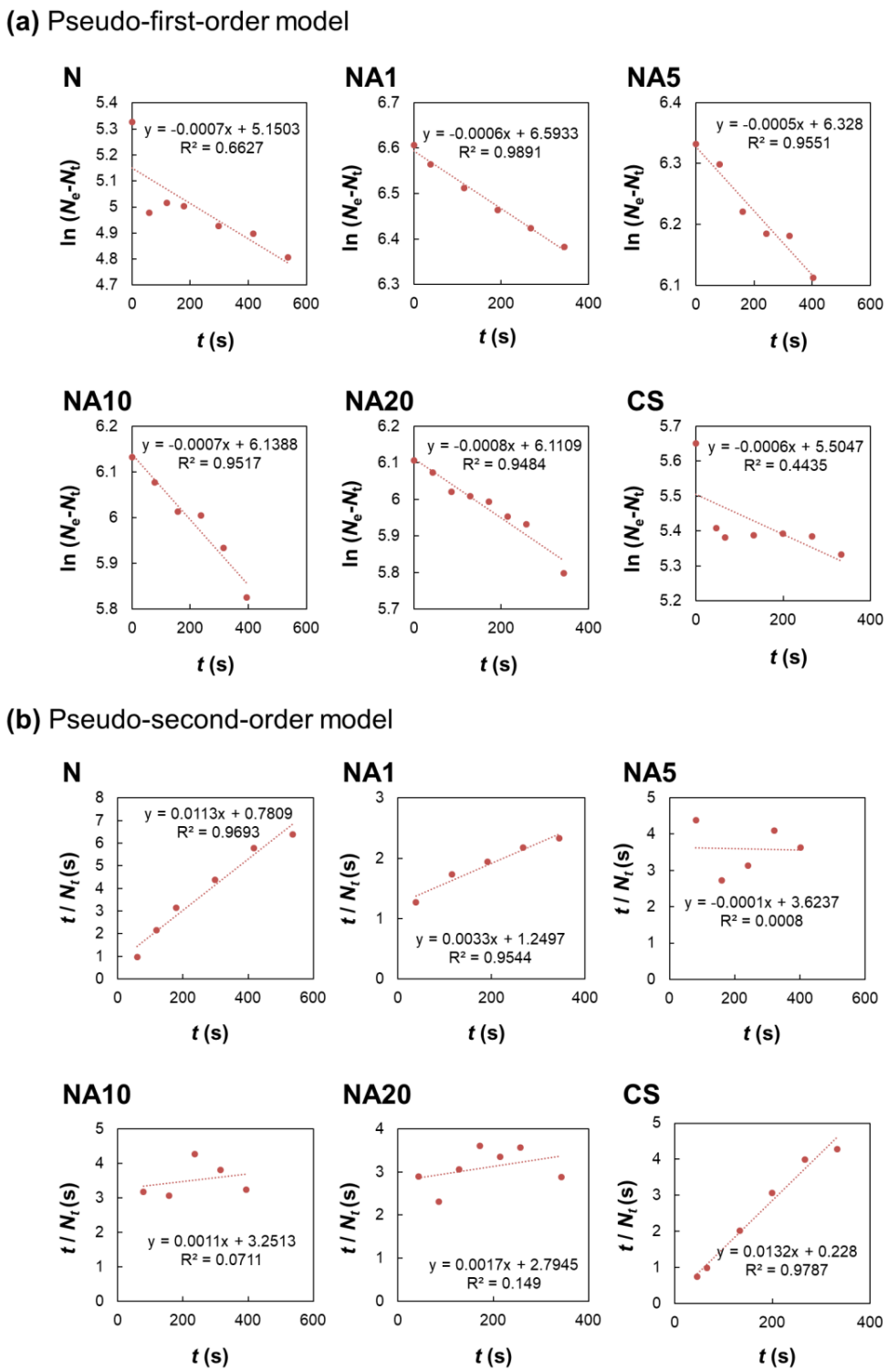

Figure 2-18. Adsorption kinetics for N, NA1, NA5, NA10, NA20, and CS microgels at the air/water interface at T_N 0~0.5 with (a) the pseudo-first-order model, and (b) the pseudo-second-order model.

2-3-6. The Deformation of Single Polyelectrolyte Microgels upon Adsorption at the Air/Water Interface

In order to investigate the deformation of polyelectrolyte microgels at the air/water interface, larger microgels, which can be visualized clearly by fluorescent microscopy, were synthesized by modified precipitation polymerization according to the previous report.[42] Different from the previous study,[42] and in order to avoid the potentially deleterious effects of impurities such as fluorescent molecules of R6G, on the deformation of the polyelectrolyte microgels, the fluorescent molecules were covalently immobilized in the microgels. For that purpose, fluorescent $Ru(bpy)_3$ complexes were immobilized in micron-sized polyelectrolyte (NRu) microgels, synthesized by a modified precipitation polymerization,[42] which revealed that their EPM was affected by the presence of NaCl (1.28×10^{-8} m^2/Vs in pure water; 0.33×10^{-8} m^2/Vs in 1 mM NaCl). The NRu microgels could be clearly visualized in water by fluorescence microscopy, and the deformation of individual microgels could be recorded at the air/water interface (**Figure 2-19(a)**). In order to clarify the influence of the charge of the microgels on their deformation, the deformation of the charge-screened NRu microgels was also investigated quantitatively in 1 mM NaCl solution (**Figure 2-19(b)**). It should be noted here that the fluorescence intensity of the microgels was reduced considerably (see images taken at 2.0 and 5.0 s), which might be due to the decreased density of the polymers (or fluorescent molecules) after the substantial deformation at the interface. Here, the author applied a pseudo-second-order model to analyze the deformation kinetics[42] of the microgels at the air/water interface:

$$\frac{t}{D_t} = \frac{t}{D_s} + \frac{1}{k_2 D_e^2} \tag{2-5}$$

where D_s and D_t (μm) represent the size of the microgels adsorbed at the air/water interface at a specific and arbitrary time t (s), respectively, whereby k_2 (μm^{-1} s^{-1}) refers to the rate constant of the pseudo-second-order model. The R^2 value of the models was ~1, indicating that the deformation could be applied to such models (**Figure 2-19(c)**). The fitting-derived deformation rate constant, k_2, decreased for the charge-screened microgels compared to those examined in pure water ($k_{2,water}$ = 1.9 μm^{-1} s^{-1}; $k_{2,NaCl}$ = 0.57 μm^{-1} s^{-1}) (**Table 2-5**). In a previous study,[42] softer microgels with a lower degree of crosslinking showed lower values of k_2, suggesting that charged microgels do not easily deform upon adsorption at the air/water interface. This may be due to (i)

electrostatic repulsive interactions between the polyelectrolyte microgels and the interface and/or (ii) a restricted deformation of harder polyelectrolyte microgels.

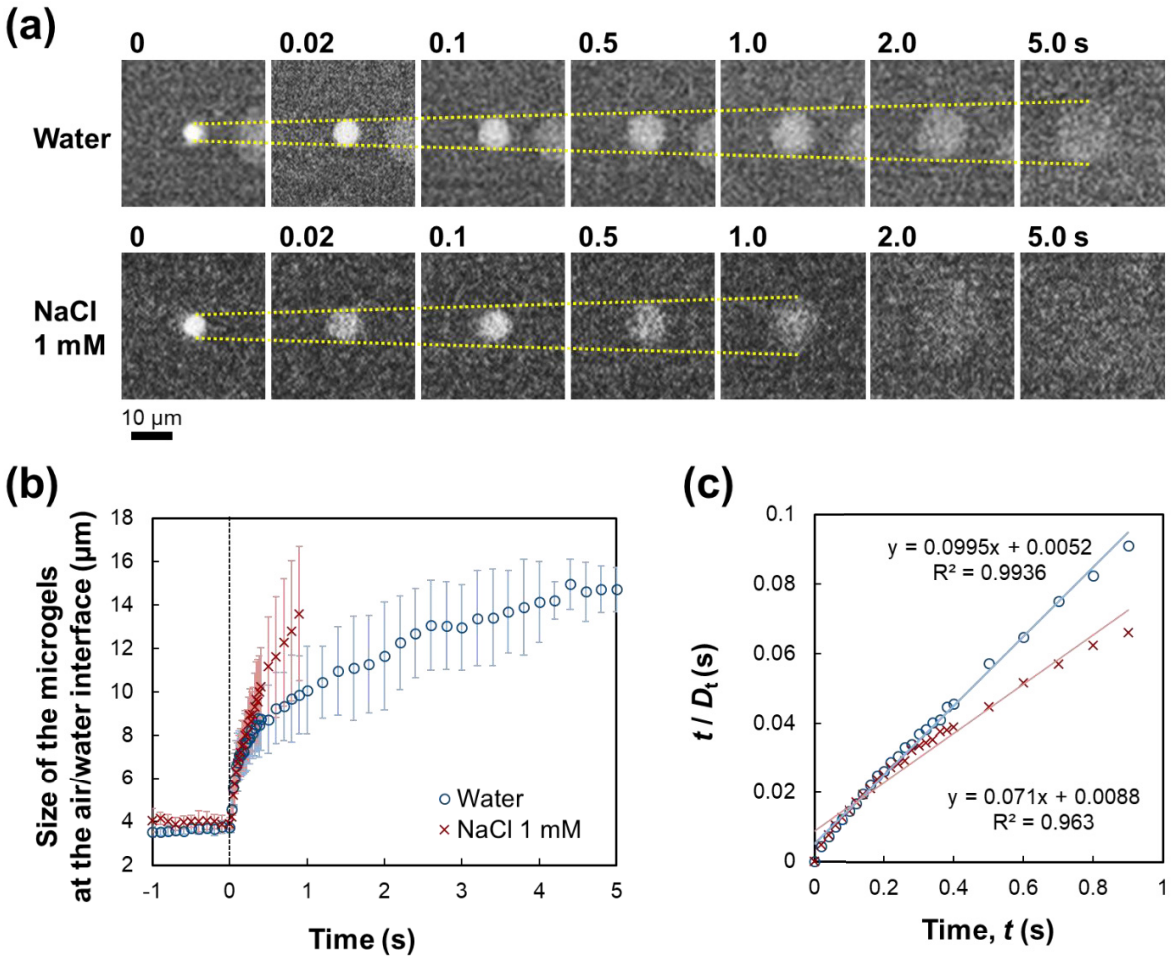

Figure 2-19. (a) Fluorescence microscopy images of NRu microgels upon adsorption at the air/water interfaces recorded with a high-speed camera. (b) Time evolution of the size of the NRu microgels upon adsorption at the air/water interface (○) in water and (×) in aqueous NaCl (1 mM; N = 10). (c) Plots of the pseudo-second-order kinetic for the deformation of the NRu microgels.

Table 2-5. The parameters for the deformation kinetics of the NRu microgels upon adsorption at the air/water interface.

Solvent	Pseudo-second order			Experimental values
	R^2	k_2 (μm^{-1} s^{-1})	$D_{t\sim1}$ (μm)	$D_{t\sim1}$ (μm)
Water	0.9936	1.9	10.0	9.87
NaCl solution	0.9630	0.57	14.1	13.6

2-4. Conclusions

The introduction of charged groups in microgels drastically influences their behavior at the air/water interface upon drying sessile droplets. Firstly, the adsorption of charged microgels at the air/water interface decreases, irrespective of the number of charged groups present (1 ≤ AAc ≤ 20 mol%). Secondly, in contrast to the control N microgels, charged microgels adsorbed at the air/water interface are more mobile, and the microgels are not highly entangled with each other. Thirdly, even though the more mobile charged microgels are arranged at the air/water interface, the formed structures can not be transferred onto the solid substrates without disrupting the structures. Thus, the resulting thin films are macroscopically inhomogeneous. Fourthly, the deformation of single polyelectrolyte microgels is relatively fast, irrespective of the charged and charge-screened microgels. However, the degree of deformation is suppressed by the presence of charged groups at the air/water interface. Fifthly, the aforementioned effect of the charged groups immobilized within the microgels can be ignored by charge-screening, and then, the interfacial behavior becomes similar to that of the control N microgels.

These findings regarding the interfacial behavior of polyelectrolyte microgels at the air/water interface can be expected to promote further developments of applications concerning e.g. foams and emulsions stabilized by microgels, where the understanding of the adsorption behavior of functional microgels at the interface is crucial.

2-5. References

(1) Holtz, J. H.; Asher, S. A. Polymerized colloidal crystal hydrogel films as intelligent chemical sensing materials. *Nature* **1997**, *389*, 829-832.

(2) Kim, J.; Serpe, M. J.; Lyon, L. A. Photoswitchable Microlens Arrays. *Angew. Chem. Int. Ed.* **2005**, *44*, 1333-1336.

(3) Su, S.; Ali, M. M.; Filipe, C. D. M.; Li, Y.; Pelton, R. Microgel-Based Inks for Paper-Supported Biosensing Applications. *Biomacromolecules* **2008**, *9*, 935-941.

(4) Gao, Y.; Xu, W.; Serpe, M. J. Free-standing poly (*N*-isopropylacrylamide) microgel-based etalons. *J. Mater. Chem. C* **2014**, *2*, 5878-5884.

(5) Karg, M. ; Hellweg, T. ; Mulvaney, P. Self-Assembly of Tunable Nanocrystal Superlattices Using Poly-(NIPAM) Spacers. *Adv. Funct.Mater.* **2011**, *21*, 4668-4676.

(6) Snowden, M. J.; Thomas, D.; Vincent, B. Use of colloidal microgels for the absorption of heavy metal and other ions from aqueous solution. *Analyst* **1993**, *118*, 1367-1369.

(7) Gelissen, A. P. H.; Scotti, A.; Turnhoff, S. K.; Janssen, C.; Radulescu, A.; Pich, A.; Rudov, A. A.; Potemkin, I. I.; Richtering, W. An anionic shell shields a cationic core allowing for uptake and release of polyelectrolytes within core–shell responsive microgels. *Soft Matter* **2018**, *14*, 4287-4299.

(8) Kureha, T.; Suzuki, D. Nanocomposite Microgels for the Selective Separation of Halogen Compounds from Aqueous Solution. *Langmuir* **2018**, *34*, 837-846.

(9) Ngai, T.; Behrens, S. H.; Auweter, H. Novel emulsions stabilized by pH and temperature sensitive microgels. *Chem. Commun.* **2005**, *0*, 331-333.

(10) Fujii, S.; Read, E. S.; Binks, B. P.; Armes, S. P. Stimulus-Responsive Emulsifiers Based on Nanocomposite Microgel Particles. *Adv. Mater.* **2005**, *8*, 1014-1018.

(11) Suzuki, D.; Tsuji, S.; Kawaguchi, H. Janus Microgels Prepared by Surfactant-Free Pickering Emulsion-Based Modification and Their Self-Assembly. *J. Am. Chem. Soc.* **2007**, *129*, 8088-8089.

(12) Richtering. W. Responsive Emulsions Stabilized by Stimuli-Sensitive Microgels: Emulsions with Special Non-Pickering Properties. *Langmuir* **2012**, *28*, 17218-17229.

(13) Massé, P.; Sellier, E.; Schmitt, V.; Ravaine, V. Impact of Electrostatics on the Adsorption of Microgels at the Interface of Pickering Emulsions. *Langmuir* **2014**, *30*, 14745-14756.

(14) Suzuki, D.; Taniguchi, H.; Yoshida, R. Autonomously Oscillating Viscosity in Microgel Dispersions. *J. Am. Chem. Soc.* **2009**, *131*, 12058-12059.

(15) Matsui, S.; Inui, K.; Kumai, Y.; Yoshida, R.; Suzuki, D. Autonomously Oscillating Hydrogel Microspheres with High-Frequency Swelling/deswelling and Dispersing/flocculating Oscillations. *ACS Biomater. Sci. Eng.* **2019**, 5, 5615-5622.

(16) Anselmo, A. C.; Mitragotri, S. Impact of particle elasticity on particle-based drug delivery systems. *Adv. Drug Delivery Rev.* **2017**, *108*, 51-67.

(17) Tahara, Y.; Akiyoshi, K. Current advances in self-assembled nanogel delivery systems for immunotherapy. *Adv. Drug Delivery Rev.* **2015**, *95*, 65-76.

(18) McClements, D. J. Encapsulation, protection, and delivery of bioactive proteins and peptides using nanoparticle and microparticle systems: A review. *Adv. Colloid. Interface Sci.* **2018**, *253*, 1-22.

(19) Pelton, R. H.; Chibante, P. Preparation of Aqueous Latices with *N*-Isopropylacrylamide. *Colloids Surf.* **1986**, *20*, 247-256.

(20) Pelton, R. Temperature-sensitive aqueous microgels. *Adv. Colloid Interface Sci.* **2000**, *85*, 1-33.

(21) Hoare, T.; Pelton, R. Highly pH and Temperature Responsive Microgels Functionalized with Vinylacetic Acid. *Macromolecules* **2004**, *37*, 2544-2550.

(22) Karg, M.; Pastoriza-Santos, I.; Rodriguez-González, B.; von Klitzing, R.; Wellert, S.; Hellweg, T. Temperature, pH, and Ionic Strength Induced Changes of the Swelling Behavior of PNIPAM-Poly(allylacetic acid) Copolymer Microgels. *Langmuir* **2008**, *24*, 6300-6306.

(23) Lapeyre, V.; Gosse, I.; Chevreux, S.; Ravaine, V. Monodispersed Glucose-Responsive Microgels Operating at Physiological Salinity. *Biomacromolecules* **2006**, *7*, 3356-3363.

(24) Nayak, S.; Lyon, L. A. Photoinduced Phase Transitions in Poly(*N*-isopropylacrylamide) Microgels. *Chem. Mater.* **2004**, *16*, 2623-2627.

(25) Kureha, T.; Aoki, D.; Hiroshige, S; Iijima, K.; Aoki, D.; Takata, T.; Suzuki, D. Decoupled Thermo- and pH-responsive Hydrogel Microspheres Cross-linked by Rotaxane Networks. *Angew. Chem., Int. Ed.* **2017**, *56*, 15393-15396.

(26) Hoshino, Y.; Imamura, K.; Yue, M.; Inoue, G.; Miura, Y. Reversible Absorption of CO_2 Triggered by Phase Transition of Amine-Containing Micro- and Nanogel Particles. *J. Am. Chem. Soc.* **2012**, *134*, 18177-18180.

(27) Yue, M.; Imai, K.; Yamashita, C.; Miura, Y.; Hoshino, Y. Effects of Hydrophobic Modifications and Phase Transitions of Polyvinylamine Hydrogel Films on Reversible CO_2

Capture Behavior: Comparison between Copolymer Films and Blend Films for Temperature-Responsive CO_2 Absorption. *Macromol. Chem. Phys.* **2017**, *218*, 1600570.

(28) Yue, M.; Hoshino, Y.; Ohshiro, Y.; Imamura, K.; Miura, Y. Temperature-Responsive Microgel Films as Reversible Carbon Dioxide Absorbents in Wet Environment *Angew. Chem., Int. Ed.* **2014**, *53*, 2654-2657.

(29) Yue, M.; Hoshino, Y.; Miura, Y. Design rationale of thermally responsive microgel particle films that reversibly absorb large amounts of CO_2: fine tuning the pK_a of ammonium ions in the particles. *Chem. Sci.* **2015**, *6*, 6112-6123.

(30) Hoare, T.; Pelton, R. Charge-Switching, Amphoteric Glucose-Responsive Microgels with Physiological Swelling Activity. *Biomacromolecules* **2008**, *9*, 733-740.

(31) Nerapusri, V.; Keddie, J. L.; Vincent, B.; Bushnak, I. A. Swelling and Deswelling of Adsorbed Microgel Monolayers Triggered by Changes in Temperature, pH, and Electrolyte Concentration. *Langmuir* **2006**, *22*, 5036-5041.

(32) Sorrell, C. D.; Lyon, L. A. Bimodal Swelling Responses in Microgel Thin Films. *J. Phys. Chem. B* **2007**, *111*, 4060-4066.

(33) Tsuji, S.; Kawaguchi, H. Colored Thin Films Prepared from Hydrogel Microspheres. *Langmuir* **2005**, *21*, 8439-8442.

(34) Sorrell, C. D.; Lyon, L. A. Deformation Controlled Assembly of Binary Microgel Thin Films. *Langmuir* **2008**, *24*, 7216-7222.

(35) Zavgorodnya, O.; Serpe, M. J. Assembly of poly(*N*-isopropylacrylamide)-*co*-acrylic acid microgel thin films on polyelectrolyte multilayers: Effects of polyelectrolyte layer thickness, surface charge, and microgel solution pH. *Colloid. Polym. Sci.* **2011**, *289*, 591-602.

(36) Horigome, K.; Suzuki, D. Drying Mechanism of Poly(*N*-isopropylacrylamide) Microgel Dispersions. *Langmuir* **2012**, *28*, 12962-12970.

(37) Suzuki, D.; Horigome, K. Assembly of Oppositely Charged Microgels at the Air/Water Interface. *J. Phys. Chem. B* **2013**, *117*, 9073-9082.

(38) Takizawa, M.; Sazuka, Y.; Horigome, K.; Sakurai, Y.; Matsui, S.; Minato, H.; Kureha, T.; Suzuki, D. Self-Organization of Soft Hydrogel Microspheres during the Evaporation of Aqueous Droplets. *Langmuir* **2018**, *34*, 4515-4525.

(39) Honda, K.; Sazuka, Y.; Iizuka, K.; Matsui, S.; Uchihashi, T.; Kureha, T.; Shibayama, M.; Watanabe, T.; Suzuki, D. Hydrogel Microellipsoids that Form Robust String-like Assemblies at the Air/Water Interface. *Angew. Chem., Int. Ed.* **2019**, *131*, 7372-7376.

(40) Karg, M.; Pich, A.; Hellweg, T.; Hoare, T.; Lyon, L. A.; Crassous, J. J.; Suzuki, D.; Gumerov, R. A.; Schneider, S.; Potemkin, I. I.; Richtering, W. Nanogels and microgels: From model colloids to applications, recent developments and future trends. *Langmuir* **2019**, *35*, 6231-6255.

(41) Pieranski, P. Two-Dimensional Interfacial Colloidal Crystals. *Phys. Rev. Lett.* **1980**, *45*, 569-572.

(42) Minato, H.; Murai, M.; Watanabe, T.; Matsui, S.; Takizawa, M.; Kureha, T.; Suzuki, D. The deformation of hydrogel microspheres at the air/water interface. *Chem. Commun.* **2018**, *54*, 932-935.

(43) Ghosh, P. K.; Spiro, T. G. Photoelectrochemistry of Tris(bipyridyl)ruthenium(II) Covalently Attached to n-Type SnO_2. *J. Am. Chem. Soc.* **1980**, *102*, 5543-5549.

(44) Jones, C. D.; Lyon, L. A. Dependence of Shell Thickness on Core Compression in Acrylic Acid Modified Poly(*N*-isopropylacrylamide) Core/Shell Microgels. *Langmuir* **2003**, *19*, 4544-4547.

(45) Urayama, K.; Saeki, T.; Cong, S.; Uratani, S.; Takigawa, T.; Murai, M.; Suzuki, D. A simple feature of yielding behavior of highly dense suspensions of soft micro-hydrogel particles. *Soft Matter* **2014**, *10*, 9486-9495.

(46) Crocker, J. C.; Grier, D. G. Methods of Digital Video Microscopy for Colloidal Studies. *J. Colloid Interf. Sci.* **1996**, *179*, 298-310.

(47) Meng, Z.; Cho, J. K.; Debord, S.; Breedveld, V.; Lyon, L. A. Crystallization Behavior of Soft, Attractive Microgels. *J. Phys. Chem. B* **2007**, *111*, 6992-6997.

(48) Ponratnam, S.; Kapur, S. L. Reactivity ratios of ionizing monomers in aqueous solution. Copolymerization of acrylic and methacrylic acids with acrylamide. *Macromol. Chem.* **1977**, *178*, 1029-1038.

(49) Hoare, T.; McLean, D. Kinetic Prediction of Functional Group Distributions in Thermosensitive Microgels. *J. Phys. Chem. B* **2006**, *110*, 20327-20336.

(50) Watanabe, T.; Kobayashi, C.; Song, C.; Murata, K.; Kureha, T.; Suzuki, D. Impact of Spatial Distribution of Charged Groups in Core Poly(*N*-isopropylacrylamide)-Based Microgels on the

Resultant Composite Structures Prepared by Seeded Emulsion Polymerization of Styrene. *Langmuir* **2016**, *32*, 12760-12773.

(51) Jones, C. D.; Lyon, L. A. Shell-Restricted Swelling and Core Compression in Poly(*N*-isopropylacrylamide) Core-Shell Microgels. *Macromolecules* **2003**, *36*, 1988-1993.

(52) Geisel, K.; Isa, L.; Richtering, W. Unraveling the 3D Localization and Deformation of Responsive Microgels at Oil/Water Interfaces: A Step Forward in Understanding Soft Emulsion Stabilizers. *Langmuir* **2012**, *28*, 15770-15776.

(53) Iyer, A. S.; Lyon, L. A. Self-Healing Colloidal Crystals. *Angew. Chem.* **2009**, *121*, 4632-4636; *Angew. Chem., Int. Ed.* **2009**, *48*, 4562-4566.

(54) Scotti, A.; Gasser, U.; Herman, E. S.; Pelaez-Fernandez, M.; Han, J.; Menzel, A.; Lyon, L. A.; Fernández-Nieves, A. The role of ions in the self-healing behavior of soft particle suspensions. *Proc. Natl. Acad. Sci. U.S.A.* **2016**, *113*, 5576-5581.

(55) Dugyala, V. R.; Muthukuru, J. S.; Mani, E.; Basavaraj, M. G. Role of electrostatic interactions in the adsorption kinetics of nanoparticles at fluid-fluid interfaces. *Phys. Chem. Chem. Phys.* **2016**,*18*, 5499-5508.

(56) Inraelachvili, J. N. *Intermolecular and surface forces* Academic press, 3rd edn, 2011.

(57) Kureha, T.; Shibamoto, T.; Matsui, S.; Sato, T.; Suzuki, D. Investigation of Changes in the Microscopic Structure of Anionic Poly(*N*-isopropylacrylamide-*co*-Acrylic acid) Microgels in the Presence of Cationic Organic Dyes toward Precisely Controlled Uptake/Release of Low-Molecular-Weight Chemical Compound. *Langmuir* **2016**, *32*, 4575-4585.

(58) Azizian, S. Kinetic Models of Sorption: A Theoretical Analysis. *J. Colloid Interface Sci.* **2004**, *276*, 47-52.

ii. Summary

In this thesis, the dynamic interfacial behavior, i.e., the adsorption and deformation of soft deformable microgels at the air/water interface was revealed by direct *in situ* observation with optical/fluorescence microscopy. Firstly, the deformation dynamics of a single microgel upon adsorption at the air/water interface was monitored and quantitatively evaluated using larger micron-sized microgels which were prepared by a modified precipitation polymerization method. Secondly, the effect of charge groups incorporated in microgels was clarified on the adsorption and deformation behavior of microgels at the air/water interface, which demonstrates that the incorporated charge is a factor that may affect the adsorption, interpenetration between the neighboring microgels, and deformation of microgels at the interface. These findings progress the understanding of some aspects of their interfacial behavior that theoretically and computationally describing has been difficult.

Recently, the microgel behavior at the fluid interface such as air/water or oil/water interface has been investigated using not only various experimental techniques but also computer simulations. A highly accurate simulation can immediately examine the effect of a change of a microgel morphology or an environmental state in the interfacial behavior of microgels. However, computational studies have included some assumptions in the microgel structure. For instance, a microgel model having a homogeneous cross-linking density have been assumed although the experimentally synthesized microgels exhibit an inhomogeneous structure, where the cross-linking density is higher at the center of the microgels due to the difference in the reactivity ratio and hydrophilicity/hydrophobicity between the cross-linker and monomers. Therefore, experimentally understanding the morphology and the effect of each parameter of microgels (i.e., size, softness, chemical composition and charge) in their interfacial behavior is of paramount importance. The findings of this thesis can be expected to develop the theoretically and computationally insight about the interfacial behavior of microgels at the fluid interface, which will promote further developments of many applications including foams (air/water interface) and Pickering emulsions (oil/water interface) stabilized by soft deformable microgels.

ChemComm

COMMUNICATION

Cite this: *Chem. Commun.*, 2018, 54, 932

Received 15th December 2017, Accepted 5th January 2018

DOI: 10.1039/c7cc09603h

rsc.li/chemcomm

The deformation of hydrogel microspheres at the air/water interface†

Haruka Minato,[a] Masaki Murai,[a] Takumi Watanabe,[a] Shusuke Matsui,[a] Masaya Takizawa,[a] Takuma Kureha *[a] and Daisuke Suzuki *[ab]

The deformation of soft hydrogel microspheres (microgels) adsorbed at the air/water interface was investigated for the first time using large poly(*N*-isopropyl acrylamide)-based microgels synthesized by a modified aqueous precipitation polymerization method. The deformation of the micron-sized soft microspheres could be visualized clearly and analyzed quantitatively at the air/water interface.

The "softness" of colloidal particles is crucial for their functions in the human body; for instance, red blood cells (RBCs) carry oxygen/carbon dioxide in capillaries whose diameter is much smaller than that of RBCs. Unlike RBCs, soft particles, hereafter denoted as hydrogel microspheres (microgels), can be synthesized artificially. Microgels are colloidal particles of cross-linked polymeric networks with high contents of water (>90%) that deform or deswell under external stress. The "softness" of microgels plays a crucial role in many applications including coatings,[1] food,[2] cosmetics,[3] colloidal crystals/glasses,[4] drug delivery systems,[5] biomaterials,[6] catalysts,[7] and stabilizers for oil/water (emulsions) and air/water (foams) interfaces.[8]

In order to further develop these applications and create new applications for soft colloidal particles, understanding the interfacial behavior of microgels is highly important. Poly(*N*-isopropyl acrylamide) (pNIPAm) microgels are representative thermo-responsive microgels;[9] they show surface activity and adsorb at the air/water interface, which was first studied using the pendant-drop method.[10] This surface tension technique has been frequently used to discuss the adsorption behavior of soft pNIPAm-based microgels at the air/water interface.[10–12] These studies demonstrate the importance of softness, *i.e.*, the degree of cross-linking in microgels, on the adsorption at the air/water interface. Recently, detailed structural information of adsorbed microgels has been studied using neutron reflectivity measurements,[13] and transmission X-ray microscopy at the oil/water interface.[14] Although the understanding of the interfacial behavior of soft microgels has progressed, the direct visualization of the interfacial dynamic behavior of individual soft microgels has, to the best of our knowledge, not yet been reported. Therefore, details on the interfacial behavior of soft microgels at the air/water or oil/water interface remains unclear and a matter of debate.

In order to better understand the interfacial behavior of soft microgels, we examined for the first time the deformation dynamics of individual large microgels (>6 μm) that were developed unexpectedly directly at the air/water interface by fluorescence microscopy using a high-speed camera. It should be noted that our group has recently reported that negatively charged softer colloidal particles show faster adsorption on positively charged solid substrates. This was demonstrated by high-speed atomic force microscopy (AFM), which allowed us to observe aqueous systems in real time (1 frame per s).[15] However, this technique cannot be applied to systems at the air/water or oil/water (*i.e.*, liquid) interfaces.

Since the first pNIPAm microgels have been synthesized by precipitation polymerization,[9a,b] the largest uniform pNIPAm-based microgels (4.7 μm, pH = 10) have been reported by the Ngai group.[16] These microgels were obtained from initially increasing gradually the temperature of the reaction solution,[17] and adding the comonomers in aqueous solution in a continuous manner. In this context, we found that much larger microgels can be obtained when a small amount of the cross-linker *N*,*N*′-methylenebis(acrylamide) (BIS) is added at the beginning of the polymerization (see Scheme S1, ESI†).

We confirmed that this method can also be applied to pure BIS-cross-linked pNIPAm microgels (both negatively and positively charged), pNIPAm-based microgels copolymerized with charged acrylic acid or reactive glycidyl methacrylate monomers

[a] *Graduate School of Textile Science & Technology, Shinshu University, 3-15-1 Tokida Ueda, Nagano 386-8567, Japan. E-mail: d_suzuki@shinshu-u.ac.jp, 15st105g@shinshu-u.ac.jp*

[b] *Division of Smart Textiles, Institute for Fiber Engineering, Interdisciplinary Cluster for Cutting Edge Research, Shinshu University, 3-15-1 Tokida Ueda, Nagano 386-8567, Japan*

† Electronic supplementary information (ESI) available: Experimental details, optical/fluorescence microscope images, and a movie, as well as a size analysis of the microgels, electrophoretic mobility, and deformation kinetic parameters. See DOI: 10.1039/c7cc09603h

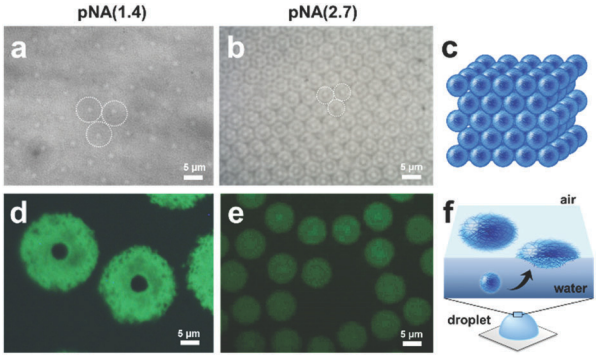

Fig. 1 Optical microscopy images of (a) pNA(1.4) and (b) pNA(2.7) microgels packed in a rectangle capillary at the critical concentration (C^*, ϕ_{eff} = 1.0). The white dotted lines indicate the surface of individual microgels. It should be noted that random motion was not observed in (a) (see Movie S1, ESI†). (c) Scheme of hexagonal close-packed crystal structures. Fluorescence microscopy images of the same (d) pNA(1.4) and (e) pNA(2.7) microgels adsorbed at the air/water interface of a dispersion droplet. (f) Scheme of adsorbed microgels at the air/water interface. It is noteworthy that the dispersions were mixed with Rhodamine 6G, and subsequently centrifuged to remove any excess R6G. These samples were observed at room temperature. Poly(NIPAm-*co*-acrylic acid) microgels denoted as pNA(*X*), where *X* indicates the BIS concentration (mol%) in the shell.

(which in turn may incorporate various functional molecules),[18] and p(NIPAm-*co*-tris(2,2′-bipyridyl)) ruthenium(II) complex microgels, which exhibit autonomous swelling/deswelling and flocculating/dispersing oscillation[19] (Table S1 and Fig. S1, ESI†). In the present study, we selected poly(NIPAm-*co*-acrylic acid) microgels, henceforth denoted as pNA(*X*), where *X* indicates the BIS concentration (mol%) in the shell, for further studies, as their diameter was the largest among all the aforementioned microgels. The detail mechanism of the modified precipitation polymerization will be discussed elsewhere.

Fig. 1a shows pNA(1.4) microgels packed in a rectangle capillary as observed by optical microscopy (6.3 μm, pH = 7, 25 °C). Here, the microgels were examined at the critical concentration (C^*, ϕ_{eff} = 1.0), where polymer chains on the microgels begin to contact each other. It should be noted that the shells of the microgels are almost transparent, as they have been highly expanded by water; however, the pNA microgels are indeed closely packed as no random movement was observed (Movie S1, ESI†). Subsequently, the deformation of the pNA(1.4) microgels was examined at the air/water interface of a dispersion droplet deposited on a glass substrate at pH = 7 and 25 °C (Fig. 1d). To visualize all the microgels, fluorescent Rhodamine 6G (R6G) was adsorbed on the pNA microgels by electrostatic attraction with the acrylic acid moieties. As a result, highly deformed microgels were visualized at the air/water interface, whose diameter increased to 20 μm (CV = 9%, N = 50), which is more than three times that of the spherical microgels. In the fluorescence microscopy images, core (dark part)–shell (green fluorescence part) microgels were observed. By optical microscopy, only the cores could be visualized, and a size of 4 μm was calculated (Fig. S2, ESI†), indicating that the polymer density in the shell is too low to visualize due to the limited resolution of the optical microscope. The highly spread thin shell was only visible upon adding the fluorescent dye.

To gain insight into how microgels are deformed at the air/water interface, the exact moment of the adsorption of the microgels was monitored by fluorescence microscopy using a high-speed camera (Fig. 2). For the pNA(1.4) microgels shown in Fig. 2, the size of the microgels spread radially at the interface became 17 μm within 0.1 s. Subsequently, the size gradually increased to ~20 μm within 1 s, where it reached an equilibrium. To evaluate the impact of the microgel softness on the deformation kinetics, pNA microgels with a higher BIS concentrations in the shell were prepared (pNA(2.7); Table S1 (ESI†) and Fig. 1b and e). We confirmed that the deformation of the stiffer pNA(2.7) microgels at the interface was fast, similar to that of the softer pNA(1.4) microgels, although the highly cross-linked pNA(2.7) microgels were only slightly deformed at the air/water interface (Fig. 2b). The degree of deformation is defined as D_{ads}/D_{C^*}, where D_{ads} represents the size of the microgels adsorbed at the interface and D_{C^*} represents the diameter of the microgels packed in a rectangle capillary at C^* (Fig. 1a and b). In this case, D_{ads}/D_{C^*} was 3.2 for pNA(1.4) and 1.9 for pNA(2.7) in the equilibrium state. In our previous work,[15] we were unable to quantify the kinetics of deformation of the microgels at the solid/water interface due to the lack of

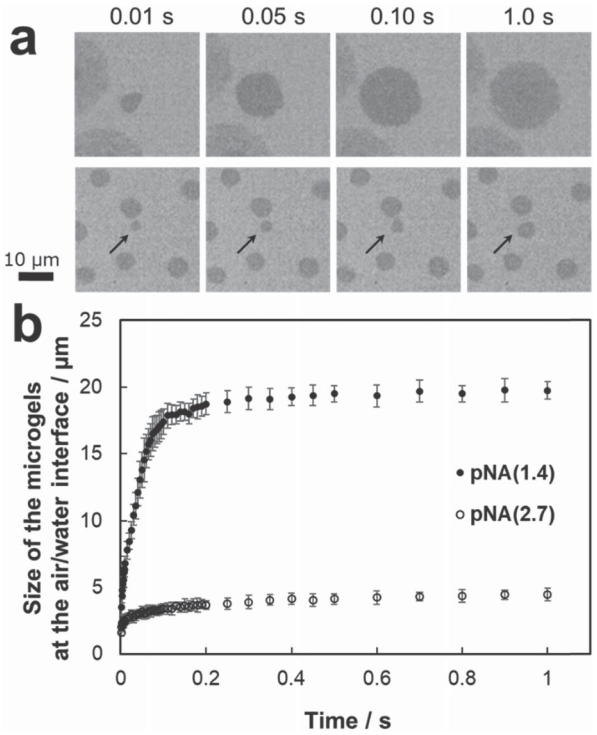

Fig. 2 (a) pNA(1.4) and pNA(2.7) microgels upon adsorption at the air/water interfaces visualized by fluorescence microscopy equipped with a high-speed camera at pH = 3 and 25 °C. It should be noted that these images were recorded in grey scale. (b) Time evolution of the size of pNA(1.4) and pNA(2.7) microgels upon adsorption at the air/water interface (N = 10). Movie S2 and S3 (ESI†) show the moment of adsorption and deformation of individual pNA(1.4) and pNA(2.7) microgels at the air/water interface, respectively.

time resolution of the high-speed AFM (1 frame per s); nevertheless, it was possible to observe the deformation of all the tested microgels at these interfaces.[15] However, in the present study, we were able to confirm for the first time that the deformation kinetics at the air/water interface is so fast that the softness or cross-link density of the microgels does not exert a significant impact.

In order to understand the deformation in more detail, the deformation dynamics were analyzed using time-lapse images. Pseudo-first-order and the pseudo-second-order equations were applied to analyze the deformation kinetics.[20] These kinetic models can be expressed in linear form as follows:

$$\log(D_e - D_t) = \log(D_e) - (k_1/2.303)t \quad (1)$$

$$(t/D_t) = 1/k_2 D_e^{\,2} + (1/D_e)t \quad (2)$$

where D_e and D_t (μm) represent the size of microgels adsorbed at the air/water interface at equilibrium and at arbitrary time t (s), respectively. k_1 (s^{-1}) is the rate constant of the pseudo-first-order model, while k_2 (μm μm^{-1} s^{-1}) is the rate constant of the pseudo-second-order model.

Fig. 3 shows the plots of pseudo-first-order and the pseudo-second-order kinetics for the deformation of pNA(1.4) and pNA(2.7) microgels. The correlation coefficient (R^2) of the pseudo-second-order model was ~1, and that of the pseudo-first-order model was not, indicating a good fit of the pseudo-second-order model for these microgels (Table S2, ESI†). It suggests that one part of the deformation dynamics should be explained by a two-stage deformation speed; during the first stage, the microgels rapidly deform at the air/water interface, which is caused by a collision of the microgels at the air/water interface. During the second stage, the surface-active polymer chains on the microgel gradually spread to stabilize the interface thermodynamically. Here, the deformation rate of the microgels during the first stage was calculated from the fitted line (Fig. S3, ESI†), affording deformation rates (v) of 95 μm s^{-1} and 24 μm s^{-1} for pNA(1.4) and pNA(2.7), respectively. Although the initial deformation rate, v, of these microgels was significantly different, it seems that the deformation of the microgels is completed very quickly, *i.e.*, within a few seconds regardless of the degree of cross-linking (*i.e.*, irrespective of the softness).

Finally, the time-dependent deformation of pNA(1.4) microgels at the air/water interface in a dilute microgel dispersion (~0.003 wt%) was monitored during drying (Fig. 4). In our previous studies,[21] the structure of the adsorbed microgels at the air/water interface could not be determined due to limitations of the resolution. In this study, however, given that the thin shell of the microgels can be visualized, we could confirm for the first time that the adsorbed and highly deformed microgels gradually engage in contact with each other (Fig. 4a and b), before the size of the microgels largely decreases with decreasing interfacial area upon drying. The degree of deformation of the pNA(1.4) microgels decreased with time from D_{ads}/D_{C^*} = 3.2 (1 min) to 3.0 (36 min) and 2.4 (42 min).

It is also noteworthy that the method reported herein for the synthesis of large microgels may also be applicable to other microgels, such as autonomously oscillating microgels,[19] although the detailed mechanism of the polymerization should be clarified experimentally. This investigation on the interfacial behavior of large microgels may thus open new research avenues in the areas of fundamental colloidal chemistry and applied materials chemistry.

In conclusion, the deformation kinetics of soft pNIPAm-based microgels upon adsorption at the air/water interface was quantified for the first time using large pNIPAm-based microgels synthesized by a modified aqueous precipitation polymerization technique. The deformation process of the microgels upon adsorption at the interface was visualized and analyzed directly. The microgels adsorbed and deformed very quickly at the air/water interface, and the deformation kinetics could be feasibly explained using a pseudo-second-order model. Additionally, the highly deformed microgels adsorbed at the interface finally engaged in contact with each other, before gradually deforming during drying. Moreover, the method to produce such large microgels was also successfully applied to other functional microgels. Therefore, these new findings for the evaluation of

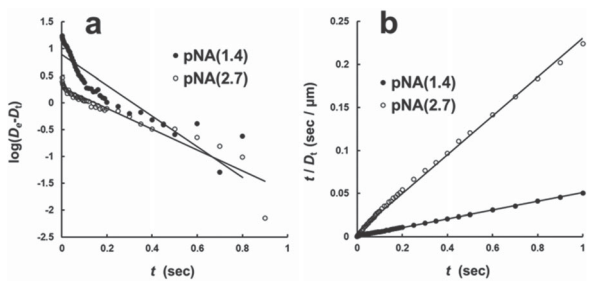

Fig. 3 Plots of (a) pseudo-first-order eqn (1) and (b) pseudo-second-order kinetic (eqn (2)) for the deformation of pNA(1.4) and pNA(2.7) microgels at the air/water interface; recorded with a fluorescence microscope equipped with a high-speed camera.

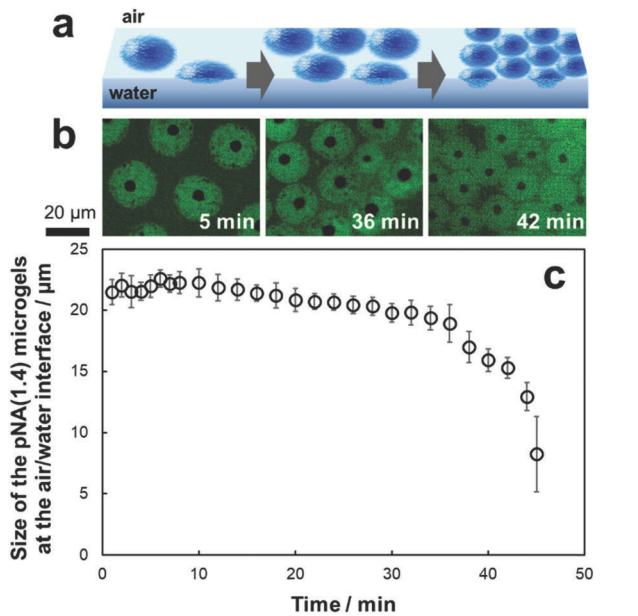

Fig. 4 (a) Scheme, (b) fluorescence microscopy images and (c) size of pNA(1.4) microgels at the air/water interface of dilute microgel droplets as a function of time during evaporation of the solvent (N = 30).

the "softness" of microgels at the air/water interface may promote the development of new applications related to the interfacial behavior of microgels.

D. S. acknowledges a Grant-in-Aid for Young Scientists (A) (17H04892) and for Scientific Research on Innovative Areas (JP26102517 and JP16H00760) from the Japanese Ministry of Education, Culture, Sports, Science, and Technology (MEXT). H. M. acknowledges a Grant-in-Aid for the Shinshu University Advanced Leading Graduate Program from MEXT.

Conflicts of interest

There are no conflicts to declare.

Notes and references

1 W. Li, L. Hu, J. Zhu, D. Li, Y. Luan, W. Xu and M. J. Serpe, *ACS Appl. Mater. Interfaces*, 2017, **9**, 26539–26548.
2 (*a*) D. J. McClements, *Food Hydrocolloids*, 2017, **68**, 238–245; (*b*) L. Gu, Y. Su, Z. Zhang, B. Zheng, R. Zhang, D. J. McClements and Y. Yang, *J. Agric. Food Chem.*, 2017, **65**, 6919–6928.
3 I. Kaneda, A. Sogabe and H. Nakajima, *J. Colloid Interface Sci.*, 2004, **275**, 450–457.
4 (*a*) L. A. Lyon, J. D. Debord, S. B. Debord, C. D. Jones, J. G. McGrath and M. J. Serpe, *J. Phys. Chem. B*, 2004, **108**, 19099–19108; (*b*) T. Hellweg, C. D. Dewhurst, E. Brückner, K. Kratz and W. Eimer, *Colloid Polym. Sci.*, 2000, **278**, 972–978; (*c*) J. Mattsson, H. M. Wyss, A. Fernandez-Nieves, K. Miyazaki, Z. Hu, D. R. Reichman and D. A. Weitz, *Nature*, 2009, **462**, 83–86; (*d*) T. Okubo, D. Suzuki, T. Yamagata, A. Katsuno, M. Sakurai, H. Kimura and A. Tsuchida, *Colloid Polym. Sci.*, 2011, **289**, 291–299; (*e*) K. Urayama, T. Saeki, S. Cong, S. Uratani, T. Takigawa, M. Murai and D. Suzuki, *Soft Matter*, 2014, **10**, 9486–9495.
5 T. J. Merkel, S. W. Jones, K. P. Herlihy, F. R. Kersey, A. R. Shields, M. Napier, J. C. Luft, H. Wu, W. C. Zamboni, A. Z. Wang, J. E. Bear and J. M. DeSimone, *Proc. Natl. Acad. Sci. U. S. A.*, 2011, **108**, 586–591.
6 (*a*) M. Nakamoto, T. Nonaka, K. J. Shea, Y. Miura and Y. Hoshino, *J. Am. Chem. Soc.*, 2016, **138**, 4282–4285; (*b*) E. Gau, D. M. Mate, Z. Zou, A. Oppermann, A. Töpel, F. Jakob, D. Wöll, U. Schwaneberg and A. Pich, *Biomacromolecules*, 2017, **18**, 2789–2798; (*c*) L. Nuhn, S. Tomcin, K. Miyata, V. Mailänder, K. Landfester, K. Kataoka and R. Zentel, *Biomacromolecules*, 2014, **15**, 4111–4121.
7 (*a*) M. Ballauff and Y. Lu, *Polymer*, 2007, **48**, 1815–1823; (*b*) Y. Lu and M. Ballauff, *Prog. Polym. Sci.*, 2016, **59**, 86–104.
8 (*a*) T. Ngai, S. H. Behrens and H. Auweter, *Chem. Commun.*, 2005, 331–333; (*b*) S. Fujii, E. S. Read, B. P. Binks and S. P. Armes, *Adv. Mater.*, 2005, **17**, 1014–1018; (*c*) D. Suzuki, S. Tsuji and H. Kawaguchi, *J. Am. Chem. Soc.*, 2007, **129**, 8088–8089; (*d*) W. Richtering, *Langmuir*, 2012, **28**, 17218–17229; (*e*) M. Destribats, V. Lapeyre, M. Wolfs, E. Sellier, F. Leal-Calderon, V. Ravaine and V. Schmitt, *Soft Matter*, 2011, **7**, 7689–7698; (*f*) M. H. Kwok and T. Ngai, *J. Colloid Interface Sci.*, 2016, **461**, 409–418.
9 (*a*) R. H. Pelton and P. Chibante, *Colloids Surf.*, 1986, **20**, 247–256; (*b*) R. Pelton, *Adv. Colloid Interface Sci.*, 2000, **85**, 1–33; (*c*) B. R. Saunders and B. Vincent, *Adv. Colloid Interface Sci.*, 1999, **80**, 1–25; (*d*) S. Nayak and L. A. Lyon, *Angew. Chem., Int. Ed.*, 2005, **44**, 7686–7708; (*e*) F. A. Plamper and W. Richtering, *Acc. Chem. Res.*, 2017, **50**, 131–140; (*f*) D. Suzuki, K. Horigome, T. Kureha, S. Matsui and T. Watanabe, *Polym. J.*, 2017, **49**, 695–702.
10 J. Zhang and R. Pelton, *Langmuir*, 1999, **15**, 8032–8036.
11 O. S. Deshmukh, A. Maestro, M. H. G. Duits, D. van den Ende, M. C. Stuart and F. Mugele, *Soft Matter*, 2014, **10**, 7045–7050.
12 L. Keal, V. Lapeyre, V. Ravaine, V. Schmitt and C. Monteux, *Soft Matter*, 2017, **13**, 170–180.
13 (*a*) K. Zielińska, H. Sun, R. A. Campbell, A. Zarbakhsh and M. Resmini, *Nanoscale*, 2016, **8**, 4951–4960; (*b*) K. Zielińska, R. A. Campbell, A. Zarbakhsh and M. Resmini, *Phys. Chem. Chem. Phys.*, 2017, **19**, 17173–17179.
14 K. Geisel, K. Henzler, P. Guttmann and W. Richtering, *Langmuir*, 2015, **31**, 83–89.
15 S. Matsui, T. Kureha, S. Hiroshige, M. Shibata, T. Uchihashi and D. Suzuki, *Angew. Chem., Int. Ed.*, 2017, **56**, 12146–12149.
16 (*a*) Z. Li, M. H. Kwok and T. Ngai, *Macromol. Rapid Commun.*, 2012, **33**, 419–425; (*b*) M. H. Kwok, Z. Li and T. Ngai, *Langmuir*, 2013, **29**, 9581–9591.
17 Z. Meng, M. H. Smith and L. A. Lyon, *Colloid Polym. Sci.*, 2009, **287**, 277–285.
18 D. Suzuki and H. Kawaguchi, *Colloid Polym. Sci.*, 2006, **284**, 1443–1451.
19 (*a*) D. Suzuki, H. Taniguchi and R. Yoshida, *J. Am. Chem. Soc.*, 2009, **131**, 12058–12059; (*b*) D. Suzuki, T. Kobayashi, R. Yoshida and T. Hirai, *Soft Matter*, 2012, **8**, 11447–11449; (*c*) S. Matsui, T. Kureha, Y. Nagase, K. Okeyoshi, R. Yoshida, T. Sato and D. Suzuki, *Langmuir*, 2015, **31**, 7228–7237.
20 M. Ghaedi, A. Ansari, M. H. Habibi and A. R. Asghari, *J. Ind. Eng. Chem.*, 2014, **20**, 17–28.
21 (*a*) D. Suzuki and K. Horigome, *Langmuir*, 2011, **27**, 12368–12374; (*b*) K. Horigome and D. Suzuki, *Langmuir*, 2012, **28**, 12962–12970; (*c*) D. Suzuki and K. Horigome, *J. Phys. Chem. B*, 2013, **117**, 9073–9082.

Supporting Information

The Deformation of Hydrogel Microspheres at the Air/Water Interface

Haruka Minato,[†] Masaki Murai,[†] Takumi Watanabe,[†] Shusuke Matsui,[†] Masaya Takizawa,[†] Takuma Kureha*[†] and Daisuke Suzuki*[,†,‡]

[†] Graduate School of Textile Science & Technology, Shinshu University, 3-15-1, Tokida Ueda 386-8567 Japan

[‡] Division of Smart Textiles, Institute for Fiber Engineering, Interdisciplinary Cluster for Cutting Edge Research, Shinshu University, 3-15-1 Tokida Ueda 386-8567, Japan

*Author to whom correspondence should be addressed.
E-mail: d_suzuki@shinshu-u.ac.jp (D.S.) 15st105g@shinshu-u.ac.jp (T.K.).

Experimental Procedures

Materials

N-isopropyl acrylamide (NIPAm, 98%), glycidyl methacrylate (GMA, 95%), *N*,*N*'-methylenebis(acrylamide) (BIS, 97%), 2,2'-azobis(2-methylpropinamidine) dihydrochloride (V-50, 95%), potassium peroxodisulfate (KPS, 95%), sodium chloride (NaCl, 99.5%), Rhodamine 6G (R6G), and 3-mercaptopropane sulfonic acid (MPSA) were purchased from Wako Pure Chemical Industries and used as received. Acrylic acid (AAc, 99%) was purchased from Sigma Aldrich and used as received. The $Ru(bpy)_3$ monomer (4-vinyl-4'-methyl-2,2'-bipyridine)bis(2,2'bipyridine)ruthenium(II)bis(hexafluorophosphate) was synthesized according to a previously reported procedure.[1] Distilled and ion-exchanged (EYELA, SA-2100E1) water was used in all experiments.

Synthesis of microgels by a modified aqueous precipitation polymerization

Poly(NIPAm-*co*-AAc) core–shell hydrogel microspheres (pNA microgels) (size > 6 μm) were prepared via a modified aqueous precipitation polymerization technique (**Scheme S1**). The polymerization was performed in a three-necked round-bottom flask (200 mL) equipped with a mechanical stirrer, a condenser, and a nitrogen gas inlet. Typically, the NIPAm monomer (0.6 g), AAc comonomer (63.2 μL), and cross-linker BIS (0.0098 g) were dissolved in deionized water (55 mL). The monomer solution was heated to 40 °C under a stream of nitrogen and constant stirring (250 rpm). The solution was sparged with nitrogen for a period of at least 30 min in order to remove any dissolved oxygen. Subsequently, the free-radical polymerization was initiated with KPS

(0.055 g) dissolved in deionized water (1 mL). Immediately after the initiation, the temperature was increased from 40 °C to 60 °C using a temperature gradient of 1 °C/3 min. Thereafter, a mixture of NIPAm monomer (3.5 g), AAc comonomer (875 μL), cross-linker BIS (pNA(1.4): 0.0927 g or pNA(2.7): 0.1855 g), and NaCl (0.0204 g, 10 mM) dissolved in deionized water (35 mL) was added to the reaction mixture at a feeding rate of 0.1 mL/min using a syringe pump. After 5 h, the feeding was stopped, and the reaction was stirred for 2 h at 60 °C, after which the microgel dispersion was cooled in an ice bath to stop the polymerization. The obtained microgels were purified twice by centrifugation/re-dispersion in water using a relative centrifugal force (RCF) of 20,000 g to remove unreacted reagents and other impurities. Similar to the synthesis of pNA microgels, pure pNIPAm microgels (both positively and negatively charged), poly(NIPAm-*co*-GMA) microgels, and poly(NIPAm-*co*-Ru(bpy)$_3$) were prepared via this modified aqueous precipitation polymerization. **Table S1** summarizes the details for the polymerization and **Figure S1** shows the optical microscopy images and chemical composition of these microgels.

Characterization of the microgels

Microgels in aqueous solution were observed with an optical microscope (BX51 or BX53, Olympus) equipped with a fluorescence system (ramp: U-RFL-T, excitation: 460-495 nm, emission: 510 nm) and a digital camera (ImageX Earth Type A-5.0M Ver. 3.0.4, Kikuchi-Optical Co., Ltd.) or high-speed camera (AX50 2SA, Photron). Note that the images shown in **Figure 4** were observed with an optical microscope (Axio Scope. A1, Zeiss) equipped with a fluorescence system (ramp: HBO-100, excitation: 450-490 nm, emission: 510 nm) and a digital camera (ImageX Earth Type S-2.0M Ver. 3.1.3, KikuchiOptical Co., Ltd.). These fluorescence systems were used to excite the fluorescent dye Rhodamine 6G. The microgels were transferred into rectangular Vitrotube borosilicate capillaries (0.1 × 2.0 mm) by capillary action. In order to observe the microgels in detail, colloidal crystals of the microgels were obtained through a thermal annealing process at a concentration close to the critical concentration.

Dye labeling experiments

After labeling the obtained pNIPAm-based microgels with ~0.0001 wt% R6G at a microgel concentration of ~0.003 wt%, the samples were purified via centrifugation/re-dispersion in water using a relative centrifugal force (RCF) of 20,000 g to remove any excess R6G. The samples were observed by fluorescence microscopy.

Calculation of the critical concentration

The intrinsic viscosity ([η]) of each microgel at 25 °C was evaluated from the viscosity of sufficiently diluted dispersions measured with an Ubbelohde viscometer. As it is customary when dealing with microgels, the apparent volume fraction of the microgels (ϕ_{eff}; $\phi_{\mathrm{eff}} \equiv c[\eta]/2.5$) was employed as a simple measure of the degree of packing, although ϕ_{eff} deviates from the real volume fraction in the concentrated regime where the microgels undergo deformation, deswelling, and interpenetration. The critical concentration, C^*, was a concentration of $\phi_{\mathrm{eff}} = 1$.

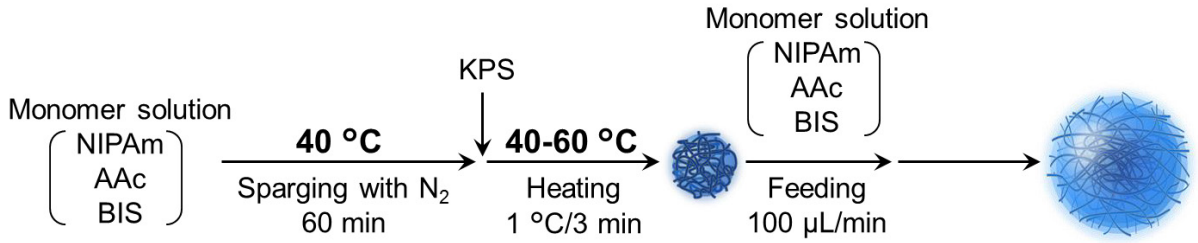

Scheme S1. pNA core–shell microgels prepared via a modified aqueous precipitation polymerization.

Table S1. Chemical composition and diameter of the pNIPAm-based microgels developed in this study

Code	Core monomer			Shell monomer					Temp. (°C)	Initiator		Diameter (N = 50)	
	NIPAm (mol%)	BIS (mol%)	AAc (mol%)	NIPAm (mol%)	AAc (mol%)	GMA (mol%)	$Ru(bpy)_3$ (mol%)	BIS (mol%)		KPS (mM)	V-50 (mM)	in a rectangle capillary (μm)	at the air/water interface (μm)
pNA(1.4)	84	1	15	69.7	28.9	-	-	1.4	40→60	3.6	-	6.3 ± 0.4	20 ± 2
pNA(2.7)	84	1	15	68.8	28.5	-	-	2.7	40→60	3.6	-	4.2 ± 0.1	7.9 ± 0.2
pN/KPS	99	1	-	99	-	-	-	1	35→60	3.6	-	2.5 ± 0.2	3.4 ± 0.1
pN/V-50	99	1	-	99	-	-	-	1	40→60	-	3.6	2.5 ± 0.1	3.5 ± 0.2
pNG	99	1	-	69	-	27	-	4	40→60	-	3.6	2.0 ± 0.1	2.4 ± 0.1
pNG-MPSA*	-	-	-	-	-	-	-	-	-	-	-	4.1 ± 0.2	4.9 ± 0.1
pNRu	99.9	0.1	-	94.7	-	-	3.7	1.6	40→60	-	3.6	4.3 ± 0.3	10 ± 1

*pNG-MPSA microgels were prepared from pNG microgels according to a previous report.[2] Briefly, a mixture of pNG microgels (0.5 g), MPSA (ten times the amount of epoxy groups in the pNG microgels), and water (45 g) was poured in a 100-mL glass vial with stirring at room temperature, and the pH was adjusted to 11 with 1 M NaOH. The reaction was continued for 24 h. The obtained pNG–MPSA microgels were purified twice by centrifugation/redispersion in water using a relative centrifugal force (RCF) of 20,000*g* to remove impurities.

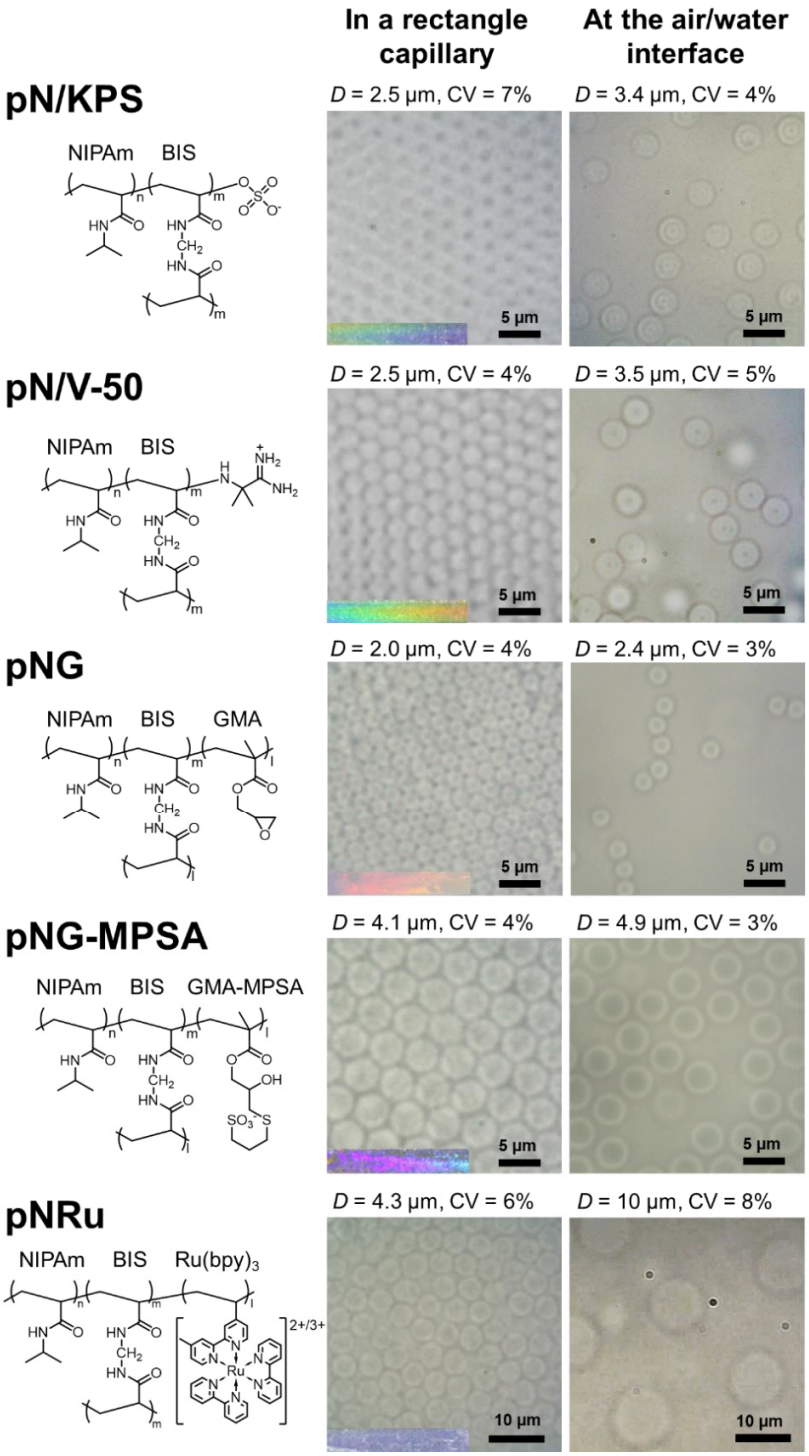

Figure S1. Optical microscopy images of different microgels. Inset photographs show colloidal crystals composed of each microgel. The microgels were observed in a rectangle capillary at high concentration (left column) and at the air/water interface (right column) of the dispersion droplets (N = 30). From these images, it is clear that these microgels are uniform, and that the applied synthetic method should be applicable to various pNIPAm-based microgels.

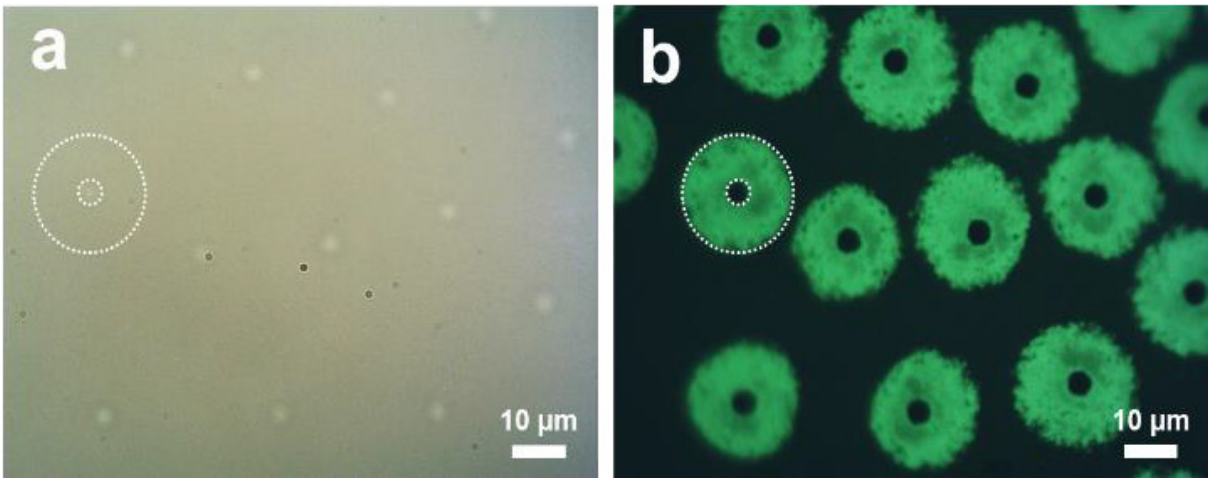

Figure S2. (a) Optical and (b) fluorescence microscopy images of the same pNA microgels after labelling with R6G dye molecules. The same area was observed at the air/water interface of the dispersion droplet at pH = 7 and 25 °C. The white dotted lines indicate the core part and the surface of an individual microgel.

Table S2. Deformation kinetic parameters of the pseudo-second-order model and parameter calculated from optical microscopy images of pNA(1.4) and pNA(2.7) microgels

Microgels	Plot parameters			Calculated parameter
	k_2 (μm^{-1} sec^{-1})	D_e (μm)	R^2	D_{ads}/D_{C^*}
pNA(1.4)	2.74	20.1	0.9995	3.2
pNA(2.7)	10.4	4.43	0.9968	1.9

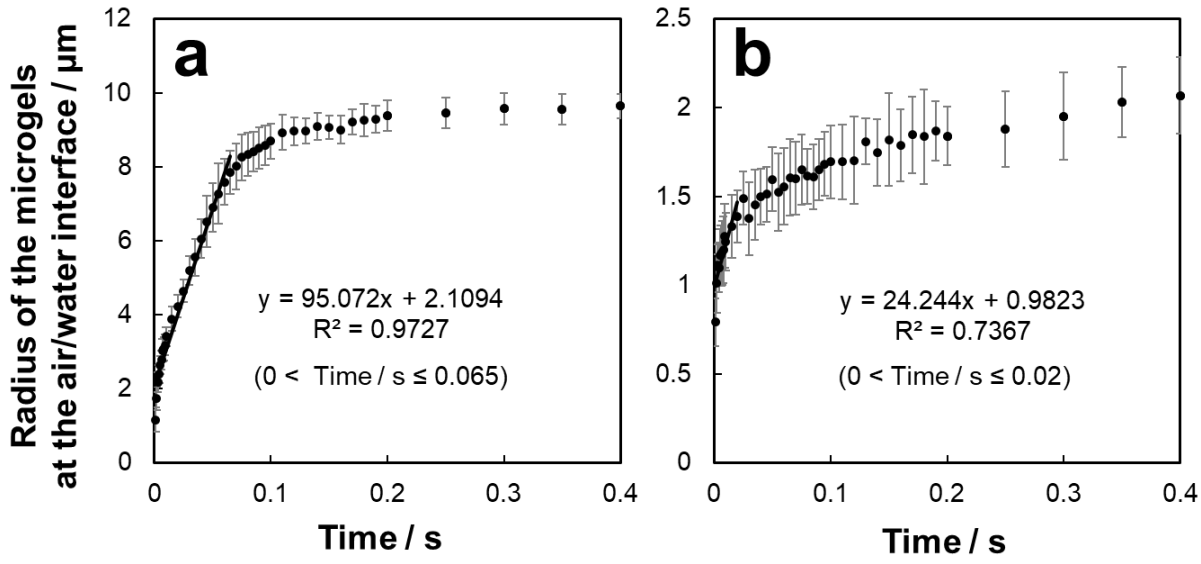

Figure S3. Radius of (a) pNA(1.4) and (b) pNA(2.7) microgels as a function of time at the air/water interface, which were calculated from the diameter (**Figure 2**).

Movie S1. Optical microscopy movie of pNA(1.4) microgels observed in a rectangle capillary.

Movie S2. Moment of adsorption and deformation of individual pNA(1.4) microgels at the air/water interface.

Movie S3. Moment of adsorption and deformation of individual pNA(2.7) microgels at the air/water interface.

REFERENCES

(1) P. K. Ghosh and T. G. Spiro, *J. Am. Chem. Soc.,* 1980, **102**, 5543-5549.
(2) D. Suzuki and H. Kawaguchi, *Colloid Polym. Sci.,* 2006, **284**, 1443-1451.

LANGMUIR
Article
Cite This: Langmuir 2019, 35, 10412−10423
pubs.acs.org/Langmuir

Effect of Charge Groups Immobilized in Hydrogel Microspheres during the Evaporation of Aqueous Sessile Droplets

Haruka Minato,[†] Masaya Takizawa,[†] Seina Hiroshige,[†] and Daisuke Suzuki*[,†,‡,§]

[†]Graduate School of Textile Science & Technology, [‡]Institute for Fiber Engineering, and [§]Research Initiative for Supra-Materials, Interdisciplinary Cluster for Cutting Edge Research, Shinshu University, 3-15-1 Tokida, Ueda, Nagano 386-8567, Japan

Supporting Information

ABSTRACT: In contrast to conventional dispersions of solid microspheres, dilute dispersions containing soft hydrogel microspheres (microgels) exhibit unique drying behavior due to their selective adsorption at the air/water interface of sessile droplets. So far, the impact of the size, chemical composition, and softness (degree of cross-linking) of microgels has been investigated. In the present study, we present the impact of charged groups introduced in the microgels on the adsorption and assembly behavior of these microgels at the air/water interface using a series of microgels with different amounts and distribution of charged groups. A series of experiments under different conditions (pH value and ionic strength) afforded information that clarified the adsorption, interpenetration, and deformation behavior of such charged microgels at the air/water interface. The results indicate that the adsorption and the deformation of charged microgels at the air/water interface are suppressed by the presence of charged groups. Moreover, charged microgels adsorbed at the interface are more dynamic and not highly entangled with each other; i.e., even though the more dynamic charged microgels are arranged at the interface, these arranged structures are disrupted upon transferring onto the solid substrates. Our findings of this study can be expected to promote the further development of applications, e.g., foams and emulsions stabilized by microgels, that crucially requires an in-depth understanding of the adsorption behavior of charged microgels at the air/water interface such as coatings.

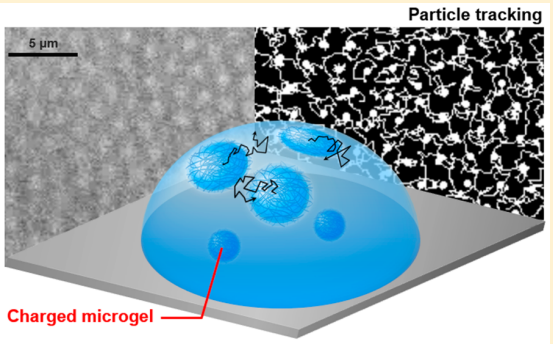

INTRODUCTION

Hydrogel microspheres (microgels), which are colloidal particles of cross-linked hydrated polymer networks, have attracted much attention due to a wide range of potential applications in, e.g., chemical or biosensors,[1−5] selective separations,[6−8] stabilizers for emulsions,[9−13] autonomous materials,[14,15] and drug-delivery systems.[16−18] The high utility of microgels can be mostly attributed to their fascinating physicochemical properties such as softness (degree of cross-linking), which can be tuned by applying external stimuli. In a series of fundamental studies, thermoresponsive poly(*N*-isopropylacrylamide) (pNIPAm) microgels (or derivatives thereof) have been widely used as they can be synthesized in uniform size by aqueous free radical precipitation polymerization.[19,20] So far, many functionalized microgels that can respond to stimuli such as changes in ionic strength or pH value, chemical reactions, light, and the presence/absence of biomolecules have been reported.[14,15,20−25] Among these functionalizations, the copolymerization with appropriately designed monomers is the most widely used and conventional approach due to the simplicity of the procedure. For instance, pH-responsive microgels are obtained from copolymerizations with, e.g., acrylic or methacrylic acid monomers.[21] Furthermore, autonomously oscillating microgels, which show periodic swelling/deswelling and assembling/disassembling oscillations, are obtained from copolymerizations with charged catalysts such as ruthenium complexes in order to be able to respond to cyclic redox reactions.[14,15]

From a materials science point of view, the assembly of such microgels is important to obtain thin films or hierarchical bulk gels that show additional functionality. For instance, films of microgels copolymerized with amine groups[26,27] show faster and increased absorption and desorption of CO_2 than those of dispersions or bulk gels.[28,29] Microgels copolymerized with phenylboronic acid groups respond to glucose, which is expected to find applications in color-changing sensors.[23,30]

So far, many methods for microgel assemblies, including dip- and spin-coating, have been reported.[31−37] Our group has been investigating the self-organization of microgels during the evaporation of aqueous sessile droplets in order to generate thin microgel films.[36−39] We have previously discovered that soft and surface-active microgels based on, e.g., pNIPAm, spontaneously adsorb on the air/water interface of the droplet when sessile droplets are evaporated.[36,40] Subsequently, the adsorbed microgels are slowly arranged at the interface, and

Received: June 25, 2019
Published: July 12, 2019

DOI: 10.1021/acs.langmuir.9b01933
Langmuir 2019, 35, 10412−10423

finally the arranged microgel monolayers are transferred onto the solid substrate,[36] which stands in sharp contrast to rigid microspheres made of, e.g., polystyrene or silica.[41] To clarify the details of the formation mechanism, understanding the behaviors of microgels at the air/water interface (e.g., adsorption, interpenetration, and deformation) is crucial. During the drying process, the size of the microgels is not crucial because the microgels are moved to the air/water interface by convection flow; however, the softness (degree of cross-linking) of the individual microgels is very important: the softer the microgels are, the faster the microgels adsorb at the air/water interface.[38] It has also been clarified that individual microgels are substantially deformed immediately upon attaching to the air/water interface, which was observed directly with an optical microscope equipped with a high-speed camera.[42]

We hypothesized that if the aforementioned charged (or functionalized) microgels could be combined with the method we developed, a variety of functionalized thin films of polyelectrolytes could potentially be obtained in an operationally simple and low-cost fashion within a short period of time, which would be useful for all applications that these microgel assemblies have already found. In this study, we initially investigated the effect of charged groups immobilized in the microgels on the self-organization during the evaporation of aqueous sessile droplets. Especially, the impact of the charged groups in the microgels on their adsorption, interpenetration, and deformation behavior at the air/water interface was systematically investigated using a series of dispersions of charged microgels. We are convinced that our results on the behavior of microgels at the air/water interface will contribute to the development of further applications for, e.g., microgel-stabilized foams and emulsions, where the understanding of the behavior of functional microgels on the air/water interface is of paramount importance.

EXPERIMENTAL DETAILS

Materials. *N*-Isopropylacrylamide (NIPAm, purity 98%), *N*,*N*′-methylenebis(acrylamide) (BIS, 97%), potassium peroxodisulfate (KPS, 95%), 2,2′-azobis(2-methylpropinamidine) dihydrochloride (V-50, 95%), rhodamine 6G (R6G), disodium hydrogen phosphate (99%), citric acid (98%), hydrochloric acid (HCl), hydroxide solution (NaOH), and sodium chloride (NaCl, 99.5%) were purchased from FUJIFILM Wako Pure Chemical Corporation (Japan) and used as received. Acrylic acid (AAc, 99%) was purchased from Sigma-Aldrich and used as received. The monomer (4-vinyl-4′-methyl-2,2′-bipyridine)bis(2,2′bipyridine)ruthenium(II)bis (hexafluorophosphate) ($Ru(bpy)_3$) was synthesized according to a previously reported procedure.[43] Water for all reactions, including the preparation of solutions and the purification of polymers, was initially distilled and subsequently subjected to ion exchange (EYELA, SA-2100E1). Glass substrates (Neo Micro Cover Glass, Matsunami Glass Ind., Ltd.) were used after cleaning using (1) detergent in water and (2) pure water.

Preparation of Charged Microgels. Negatively charged microgels were prepared by aqueous free radical precipitation copolymerization of NIPAm and AAc.[11] The copolymerizations were performed in a three-necked round-bottom flask equipped with a mechanical stirrer, a condenser, and a nitrogen gas inlet. The initial total concentration of each monomer for the microgels was 150 mM. Initially, the monomer solutions were prepared and dissolved in water in the three-necked round-bottom flask and heated to 70 °C under a stream of nitrogen and constant stirring (250 rpm). The solutions were allowed to stabilize for at least 30 min prior to initiating the polymerization in order to remove any dissolved oxygen. Subsequently, the free-radical polymerizations were initiated with KPS (2 mM) dissolved in water. The solutions were stirred for 4 h, and after completion of the polymerization, the obtained dispersions were cooled to room temperature. The microgels were purified via two cycles of centrifugation/redispersion in water using a relative centrifugal force (RCF) of 70 000 G for ∼90 min (Avanti J-26S XP, Beckman Coulter Inc.), followed by dialysis using cellulose tubing (36/32, Viskase Companies, Inc.) in water for around 1 week, whereby the water was changed daily. Henceforth, the obtained p(NIPAm-*co*-AAc) microgels will be denoted as NA*X*, whereby *X* represents the amount of charged AAc monomer (mol %). The pNIPAm microgels (henceforth denoted as N) were prepared by temperature-programmed precipitation polymerization to increase their size, which is necessary for evaluating the individual microgels with an optical microscope.[38] After initiation of the polymerization, the temperature of the reaction solution was gradually increased from 45 to 70 °C (1 °C/3 min). The solution was stirred for 6 h, and the obtained dispersion was cooled to room temperature. The microgels were purified via two cycles of centrifugation/redispersion in water using an RCF of 70 000 G for ∼45 min (Avanti J-26S XP, Beckman Coulter Inc.), followed by dialysis using cellulose tubing in water for 3 days, whereby the water was changed daily.

Preparation of Charged Core/Shell Microgels. To check the potential influence of the pNIPAm shell that contains the charged core on the self-organization, core/shell microgels (henceforth referred to as CS) were prepared by seeded precipitation polymerization in the presence of charged microgels.[44] The polymerization was performed in a three-necked round-bottom flask (50 mL) equipped with a mechanical stirrer, a condenser, and a nitrogen gas inlet. Initially, the flask was charged with water (18.23 g), which was heated to 70 °C under a stream of nitrogen and constant stirring (250 rpm). The water was allowed to stabilize for 30 min prior to initiating the polymerization in order to remove any dissolved oxygen. Subsequently, seed microgels (NA5, 2.08 wt %, 5.77 g) and KPS (0.016 g) dissolved in water (1 mL) were added into the system to start the polymerization. After 5 min, the core NA5 microgels had shrunk sufficiently, and a mixture of NIPAm monomer (99 mol %, 0.6720 g) and cross-linker BIS (1 mol %, 0.0096 g) dissolved in water (5 mL), which had been heated to 70 °C under a stream of nitrogen, was added to the reaction mixture. The solution was stirred for 4 h, and after completion of the polymerization, the obtained dispersions were cooled to room temperature. The microgels were purified via several cycles of centrifugation/redispersion in water to remove unreacted reagents and other impurities using an RCF of 70 000 G for ∼30 min (Avanti J-26S XP, Beckman Coulter Inc.).

Preparation of Micron-Sized, Fluorescent, and Charged Microgels. To investigate the deformation of individual microgels upon adsorption at the air/water interface, micron-sized, fluorescent, and charged poly(NIPAm-*co*-$Ru(bpy)_3$) microgels (NRu microgels) were prepared via a modified aqueous precipitation polymerization technique that we have previously reported.[42] The polymerization was performed in a three-necked round-bottom flask (300 mL) equipped with a mechanical stirrer, a condenser, and a nitrogen gas inlet. Initially, the NIPAm monomer (0.6 g) and cross-linker BIS (0.0008 g) were dissolved in deionized water (55 mL). The monomer solution was heated to 40 °C under a stream of nitrogen and constant stirring (250 rpm). After sparging with nitrogen for a period of at least 30 min, the free-radical polymerization was initiated with V-50 (0.055 g) dissolved in water (1 mL). Immediately after the initiation, the temperature was gradually increased from 40 to 60 °C (1 °C/3 min). Thereafter, a mixture of NIPAm (1.0 g), $Ru(bpy)_3$ comonomer (0.135 g), cross-linker BIS (0.053 g), and NaCl (0.1753 g, 30 mM) dissolved in deionized water (100 mL) was added to the reaction mixture at a feeding rate of 0.8 mL/min using a syringe pump. After 90 mL of the mixture was added, the reaction was stirred for 2 h at 60 °C. Finally, the obtained microgel dispersion was cooled to stop the polymerization. The microgels were purified twice by centrifugation/redispersion in water to remove unreacted reagents and other impurities, followed by dialysis in water for around 1 week. It should be noted here that the obtained NRu microgels showed absorption peaks at 288 and 457 nm and a fluorescence emission peak at 602 nm upon photoirradiation at 457 nm (Figure S1).

DOI: 10.1021/acs.langmuir.9b01933
Langmuir 2019, 35, 10412−10423

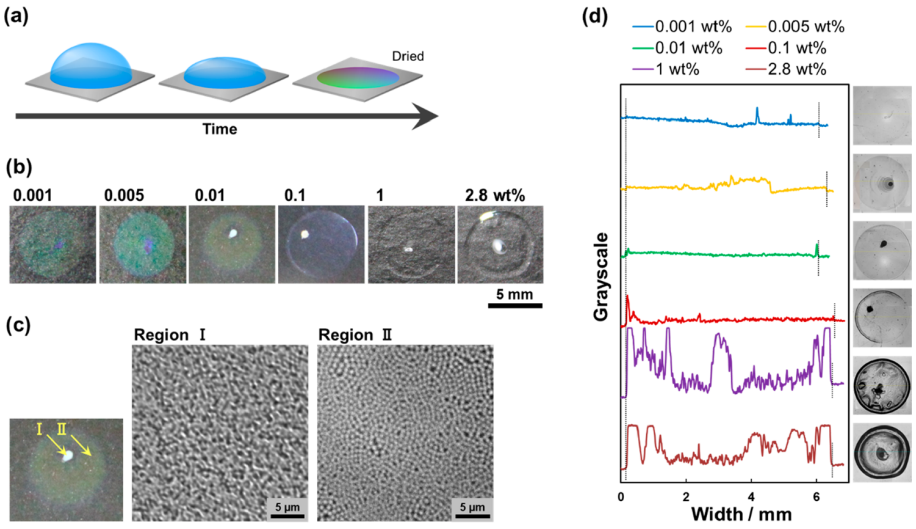

Figure 1. (a) Schematic illustration of the drying phenomenon of microgel sessile droplets. (b) Photographs of dried thin films containing N microgels formed after 30 μL of microgel droplets were dried at room temperature (~25 °C, ~70% humidity) on glass substrates at different microgel concentrations. (c) Optical microscopy images of the thin films dried at 0.01 wt %. Two of the images show an enlarged view of region I and II. (d) Plot profile of each thin film dried at different concentrations. The dotted black line shows the boundary between the film and the substrate.

Characterization of the Microgels. The microgels were examined with an optical microscope (BX51, Olympus) equipped with a digital camera (ImageX Earth Type S-2.0 M Ver.3.0.5, Kikuchi-Optical Co., Ltd.). All microgel diameters were determined by measuring the center-to-center distance between neighboring microgels in order to calculate relatively accurate microgel diameters under low-contrast conditions. For the calculations, we used the ImageJ software (1.49v, Wayne Rasband, National Institutes of Health) (N = 50) on optical microscopy images of colloidal crystals formed in glass capillaries. Colloidal crystals were prepared by transferring microgel dispersions into rectangular Vitrotube borosilicate capillaries (0.1 × 2.0 mm) using the capillary force. The microgels concentration was tuned to the critical concentration, C^* (g/mL), where the apparent volume fraction (Φ_{eff}, $\Phi_{eff} = [\eta]C/2.5$) equals 1.[42,45] Here, Φ_{eff} was calculated from the intrinsic viscosity, while $[\eta]$ (mL/g) was measured at 25 °C using an Ubbelohde viscometer. It should be noted that Φ_{eff} is used as a simple measure for the degree of packing, even though Φ_{eff} deviates from the real volume fraction in the concentrated regime where the microgels can deform, deswell, and/or interpenetrate.[45]

The amount of acrylic acid introduced in the microgels was determined by conductometric titrations. The microgel dispersions were adjusted to pH ≈ 11 with a 1 M NaOH solution. The titrations were performed using standardized HCl solutions (0.1 or 0.01 M).

The electrophoretic mobility (EPM) of the microgels was evaluated using a Zetasizer Nano ZS instrument (Malvern Panalytical). The average EPM was calculated from three individual measurements. These measurements were conducted at a microgel concentration of 0.001 wt % at 25 °C in pure water. For the NA5 and NRu microgels, the EPM measurements were conducted at a microgel concentration of 0.001 wt % at 25 °C in a 1 mM NaCl solution in order to investigate the effect of the presence of NaCl.

The surface tension of the microgel dispersions was determined using the Wilhelmy plate method with a surface tensiometer (Automatic Surface Tensiometer Model CBVP-Z, Kyowa Interface Science Co., Ltd.) and a Pt plate at 25 °C, 24 h after placing each solution or dispersion (5 mL) in a glass dish. Average surface tension values were calculated from three individual measurements.

The amount of $Ru(bpy)_3$ monomer introduced in the microgels was estimated using UV−vis spectrophotometry measurements (V-630iRM, JASCO) at an absorbance of 458 nm, which is the wavelength of the maximum absorbance for $[Ru(bpy)_3]^{2+}$.

The absorption and emission spectra of NRu microgels were evaluated at 25 °C in pure water using a UV−vis spectrophotometer (V-630iRM, JASCO) and fluorescence spectrophotometer (FP-6300, JASCO), respectively.

Characterization of the Drying Phenomena. As a macroscopic evaluation, the shape of the sessile droplets during drying and the resulting dried structures were evaluated with a digital camera (Canon, EOS kiss ×4). The dispersions (30 μL) were dried on glass substrates (Neo Micro Cover Glass, Matsunami Glass Ind., Ltd.) at 25 ± 2 °C (Figure 1a). These substrates were used after cleaning with (1) detergent in water and (2) pure water. The homogeneity of the distribution of the microgels in the films was compared by evaluating the grayscale, which was calculated using the "plot profile (ImageJ software)" of a straight line drawn on the observed optical microscopy images at the center of each film. In the optical microscopy observations, the images are darkened in the presence of packed microgels.

As a microscopic evaluation, the air/water interface at the center and the edge of the sessile droplet (1 μL) was observed at 25 ± 2 °C with an optical microscope (BX51, Olympus) equipped with a digital camera (ImageX Earth Type S-2.0 M Ver.3.0.5, Kikuchi-Optical Co., Ltd.). The number of microgels adsorbed at the air/water interface was calculated based on the optical microscopy movies. The pH value of the dispersions was controlled using McIlvaine buffers composed of 50 mM disodium hydrogen phosphate and 25 mM citric acid or using simple electrolytes such as HCl, NaOH, and NaCl. Here, the concentration of the microgel dispersions was calculated based on the weight of the microgels after drying. The concentrations of dispersions were decreased or increased by diluting (with water) or centrifuging the dispersions, respectively.

Evaluation of the Mean-Squared Displacements. To quantify the motion of microgels at the air/water interface, the microgel positions in an image time series recorded by optical microscopy were analyzed using the mean-squared displacement (MSD) as a function of the lag time (τ).[46,47] The particle-tracking data were obtained by tracking the position of the microgels in a movie of ~6 s (30 frame s^{-1}) using the "Pointing Cell Tracking" tool of the ImageJ software. The MSD of microgels adsorbed at the interface is given by

$$\mathrm{MSD}(\tau) = \langle (r_i(t+\tau) - r_i(t))^2 \rangle_{i,t} \quad (1)$$

where $r_i(t)$ is the position vector of ith particle at time t, and $\langle\rangle_{i,t}$ indicates the average over the data of the microgels. In the liquid

DOI: 10.1021/acs.langmuir.9b01933
Langmuir 2019, 35, 10412−10423

Table 1. Chemical Composition and Characteristics of the Negatively Charged Microgels

c	NIPAm (mol %)	BIS (mol %)	AAc (mol %)	diameter (nm)	−COOH content (mmol/g)	EPM (10^{-8} $m^2/(V\ s)$)	$[\eta]$ (mL/g)
[a]N	99	1	–	939 ± 68	N.D.	−1.26 ± 0.07	59.7
NA1	98	1	1	745 ± 75	0.11	−1.90 ± 0.03	79.7
NA5	94	1	5	1167 ± 50	0.42	−2.08 ± 0.18	166
NA10	89	1	10	1178 ± 104	1.18	−2.24 ± 0.03	163
NA20	79	1	20	1251 ± 61	2.22	−2.81 ± 0.06	322
NA50	49	1	50	1549 ± 108	5.18	−2.84 ± 0.14	482
[b]CS	99	1	–	1082 ± 73	0.24	−1.24 ± 0.05	41.0

[a]Reproduced with permission from ref 38. Copyright (2018) American Chemical Society. [b]Core/shell (CS) microgels were prepared by seeded precipitation polymerization using NA5 microgels as seeds.

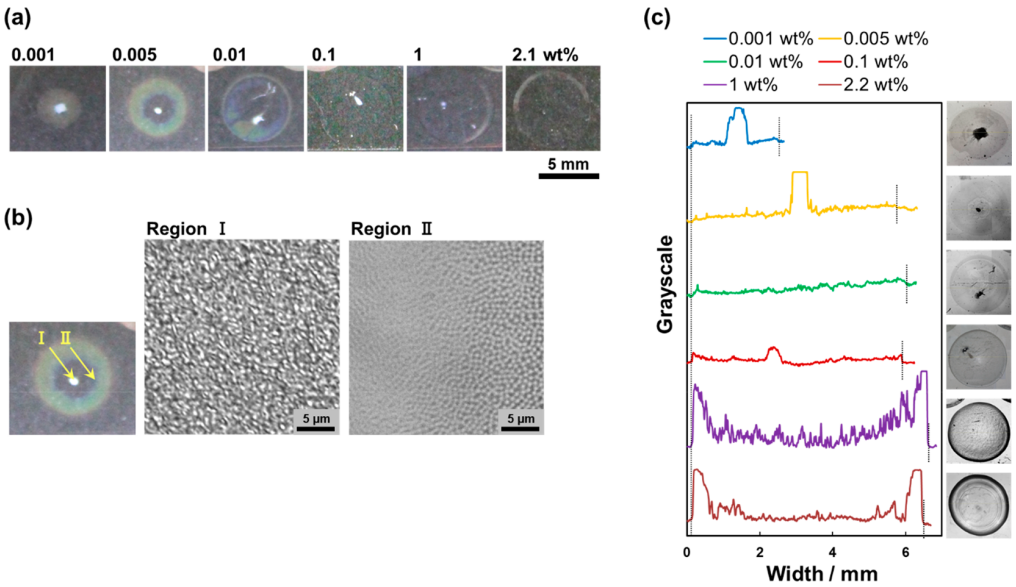

Figure 2. (a) Photographs of dried thin films containing NA5 microgels. Thirty microliters of droplets were dried at room temperature (~25 °C, ~70% humidity) on glass substrates at different NA5 microgel concentrations. (b) Optical microscopy images of a thin film dried at 0.005 wt %. Two of the images show an enlarged view of region I and II. (c) Plot profile of each thin film dried at different concentrations. The dotted black line shows the boundary between the film and the substrate.

regime, where the particle motion is expected to be purely diffusive, the MSD should be proportional to the lag time, τ

$$\mathrm{MSD}(\tau) = 2dD\tau \quad (2)$$

where d is the dimensionality of the displacement vectors and D is the self-diffusion coefficient. The movie of the microgels adsorbed at the air/water interface only provides their movement in two dimensions, and therefore $d = 2$ for the obtained optical microscopy movies.[47]

Deformation Analysis of Individual Charged Microgels. The deformation of microgels at the air/water interface of droplets was observed with an optical microscope (BX53, Olympus) equipped with a fluorescence system (ramp: U-RFL-T, wavelength: 451−485 and 541−565 nm) and a high-speed camera (monochrome AX50 2SA, Photron). It should be noted here that the deformation was observed for only a few minutes after the dispersion droplet was deposited onto the glass substrate in order to ignore the influence of the increasing salt concentration as a result of the drying of the water.

RESULTS AND DISCUSSION

Synthesis and Characterization of the Polyelectrolyte Microgels. First, charged (or polyelectrolyte) microgels were synthesized by a conventional free radical precipitation polymerization with NIPAm and AAc, where the feed ratio of AAc was changed (NA*X* microgels, $1 \leq X \leq 50$ mol %). The size of all (~1 μm) was uniform, which was confirmed by optical microscopy images for a concentration of C^* for these microgels (Table 1, Figure S2a−f). The number of carboxyl groups incorporated in the microgels increased with increasing the proportion of the AAc fed during the polymerization (Table 1), and thus, the EPM, which is an indicator of the surface-charge density, showed negative values for all NA microgels. It has been reported that relatively uniform charge distribution in microgels is realized for poly(NIPAm-*co*-AAc) microgels prepared by precipitation polymerization, as the reactivity ratios of NIPAm and AAc are similar ($r_1 = 0.57$ and $r_2 = 0.32$).[48−50] Thus, we assumed that the amount of carboxyl groups would increase both on the surface and within the microgels. Indeed, the EPM values gradually decreased upon increasing the incorporated amount of AAc (Table 1), indicating that the surface-charge density originates from the carboxyl group increase. Additionally, the intrinsic viscosity $[\eta]$, which is an indicator of the degree of swelling, increased with the amount of incorporated AAc (Table 1), indicating that the amount of carboxyl groups increased within the microgels and on the surface.

Next, core/shell structures were formed by adding AAc-free pNIPAm hydrogel shell onto NA5 microgels by seeded precipitation polymerization in order to investigate the effect of the charge distribution of the microgels on the drying

DOI: 10.1021/acs.langmuir.9b01933
Langmuir 2019, 35, 10412−10423

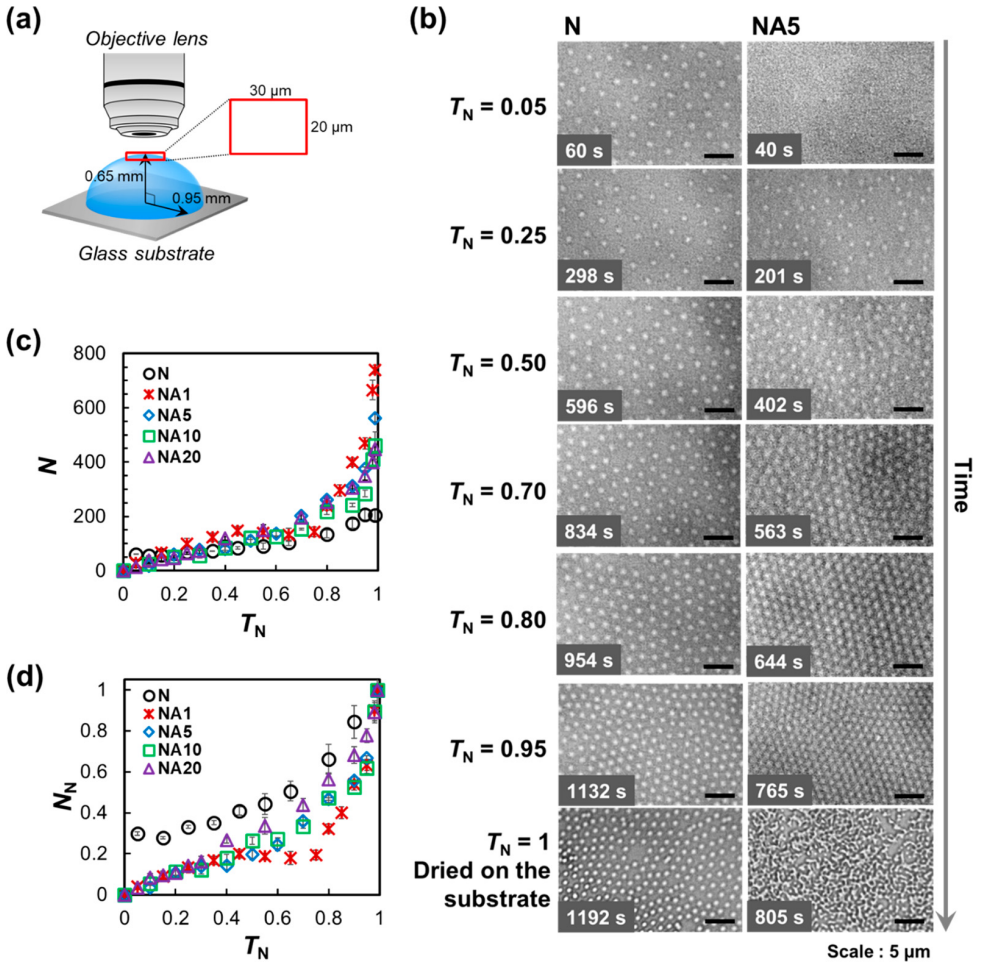

Figure 3. (a) Schematic illustration of the microscopic observation of the sessile droplets. The air/water interface at the center of the droplets was observed with an optical microscope. (b) Optical microscopy images of N and NA5 microgels at the air/water interface of each droplet on glass substrates as a function of the normalized time, T_N. Optical microscopy images of the NA1, NA10, and NA20 microgels are shown in Figure S5. It should be noted here that the NA50 microgels could not be observed due to their low contrast. (c) Adsorbed amount, N, and (d) normalized adsorbed amount, N_N, for each microgel as a function of T_N. The droplets were dried at room temperature (~25 °C, ~40% humidity) at concentrations of 0.003 wt % (N) or 0.005 wt % (NA1, NA5, NA10, and NA20).

behavior (Figure S2g).[44,51] After the shell was formded, the amount of carboxyl groups in the microgels decreased to approximately 50% (core NA5 microgels: 0.42 mmol/g; CS microgels: 0.24 mmol/g), indicating that a shell of similar weight was formed on the core microgel (NA5). In addition, the EPM value of the CS microgels approached that of AAc-free N microgels (EPM: -1.26×10^{-8} m^2/(V s) (N microgels), -2.08×10^{-8} m^2/(V s) (core NA5 microgels), and -1.24×10^{-8} m^2/(V s) (CS microgels)), suggesting that the core was completely covered with the shell. In addition, the $[\eta]$ value of the CS microgels was considerably lower than that of the core NA5 microgels, indicating that the shell restricts the swelling of the core, which has already been reported.[51]

Macroscopic Evaluation of Drying Microgel Sessile Droplets. As schematically illustrated in Figure 1a and reported in our previous study,[36,38] the self-organization of microgels was investigated at very low (~0.001 wt %) microgel concentrations, where soft and surface-active microgels are regularly arranged at the air/water interface, and the resulting films on the solid substrate exhibit iridescent structural colors. Therefore, in this study, we initially checked the dependence of the microgel concentration on the drying phenomenon. Figure 1b shows the result for N microgels (without AAc groups), i.e., the same ones used in our previous study.[38] Similar to our previous study, homogeneous monolayer films with iridescent structural colors were obtained at low microgel concentrations (0.001, 0.005 wt %). Upon increasing the concentration, a white dot appeared near the center of the dried films (≥0.01 wt %). As shown in Figure 1c, the microgels were more concentrated in the white dot (region I) than in region II (microgel size: 353 ± 91 nm (region I); 598 ± 71 nm (region II); N = 50). The white dot was formed at that position, where water was present up to complete evaporation of the droplet (Figure S3b, Movie S1) due to the transportation of excess microgels present in the bulk solution to this position by the convention flow. Furthermore, ringlike stains were observed for higher microgel concentrations (≥0.1 wt %, Figure 1b, d). These data indicate that excess microgels, i.e., N microgels dispersed within the droplets, are moved to the edge of the droplet by convection flow to form ringlike stains (Figure 1b, d, Figure S3c) or concentrated near the center of the droplet

DOI: 10.1021/acs.langmuir.9b01933
Langmuir 2019, 35, 10412−10423

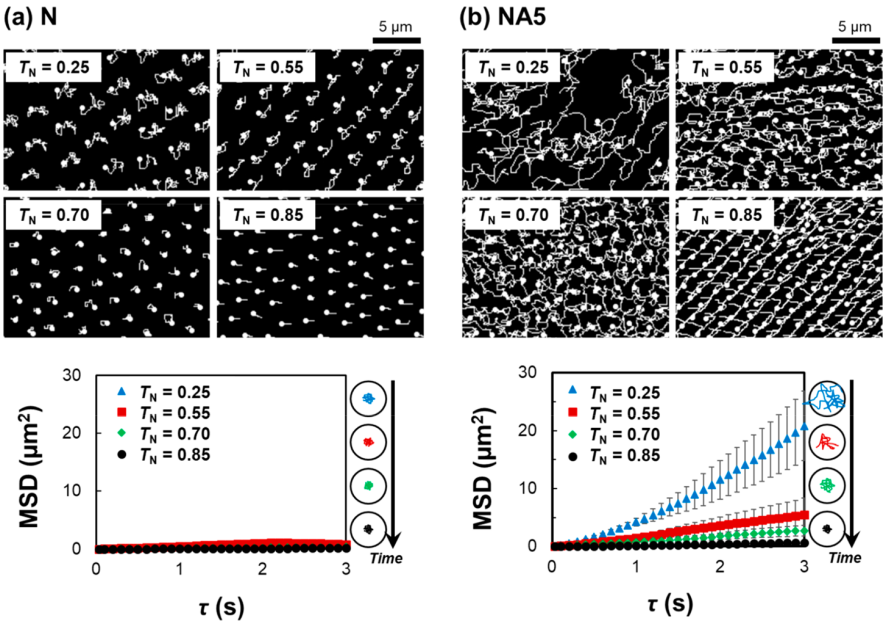

Figure 4. Particle-trajectory images and MSD plots of (a) N and (b) NA5 microgels adsorbed at the air/water interface of the sessile droplets at T_N = 0.25, 0.55, 0.70, and 0.85. The droplets were dried at room temperature (~25 °C, ~40% humidity) at 0.003 wt % (N) and 0.005 wt % (NA5) on a glass substrate.

(Figure 1c, Figure S3b, Movie S1), although these phenomena were not observed for lower microgel concentrations.

In contrast, homogeneous monolayer films showing iridescent colors could not be obtained for NA5 polyelectrolyte microgels, not even at low concentrations (0.001 and 0.005 wt % in Figure 2a). The appearance of white dots (Figure 2b) and ringlike stains (Figure 2c) was, as mentioned above, dependent on the concentration, albeit in a slightly different manner. It should be noted here that the homogeneous monolayer films could not be obtained for any of the negatively charged NA*X* microgels ($1 \leq X \leq 20$ mol %) at low concentrations (Figure S4a–c). In the case of the NA50 microgels, the resulting films could not be visualized and the boundary between films and the glass substrate could not be recognized as the NA50 microgels were highly swollen by water. However, homogeneous thin films showing iridescent colors could be obtained in the case of CS microgels, which contain a pNIPAm shell layer on a NA5 core, dried at low concentrations (0.001 wt % in Figure S4d). These results suggest that charged groups attached near the surface of the microgels affect the individual microgel motion within the sessile droplets.

Evaluation of Individual Polyelectrolyte Microgel Movements at the Air/Water Interface. Then, we microscopically investigated the drying process of the sessile droplets. First, the center of the droplet was monitored by optical microscopy (Figure 3a). At the early stage ($T_N \sim 0.05$; the normalized time, $T_N = T/T_{dried}$, where T and T_{dried} denote the arbitrary time and the time for complete drying, respectively.), as reported in our previous work,[38] control N microgels were immediately adsorbed and arranged with intervals at the air/water interface after dropping a dispersion (1 μL) on a glass substrate (Figure 3b). Then, the adsorbed amount, N (or normalized amount, $N_N = N/N_{dried}$, where N_{dried} denotes the adsorbed amount per unit of interfacial area when the droplet is completely dry) at the interface increased until completely drying, as the adsorbed and highly deformed microgels at the interface were increasingly compressed given that the total surface area of the sessile droplets decreased due to evaporation of water (Figure 3c, d).[38,42] Finally, the ordered structures formed at the interface were transferred onto the substrate without any structural disruption (Figure 3b: N).[38] In the case of the NA5 microgels, on the other hand, the microgels did not adsorb on the air/water interface at the early stage of drying (Figure 3b: NA5, $T_N \sim 0.05$). However, as time proceeded ($T_N \sim 0.25$), the microgels gradually adsorbed on and arranged at the interface (Figure 3b–d). Here, in contrast to the N microgels, there was no interval between the NA5 microgels (e.g., the images taken at $T_N \sim 0.70$, 0.80, 0.95). In the N microgel case, there are low-density polymers on the shell of the deformed microgels in the interval between the microgels,[42] which might be due to the suppression of the deformation of charged microgels at the air/water interface. It should be noted here that similar results were reported when charged microgels are observed at the oil/water interface.[13,52] Additionally, NA5 microgels are thermally fluctuated at the interface (vide infra). Furthermore, different from N microgels, the arranged structures of the NA5 microgels formed at the interface were not transferred without disrupting the structures when the water was completely evaporated (Figure 3b: NA5, $T_N \sim 1$). Similar behavior to that of the NA5 microgels was observed in the case of the NA1, NA10, and NA20 microgels (Figure 3c, d, Figure S5), indicating that the charged groups immobilized in the microgels lower the adsorption rate of the microgels at the air/water interface and affect each characteristic process of the drying behavior of the microgel dispersions.

To clarify the reason why the thin films of charged microgels are inhomogeneous, the drying behavior of the edge of the sessile droplets containing microgels was monitored (Figure S6). In the case of the control N microgels, no microgels were seen due to a large curvature at the early stage (Figure S6a: $T_N \sim 0.1$, 0.2). As time proceeded ($T_N \sim 0.5$), the microgels adsorbed at the air/water interface both at the center and at

DOI: 10.1021/acs.langmuir.9b01933
Langmuir 2019, 35, 10412–10423

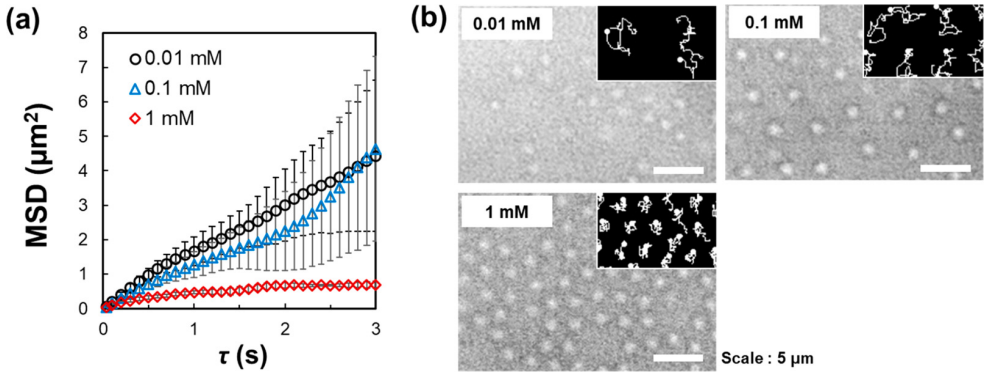

Figure 5. (a) Plots of MSD as a function of the lag time, τ, and (b) optical microscopy images with particle-trajectory images of the NA5 microgels at different NaCl concentrations at $T_N \sim 0.25$ (insets). The sessile droplets were dried at room temperature (~25 °C, ~ 40% humidity) at 0.005 wt % on a glass substrate.

the edge of the same sessile droplet, suggesting that N microgels regularly pack over the whole area of the air/water interface. Upon drying, the arranged structure of the N microgels gradually transferred from the edge without disruption (Figure S6a: $T_N \sim 0.6$, 0.7; Movie S2). On the other hand, NA5 microgels gradually adsorbed to the interface at the edge and at the center of the sessile droplet (Figure S6b). While NA5 microgels continued to adsorb at the interface at the edge, the adsorbed NA5 microgels were carried from the edge to the center on the interface of the droplet by convection flow, even upon drying (Figure S6b: e.g., $T_N \sim 0.5$, 0.7, 0.8; Movie S3). Due to this drying behavior, NA5 microgels were uniformly arranged at the edge of the thin film on the substrate after drying. Getting closer to the center of the droplet, the impact of the convection flow on the microgel arrangement lowered, and the adsorbed NA5 microgels were disordered when they were transferred onto the glass substrate (Figure S6c, Movie S4).

As has been described above, the microgels fluctuate at the air/water interface. Therefore, we subsequently examined the dynamic motion of the N microgels and polyelectrolyte microgels at the interface. The trajectory of the microgels was tracked as shown in Figure 4 and Figure S7, which indicates that from the early stage of drying, individual N microgels are hardly moving at the interface (Figure 4a, Movie S5: $T_N = \sim 0.7$). On the other hand, individual NA5 microgels are moving considerably in two dimensions (Figure 4b, Movie S6: $T_N = \sim 0.7$), even though they are adsorbed at the air/water interface. These movements were quantitatively evaluated, and the results are shown as MSD plots (Figure 4) using eq 1. For the N microgels, the slope of the MSD plots and the self-diffusion values calculated from eq 2 were close to 0 for each T_N (Figure 4a, Table S1), indicating that the microgel movements are highly restricted at the air/water interface, even at the early stage of the drying process ($T_N \sim 0.25$). On the other hand, the diffusivity of the NA5 microgels was significantly higher than that of the N microgels (Figure 4b, Table S1), and their self-diffusion coefficients were much larger than those of N microgels at $T_N \sim 0.25$ (Table S1). As time proceeded, the self-diffusion coefficient values of the NA5 microgels gradually decreased with increasing packing density of the microgels at the air/water interface (Table S1). It should be noted here that at $T_N \sim 0.85$, each NA5 microgel moved in the same direction (Figure 4b: $T_N \sim 0.85$), which is due to the microgels moving at the interface from the edge of the droplet during evaporation (Figure S6b, Movie S3). Although the value approximated 0 at $T_N \sim 0.85$, the NA5 microgel movements were not completely restricted, which might be a reason why the arranged structures of the NA5 microgels were not transferred onto the substrate without disruption during evaporation.

The fact that charged microgels at the air/water interface are relatively mobile is different fromn the behavior of previous work on colloidal crystals packed charged microgels, where movement is highly restricted due to different osmotic pressure between the inside and the outside of the microgels.[53,54] The difference may be due to the repulsive interactions between charged microgels at the air/water interface. In our previous work,[38] we confirmed that N microgels arranged at the air/water interface are highly deformed and that neighboring microgels are highly interpenetrated. Therefore, the arranged structures of the N microgels can be transferred onto the solid substrate without disruption. Therefore, in addition to high crystallinity induced by osmotic pressure, it seems feasible to conclude that charged NA5 microgels adsorbed at the interface are not highly interpenetrated with each other most likely due to repulsive interactions between the NA microgels or between the NA microgels and the air/water interface. It is worthwhile noting that the NA microgels (e.g., NA20 microgels: 39.6 mNJ/m at 1.0 wt %) and the N microgels can lower the surface tension, suggesting that it is difficult to evaluate the microscopic movements of microgels exclusively by surface-tension measurements.

Effect of the pH Value, the Ionic Strength, and the Charge Distribution in Microgels on the Polyelectrolyte Microgels at the Air/Water Interface. The aforementioned results indicate an energy barrier when polyelectrolyte microgels approach the air/water interface. According to a previous report,[55] there are both attractive, i.e., van der Waals interactions, and repulsive interactions, i.e., an image-charge effect,[56] and electric double layer interactions between colloidal particles and an interface. In this study, we wanted to clarify the effect of charges immobilized on microgels on the interfacial phenomenon; therefore, we initially observed NA5 microgels at the air/water interface at pH = 3 and pH = 7, where carboxyl groups in the NA microgels are protonated and deprotonated, respectively. However, the results obtained at pH = 3 and pH = 7 were, unexpectedly, almost identical (Figure S8). Even though, different from McIlvaine buffers, simple electrolyte was used for adjusting the pH values, the

DOI: 10.1021/acs.langmuir.9b01933
Langmuir 2019, 35, 10412−10423

adsorption behaviors were similar on the drying process of the microgels at pH ∼ 3, pH ∼ 7, and pH ∼ 10 (Figure S9).

Thus, as another potential factor, the effect of the ionic strength in the sessile droplets on the static and dynamic adsorption behavior of the microgels at the air/water interface was investigated at the different concentrations of NaCl (Figure 5, Figure S10). As expected, the adsorption numbers of the charge-screened NA5 microgels at the interface increased with increasing NaCl concentration (Figure S10). Moreover, the self-diffusion coefficient values calculated from the MSD plots of the charge-screened NA5 microgels also decreased with increasing NaCl concentration, and the value approached 0 when the droplet contained 1 mM NaCl at the initial state (Figure 5, Table S2), indicating that the individual mobility of the charge-screened microgels is restricted in the presence of NaCl (-2.08×10^{-8} $m^2/(V\ s)$ in pure water; -1.68×10^{-8} $m^2/(V\ s)$ in 1 mM NaCl). In this case, the electrostatic repulsive interactions both between the polyelectrolyte microgels and between the microgels and the interface should decrease with increasing ionic strength as the electric double layer ($1/\kappa$) of the particles is defined as $\kappa \propto \sqrt{n}$, where n is the salt concentration. Thus, the thickness of the electric double layer of the polyelectrolyte microgels decreases with increasing salt concentrations. In addition, the image-charge effect, which is also an electrostatic repulsive interaction, decreased in the presence of NaCl.[55] Hence, the presence of NaCl lowers not only the energy barrier between the microgels and the air/water interface but also the repulsive interactions between the microgels adsorbed at the interface. These results confirm that a slight increase in ionic strength (∼1 mM NaCl) affects the interfacial behavior of polyelectrolyte NA5 microgels; therefore, the effect of pH value on the microgel adsorption behavior was not observed as the buffer solutions contain substantially higher concentrations of ions than those used in the NaCl tests.

Next, different from the conditions when NaCl was not added, the arranged structures of the charge-screened microgels at the air/water interface were transferred onto the substrates without significant disruptions after drying (Figure S10a; [NaCl] = 1 mM; $T_N \sim 1$), suggesting that the adsorbed polyelectrolyte microgels at the interface are highly interpenetrated with each other due to weaker repulsive interactions between the microgels. Although the resulting microgel-monolayer film included salt as an additive, the salt could be easily removed by washing with pure water, which afforded a homogeneous monolayer film showing iridescent colors (Figure S11). Furthermore, the negatively charged polyelectrolyte microgels could also be charge-screened in the presence of cationic dyes such as Rhodamine 6G (R6G), which interact electrostatically with charged carboxyl groups in the microgels.[57] After drying the dispersion of the polyelectrolyte microgels charge-screened with R6G, almost homogeneous monolayer films were obtained (Figure S12). These results indicate that charge-screened polyelectrolyte microgels show self-organization during drying of sessile droplets and create homogeneous monolayer films similar to the control N microgels as previously reported by our group.[38]

Next, we investigated the effect of the charge distribution in the microgels on the interfacial behavior using core/shell (CS) microgels, where the polyelectrolyte NA5 microgels are covered with AAc-free pNIPAm hydrogel shells. The CS microgels adsorbed on the air/water interface during the early stage ($T_N \sim 0.05$) of the drying process (Figure 6a, b).

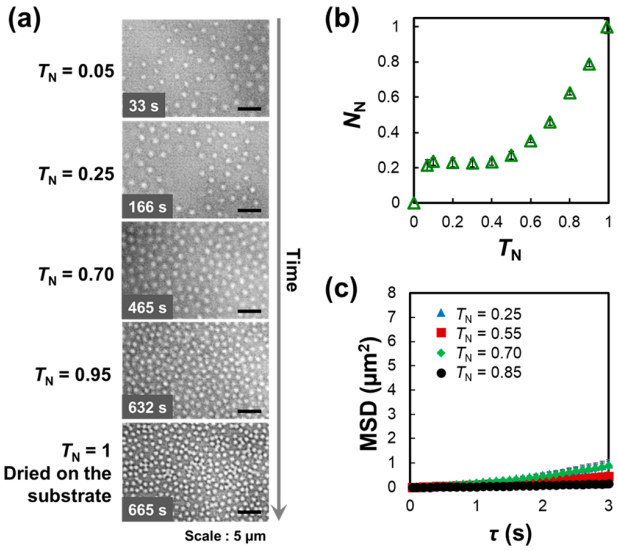

Figure 6. (a) Optical microscopy images of the CS microgels at the air/water interface of the droplets on glass substrates as a function of T_N. (b) Normalized adsorbed amount, N_N, for each charged microgel as a function of T_N. (c) The plots of MSD as a function of the lag time, τ, of the CS microgels. The droplets were dried at room temperature (∼25 °C, ∼60% humidity) at a concentration of 0.005 wt %.

Subsequently, the normalized adsorbed amount, N_N, did not change from $T_N \sim 0.1$ to $T_N \sim 0.4$ (Figure 6b) before N_N increased gradually because the microgels were compressed with each other due to the decrease of the interfacial area upon evaporation, which is similar to the control N microgels.[38] Moreover, the MSD plots show that the movement of the CS microgels adsorbed at the interface is also restricted (Figure 6c), which is also similar to the behavior of the control N microgels.[38] These results indicate that charge groups located near the surface of the polyelectrolyte microgels are crucial to control the interfacial behavior of the microgels.

Analysis of the Adsorption Behavior of Polyelectrolyte Microgels at the Air/Water Interface. In order to understand the adsorption process of polyelectrolyte microgels at the air/water interface ($T_N < \sim 0.5$), the following pseudo-first-order equation[58] and pseudo-second-order equation[38,58] were applied to the experimental data:

$$\ln(N_e - N_t) = \ln N_e - K_1 t \quad (3)$$

$$\frac{t}{N_t} = \frac{t}{N_e} + \frac{1}{K_2 N_e^2} \quad (4)$$

where N_e and N_t are the adsorbed amount at equilibrium ($T_N = 1.0$) and at the time t (s), while K_1 (s^{-1}) and K_2 (s^{-1}) represent the adsorption rate constant of the pseudo-first-order model and the pseudo-second-order model, respectively. The resulting correlation coefficients, R^2, of the pseudo-first-order model fitting (eq 3) were higher ($R^2 \geq 0.95$) for all polyelectrolyte microgels (NA1, NA5, NA10, NA20) than those of the pseudo-second-order model fitting (Figure S13, Table 2), which is the opposite of the trend observed for the control N microgels[38] and the CS microgels, where the shell does not contain AAc-incorporated hydrogels. The similar values of the adsorption rate constant K_1 quantitatively indicate that the adsorption kinetics do not depend on the amount of

DOI: 10.1021/acs.langmuir.9b01933
Langmuir 2019, 35, 10412−10423

Table 2. Parameters for the Adsorption Kinetics of the N, NA1, NA5, NA10, NA20, and CS Microgels at the Air/Water Interface

	pseudo-first order		pseudo-second order	
microgel	R^2	K_1 (s^{-1})	R^2	K_2 (s^{-1})
N	0.6627	–	0.9693	1.6×10^{-4}
NA1	0.9891	0.0006	0.9544	8.7×10^{-6}
NA5	0.9551	0.0005	0.0080	–
NA10	0.9517	0.0007	0.0711	–
NA20	0.9484	0.0008	0.1490	–
CS	0.4435	–	0.9787	7.6×10^{-4}

charged AAc groups immobilized in the microgels (1−20 mol %) (Table 2).

The Deformation of Single Polyelectrolyte Microgels upon Adsorption at the Air/Water Interface. In order to investigate the deformation of polyelectrolyte microgels at the air/water interface, larger microgels, which can be visualized clearly by fluorescent microscopy, were synthesized by modified precipitation polymerization according to our previous report.[42] Different from our previous study,[42] and in order to avoid the potentially deleterious effects of impurities such as fluorescent molecules of R6G on the deformation of the polyelectrolyte microgels, the fluorescent molecules were covalently immobilized in the microgels. For that purpose, fluorescent $Ru(bpy)_3$ complexes were immobilized in micron-sized polyelectrolyte (NRu) microgels, synthesized by a modified precipitation polymerization,[42] which revealed that their EPM was affected by the presence of NaCl (1.28×10^{-8} $m^2/(V\,s)$ in pure water; 0.33×10^{-8} $m^2/(V\,s)$ in 1 mM NaCl). The NRu microgels could be clearly visualized in water by fluorescence microscopy, and the deformation of individual microgels could be recorded at the air/water interface (Figure 7a). In order to clarify the influence of the charge of the microgels on their deformation, the deformation of the charge-screened NRu microgels was also investigated quantitatively in 1 mM NaCl solution (Figure 7b). It should be noted here that the fluorescence intensity of the microgels was reduced considerably (see images taken at 2.0 and 5.0 s), which might be due to the decreased density of the polymers (or fluorescent molecules) after the substantial deformation at the interface. Here, we applied a pseudo-second-order model to analyze the deformation kinetics[42] of the microgels at the air/water interface:

$$\frac{t}{D_t} = \frac{t}{D_s} + \frac{1}{k_2 D_e^2} \tag{5}$$

where D_s and D_t (μm) represent the size of the microgels adsorbed at the air/water interface at a specific and arbitrary time t (s), respectively, whereby k_2 ($\mu m^{-1}\ s^{-1}$) refers to the rate constant of the pseudo-second-order model. The R^2 value of the models was ∼1, indicating that the deformation could be applied to such models (Figure 7c). The fitting-derived deformation rate constant, k_2, decreased for the charge-screened microgels compared to those examined in pure water ($k_{2,water}$ = 1.9 $\mu m^{-1}\ s^{-1}$; $k_{2,NaCl}$ = 0.57 $\mu m^{-1}\ s^{-1}$) (Table 3). In a previous study,[42] softer microgels with a lower degree of cross-linking showed lower values of k_2, suggesting that charged microgels do not easily deform upon adsorption at the air/water interface. This may be due to (i) electrostatic repulsive interactions between the polyelectrolyte microgels

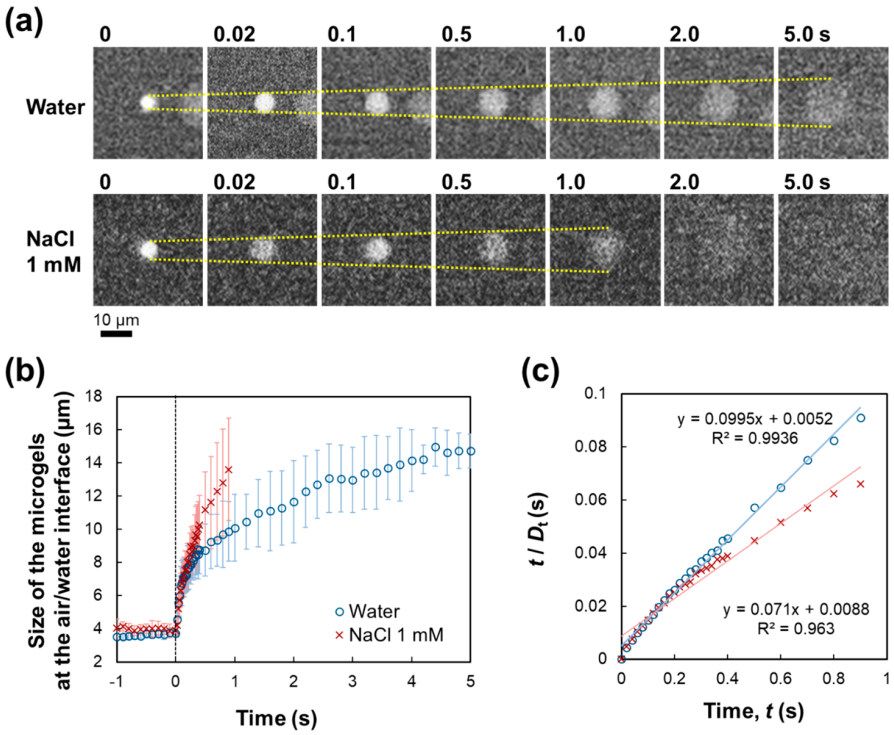

Figure 7. (a) Fluorescence microscopy images of NRu microgels upon adsorption at the air/water interfaces recorded with a high-speed camera. (b) Time evolution of the size of the NRu microgels upon adsorption at the air/water interface (○) in water and (×) in aqueous NaCl (1 mM; N = 10). (c) Plots of the pseudo-second-order kinetics for the deformation of the NRu microgels.

DOI: 10.1021/acs.langmuir.9b01933
Langmuir 2019, 35, 10412−10423

Table 3. Parameters for the Deformation Kinetics of the NRu Microgels upon Adsorption at the Air/Water Interface

	pseudo-second order			exptl values
solvent	R^2	k_2 (μm^{-1} s^{-1})	$D_{t\sim1}(\mu m)$	$D_{t\sim1}(\mu m)$
water	0.9936	1.9	10.0	9.87
NaCl solution	0.9630	0.57	14.1	13.6

and the interface and/or (ii) a restricted deformation of harder polyelectrolyte microgels.

CONCLUSIONS

The introduction of charged groups in microgels drastically influences their behavior at the air/water interface upon drying sessile droplets. First, the adsorption of charged microgels at the air/water interface decreases, irrespective of the number of charged groups present ($1 \leq$ AAc ≤ 20 mol %). Second, in contrast to the control N microgels, charged microgels adsorbed at the air/water interface are more mobile, and the microgels are not highly entangled with each other. Third, even though the more mobile charged microgels are arranged at the air/water interface, the formed structures cannot be transferred onto the solid substrates without disrupting the structures. Thus, the resulting thin films are macroscopically inhomogeneous. Fourthly, the deformation of single polyelectrolyte microgels is relatively fast, irrespective of the charged and charge-screened microgels. However, the degree of deformation is suppressed by the presence of charged groups at the air/water interface. Fifthly, the aforementioned effect of the charged groups immobilized within the microgels can be ignored by charge-screening, and then, the interfacial behavior becomes similar to that of the control N microgels.

Our findings regarding the interfacial behavior of polyelectrolyte microgels at the air/water interface can be expected to promote further developments of applications concerning, e.g., foams and emulsions stabilized by microgels, where the understanding of the adsorption behavior of functional microgels at the interface is crucial.

ASSOCIATED CONTENT

Supporting Information

The Supporting Information is available free of charge on the ACS Publications website at DOI: 10.1021/acs.langmuir.9b01933.

Optical microscopy images of colloidal crystals of individual microgels; sessile droplet observations; photographs of films after drying microgel dispersions; microscopic observations and evaluation of polyelectrolyte microgels at the air/water interface in water, in buffer solution, in sodium chloride solution, and with R6G; MSD plots and the calculated self-diffusion coefficients; fittings obtained from the pseudo-first-order and the pseudo-second-order models; individual microgel deformations (PDF)

Drying process of dispersions of the entire sessile droplets (MP4)

Microscopic observations of the sessile dispersion droplets at different observation positions during drying at the edge (AVI)

Microscopic observations of the sessile dispersion droplets at different observation positions during drying at the edge (AVI)

Microscopic observations of the sessile dispersion droplets at different observation positions during drying from the edge to the center (AVI)

Tracked time trajectories of N microgels (AVI)

Tracked time trajectories of NA5 mirogels (MP4)

AUTHOR INFORMATION

Corresponding Author

*E-mail: d_suzuki@shinshu-u.ac.jp.

ORCID

Haruka Minato: 0000-0001-6252-3032

Masaya Takizawa: 0000-0002-1169-6002

Daisuke Suzuki: 0000-0003-0444-156X

Notes

The authors declare no competing financial interest.

ACKNOWLEDGMENTS

D.S. acknowledges financial support from a Grant-in-Aid for Young Scientists (A) (17H04892) and a Grant-in Aid for Scientific Research on Innovative Areas "Molecular Engine" (19H05388) from the Japan Society for the Promotion of Science (JSPS). H.M. acknowledges financial support from a Grant-in-Aid for the Shinshu University Advanced Leading Graduate Program from the Japanese Ministry of Education, Culture, Sports, Science, and Technology. The authors thank Masaki Murai, Yuki Sakurai, and Kensuke Hosho for giving us the NRu, N, NA10, and NA20 microgels.

REFERENCES

(1) Holtz, J. H.; Asher, S. A. Polymerized colloidal crystal hydrogel films as intelligent chemical sensing materials. *Nature* **1997**, *389*, 829−832.

(2) Kim, J.; Serpe, M. J. M.; Lyon, L. A. Photoswitchable Microlens Arrays. *Angew. Chem., Int. Ed.* **2005**, *44*, 1333−1336.

(3) Su, S.; Ali, M. M.; Filipe, C. D.; Li, Y.; Pelton, R. Microgel-Based Inks for Paper-Supported Biosensing Applications. *Biomacromolecules* **2008**, *9*, 935−941.

(4) Gao, Y.; Xu, W.; Serpe, M. J. Free-standing poly (*N*-isopropylacrylamide) microgel-based etalons. *J. Mater. Chem. C* **2014**, *2*, 5878−5884.

(5) Karg, M.; Hellweg, T.; Mulvaney, P. Self-Assembly of Tunable Nanocrystal Superlattices Using Poly-(NIPAM) Spacers. *Adv. Funct. Mater.* **2011**, *21*, 4668−4676.

(6) Snowden, M. J.; Thomas, D.; Vincent, B. Use of colloidal microgels for the absorption of heavy metal and other ions from aqueous solution. *Analyst* **1993**, *118*, 1367−1369.

(7) Gelissen, A. P. H.; Scotti, A.; Turnhoff, S. K.; Janssen, C.; Radulescu, A.; Pich, A.; Rudov, A. A.; Potemkin, I. I.; Richtering, W. An anionic shell shields a cationic core allowing for uptake and release of polyelectrolytes within core−shell responsive microgels. *Soft Matter* **2018**, *14*, 4287−4299.

(8) Kureha, T.; Suzuki, D. Nanocomposite Microgels for the Selective Separation of Halogen Compounds from Aqueous Solution. *Langmuir* **2018**, *34*, 837−846.

(9) Ngai, T.; Behrens, S. H.; Auweter, H. Novel emulsions stabilized by pH and temperature sensitive microgels. *Chem. Commun.* **2005**, *0*, 331−333.

(10) Fujii, S.; Read, E. S.; Binks, B. P.; Armes, S. P. Stimulus-Responsive Emulsifiers Based on Nanocomposite Microgel Particles. *Adv. Mater.* **2005**, *17*, 1014−1018.

(11) Suzuki, D.; Tsuji, S.; Kawaguchi, H. Janus Microgels Prepared by Surfactant-Free Pickering Emulsion-Based Modification and Their Self-Assembly. *J. Am. Chem. Soc.* **2007**, *129*, 8088−8089.

DOI: 10.1021/acs.langmuir.9b01933
Langmuir 2019, 35, 10412−10423

(12) Richtering, W. Responsive Emulsions Stabilized by Stimuli-Sensitive Microgels: Emulsions with Special Non-Pickering Properties. *Langmuir* **2012**, *28*, 17218−17229.
(13) Massé, P.; Sellier, E.; Schmitt, V.; Ravaine, V. Impact of Electrostatics on the Adsorption of Microgels at the Interface of Pickering Emulsions. *Langmuir* **2014**, *30*, 14745−14756.
(14) Suzuki, D.; Taniguchi, H.; Yoshida, R. Autonomously Oscillating Viscosity in Microgel Dispersions. *J. Am. Chem. Soc.* **2009**, *131*, 12058−12059.
(15) Matsui, S.; Inui, K.; Kumai, Y.; Yoshida, R.; Suzuki, D. Autonomously Oscillating Hydrogel Microspheres with High-Frequency Swelling/deswelling and Dispersing/flocculating Oscillations. *ACS Biomater. Sci. Eng.* **2018**, DOI: 10.1021/acsbiomaterials.8b00850.
(16) Anselmo, A. C.; Mitragotri, S. Impact of particle elasticity on particle-based drug delivery systems. *Adv. Drug Delivery Rev.* **2017**, *108*, 51−67.
(17) McClements, D. J. Encapsulation, protection, and delivery of bioactive proteins and peptides using nanoparticle and microparticle systems: A review. *Adv. Colloid Interface Sci.* **2018**, *253*, 1−22.
(18) Anselmo, A.; Mitragotri, S. Advanced Impact of particle elasticity on particle-based drug delivery systems. *Adv. Drug Delivery Rev.* **2017**, *108*, 51−67.
(19) Pelton, R. H.; Chibante, P. Preparation of Aqueous Latices with *N*-Isopropylacrylamide. *Colloids Surf.* **1986**, *20*, 247−256.
(20) Pelton, R. Temperature-sensitive aqueous microgels. *Adv. Colloid Interface Sci.* **2000**, *85*, 1−33.
(21) Hoare, T.; Pelton, R. Highly pH and Temperature Responsive Microgels Functionalized with Vinylacetic Acid. *Macromolecules* **2004**, *37*, 2544−2550.
(22) Karg, M.; Pastoriza-Santos, I.; Rodriguez-González, B.; von Klitzing, R.; Wellert, S.; Hellweg, T. Temperature, pH, and Ionic Strength Induced Changes of the Swelling Behavior of PNIPAM-Poly(allylacetic acid) Copolymer Microgels. *Langmuir* **2008**, *24*, 6300−6306.
(23) Lapeyre, V.; Gosse, I.; Chevreux, S.; Ravaine, V. Monodispersed Glucose-Responsive Microgels Operating at Physiological Salinity. *Biomacromolecules* **2006**, *7*, 3356−3363.
(24) Nayak, S.; Lyon, L. A. Photoinduced Phase Transitions in Poly(*N*-isopropylacrylamide) Microgels. *Chem. Mater.* **2004**, *16*, 2623−2627.
(25) Kureha, T.; Aoki, D.; Hiroshige, S.; Iijima, K.; Aoki, D.; Takata, T.; Suzuki, D. Decoupled Thermo- and pH-responsive Hydrogel Microspheres Cross-linked by Rotaxane Networks. *Angew. Chem., Int. Ed.* **2017**, *56*, 15393−15396.
(26) Hoshino, Y.; Imamura, K.; Yue, M.; Inoue, G.; Miura, Y. Reversible Absorption of CO_2 Triggered by Phase Transition of Amine-Containing Micro- and Nanogel Particles. *J. Am. Chem. Soc.* **2012**, *134*, 18177−18180.
(27) Yue, M.; Imai, K.; Yamashita, C.; Miura, Y.; Hoshino, Y. Effects of Hydrophobic Modifications and Phase Transitions of Polyvinylamine Hydrogel Films on Reversible CO_2 Capture Behavior: Comparison between Copolymer Films and Blend Films for Temperature-Responsive CO_2 Absorption. *Macromol. Chem. Phys.* **2017**, *218*, 1600570.
(28) Yue, M.; Hoshino, Y.; Ohshiro, Y.; Imamura, K.; Miura, Y. Temperature-Responsive Microgel Films as Reversible Carbon Dioxide Absorbents in Wet Environment. *Angew. Chem., Int. Ed.* **2014**, *53*, 2654−2657.
(29) Yue, M.; Hoshino, Y.; Miura, Y. Design rationale of thermally responsive microgel particle films that reversibly absorb large amounts of CO_2: fine tuning the pK_a of ammonium ions in the particles. *Chem. Sci.* **2015**, *6*, 6112−6123.
(30) Hoare, T.; Pelton, R. Charge-Switching, Amphoteric Glucose-Responsive Microgels with Physiological Swelling Activity. *Biomacromolecules* **2008**, *9*, 733−740.
(31) Nerapusri, V.; Keddie, J. L.; Vincent, B.; Bushnak, I. A. Swelling and Deswelling of Adsorbed Microgel Monolayers Triggered by Changes in Temperature, pH, and Electrolyte Concentration. *Langmuir* **2006**, *22*, 5036−5041.
(32) Sorrell, C. D.; Lyon, L. A. Bimodal Swelling Responses in Microgel Thin Films. *J. Phys. Chem. B* **2007**, *111*, 4060−4066.
(33) Tsuji, S.; Kawaguchi, H. Colored Thin Films Prepared from Hydrogel Microspheres. *Langmuir* **2005**, *21*, 8439−8442.
(34) Sorrell, C. D.; Lyon, L. A. Deformation Controlled Assembly of Binary Microgel Thin Films. *Langmuir* **2008**, *24*, 7216−7222.
(35) Zavgorodnya, O.; Serpe, M. J. Assembly of poly(*N*-isopropylacrylamide)-*co*-acrylic acid microgel thin films on polyelectrolyte multilayers: Effects of polyelectrolyte layer thickness, surface charge, and microgel solution pH. *Colloid Polym. Sci.* **2011**, *289*, 591−602.
(36) Horigome, K.; Suzuki, D. Drying Mechanism of Poly(*N*-isopropylacrylamide) Microgel Dispersions. *Langmuir* **2012**, *28*, 12962−12970.
(37) Suzuki, D.; Horigome, K. Assembly of Oppositely Charged Microgels at the Air/Water Interface. *J. Phys. Chem. B* **2013**, *117*, 9073−9082.
(38) Takizawa, M.; Sazuka, Y.; Horigome, K.; Sakurai, Y.; Matsui, S.; Minato, H.; Kureha, T.; Suzuki, D. Self-Organization of Soft Hydrogel Microspheres during the Evaporation of Aqueous Droplets. *Langmuir* **2018**, *34*, 4515−4525.
(39) Honda, K.; Sazuka, Y.; Iizuka, K.; Matsui, S.; Uchihashi, T.; Kureha, T.; Shibayama, M.; Watanabe, T.; Suzuki, D. Hydrogel Microellipsoids that Form Robust String-like Assemblies at the Air/Water Interface. *Angew. Chem.* **2019**, *131*, 7372−7376.
(40) Karg, M.; Pich, A.; Hellweg, T.; Hoare, T.; Lyon, L. A.; Crassous, J. J.; Suzuki, D.; Gumerov, R. A.; Schneider, S.; Potemkin, I. I.; Richtering, W. Nanogels and microgels: From model colloids to applications, recent developments and future trends. *Langmuir* **2019**, *35*, 6231−6255.
(41) Pieranski, P. Two-Dimensional Interfacial Colloidal Crystals. *Phys. Rev. Lett.* **1980**, *45*, 569−572.
(42) Minato, H.; Murai, M.; Watanabe, T.; Matsui, S.; Takizawa, M.; Kureha, T.; Suzuki, D. The deformation of hydrogel microspheres at the air/water interface. *Chem. Commun.* **2018**, *54*, 932−935.
(43) Ghosh, P. K.; Spiro, T. G. Photoelectrochemistry of Tris(bipyridyl)ruthenium(II) Covalently Attached to n-Type SnO_2. *J. Am. Chem. Soc.* **1980**, *102*, 5543−5549.
(44) Jones, C. D.; Lyon, L. A. Dependence of Shell Thickness on Core Compression in Acrylic Acid Modified Poly(*N*-isopropylacrylamide) Core/Shell Microgels. *Langmuir* **2003**, *19*, 4544−4547.
(45) Urayama, K.; Saeki, T.; Cong, S.; Uratani, S.; Takigawa, T.; Murai, M.; Suzuki, D. A simple feature of yielding behavior of highly dense suspensions of soft micro-hydrogel particles. *Soft Matter* **2014**, *10*, 9486−9495.
(46) Crocker, J. C.; Grier, D. G. Methods of Digital Video Microscopy for Colloidal Studies. *J. Colloid Interface Sci.* **1996**, *179*, 298−310.
(47) Meng, Z.; Cho, J. K.; Debord, S.; Breedveld, V.; Lyon, L. A. Crystallization Behavior of Soft, Attractive Microgels. *J. Phys. Chem. B* **2007**, *111*, 6992−6997.
(48) Ponratnam, S.; Kapur, S. L. Reactivity ratios of ionizing monomers in aqueous solution. Copolymerization of acrylic and methacrylic acids with acrylamide. *Makromol. Chem.* **1977**, *178*, 1029−1038.
(49) Hoare, T.; McLean, D. Kinetic Prediction of Functional Group Distributions in Thermosensitive Microgels. *J. Phys. Chem. B* **2006**, *110*, 20327−20336.
(50) Watanabe, T.; Kobayashi, C.; Song, C.; Murata, K.; Kureha, T.; Suzuki, D. Impact of Spatial Distribution of Charged Groups in Core Poly(*N*-isopropylacrylamide)-Based Microgels on the Resultant Composite Structures Prepared by Seeded Emulsion Polymerization of Styrene. *Langmuir* **2016**, *32*, 12760−12773.
(51) Jones, C. D.; Lyon, L. A. Shell-Restricted Swelling and Core Compression in Poly(*N*-isopropylacrylamide) Core-Shell Microgels. *Macromolecules* **2003**, *36*, 1988−1993.

DOI: 10.1021/acs.langmuir.9b01933
Langmuir 2019, 35, 10412−10423

(52) Geisel, K.; Isa, L.; Richtering, W. Unraveling the 3D Localization and Deformation of Responsive Microgels at Oil/Water Interfaces: A Step Forward in Understanding Soft Emulsion Stabilizers. *Langmuir* **2012**, *28*, 15770−15776.
(53) Iyer, A. S.; Lyon, L. A. Self-Healing Colloidal Crystals. *Angew. Chem.* **2009**, *121*, 4632−4636; *Angew. Chem., Int. Ed.* **2009**, *48*, 4562−4566.
(54) Scotti, A.; Gasser, U.; Herman, E. S.; Pelaez-Fernandez, M.; Han, J.; Menzel, A.; Lyon, L. A.; Fernández-Nieves, A. The role of ions in the self-healing behavior of soft particle suspensions. *Proc. Natl. Acad. Sci. U. S. A.* **2016**, *113*, 5576−5581.
(55) Dugyala, V. R.; Muthukuru, J. S.; Mani, E.; Basavaraj, M. G. Role of electrostatic interactions in the adsorption kinetics of nanoparticles at fluid-fluid interfaces. *Phys. Chem. Chem. Phys.* **2016**, *18*, 5499−5508.
(56) Inraelachvili, J. N. *Intermolecular and surface forces*, 3rd ed.; Academic Press: Cambridge, MA, 2011.
(57) Kureha, T.; Shibamoto, T.; Matsui, S.; Sato, T.; Suzuki, D. Investigation of Changes in the Microscopic Structure of Anionic Poly(*N*-isopropylacrylamide-*co*-Acrylic acid) Microgels in the Presence of Cationic Organic Dyes toward Precisely Controlled Uptake/Release of Low-Molecular-Weight Chemical Compound. *Langmuir* **2016**, *32*, 4575−4585.
(58) Azizian, S. Kinetic Models of Sorption: A Theoretical Analysis. *J. Colloid Interface Sci.* **2004**, *276*, 47−52.

DOI: 10.1021/acs.langmuir.9b01933
Langmuir 2019, 35, 10412−10423

Supporting Information

Effect of Charge Groups Immobilized in Hydrogel Microspheres during the Evaporation of Aqueous Sessile Droplets

Haruka Minato,[†] Masaya Takizawa,[†] Seina Hiroshige,[†] and Daisuke Suzuki[*†, ‡, §]

[†]Graduate School of Textile Science & Technology, [‡]Institute for Fiber Engineering, and [§]Research Initiative for Supra-Materials, Interdisciplinary Cluster for Cutting Edge Research, Shinshu University, 3-15-1 Tokida, Ueda, Nagano 386-8567, Japan

*Author to whom correspondence should be addressed.
E-mail: d_suzuki@shinshu-u.ac.jp (D.S.).

Number of pages: 15
Number of figures: 13
Number of tables: 2

Results and Discussion.

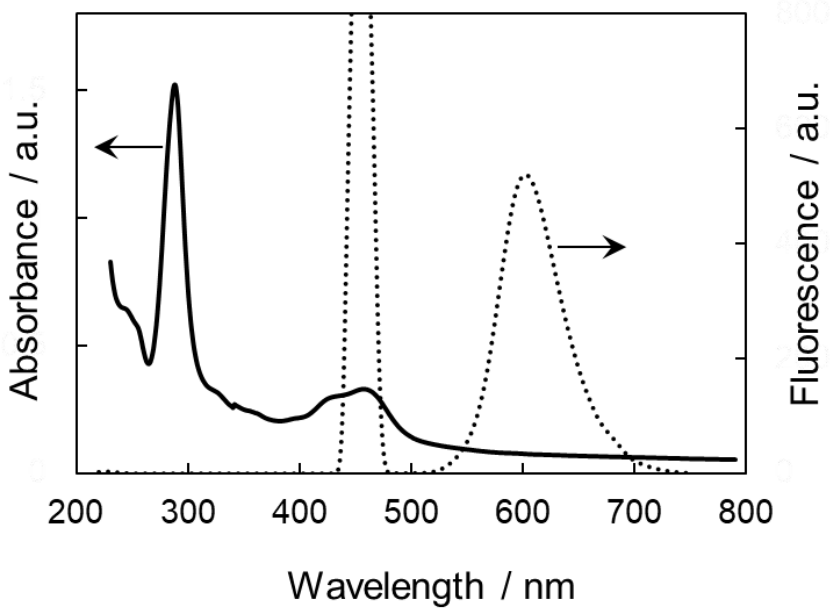

Figure S1. Absorption (solid line) and emission (dotted line) spectra of the NRu microgels in aqueous solution at 25 °C. The fluorescence emission peak at ~457 nm was detected due to measuring upon photoirradiation at 457 nm.

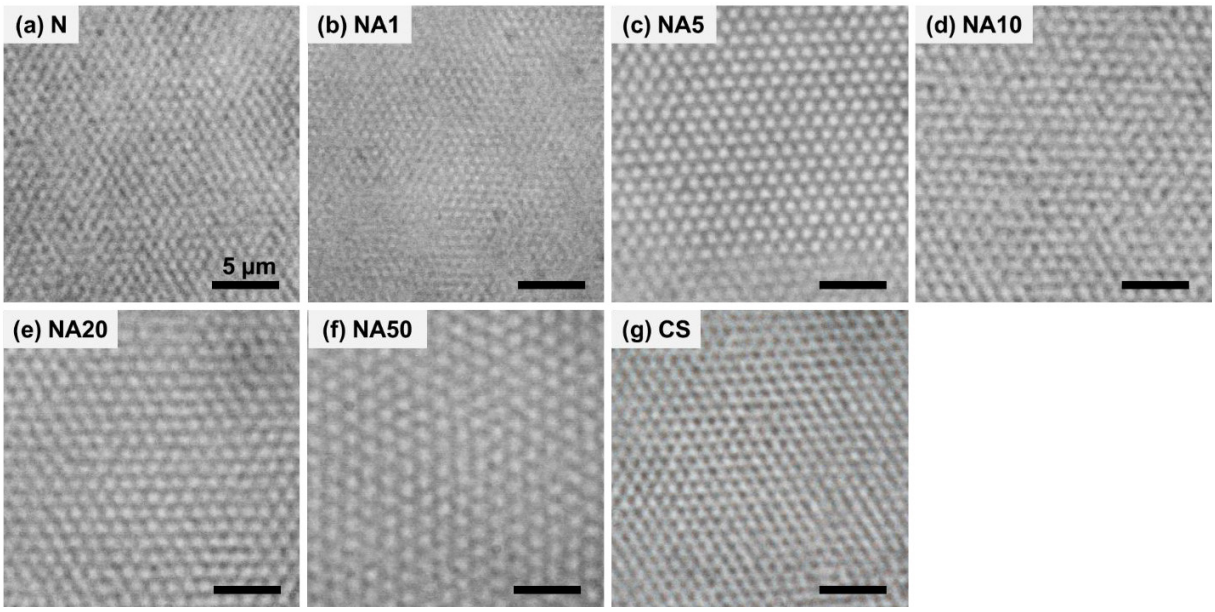

Figure S2. Optical microscopy images of colloidal crystals of (a)~(f) NAX ($1 \leq X \leq 50$) and (g) CS microgels at the critical concentration, C^*. From these images, the diameters of the microgels were calculated, and these are listed in **Table 1**.

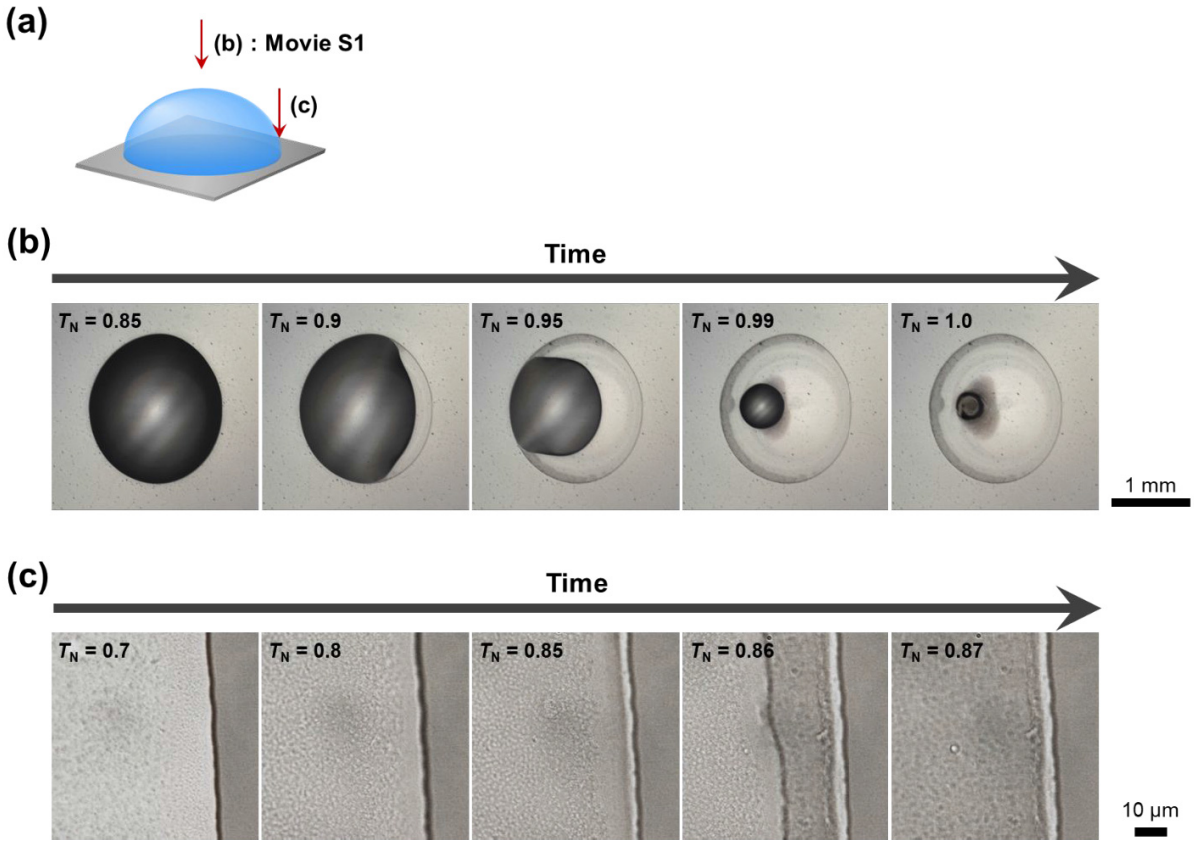

Figure S3. (a) Schematic illustration of the observation of sessile droplets by optical microscopy. (b), (c) Optical microscopy images of the sessile droplets containing N microgel dispersions (1 μL) as a function of the normalized time, T_N. The droplets (0.1 wt%) were dried at room temperature (~25 °C, ~30 % humidity). (b: **Movie S1**) The entire and (c) the edge of the droplets on the glass substrate were observed. (b) The sessile droplets were observed by reflected-light optical microscopy.

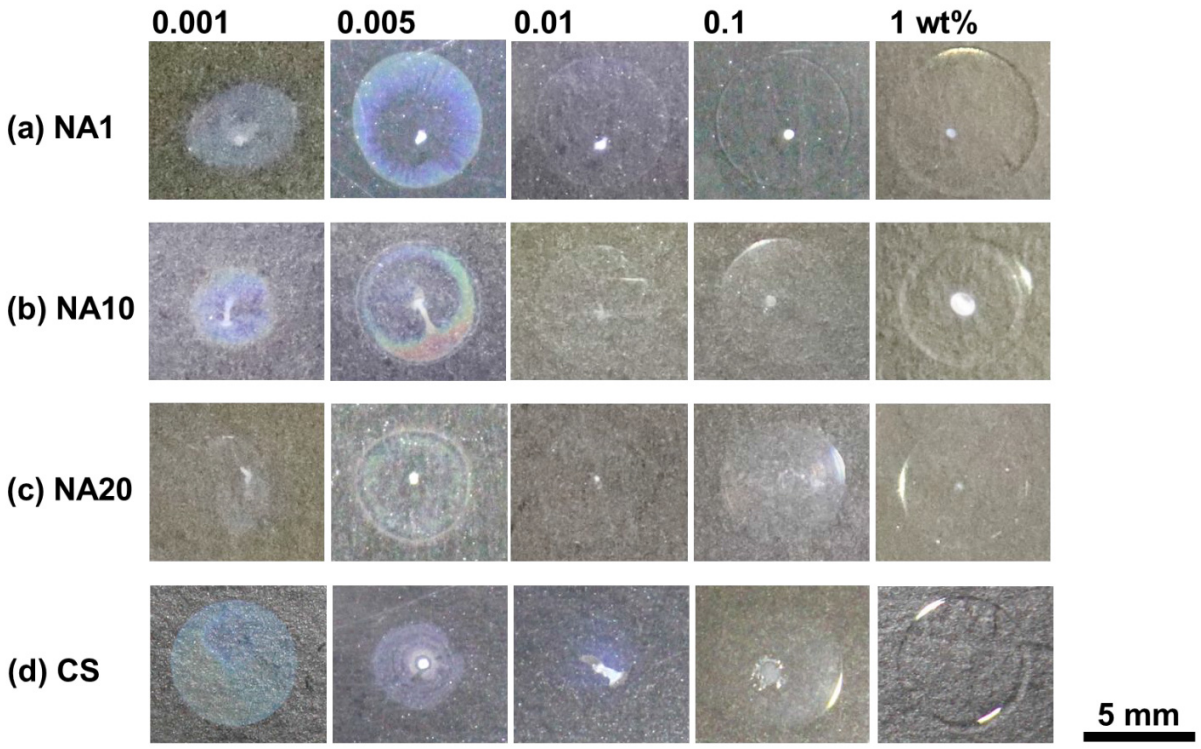

Figure S4. Photographs of the dried thin films containing (a) NA1, (b) NA10, (c) NA20, and (d) CS microgels formed after the microgel droplets (30 μL) were dried at room temperature (~25 °C, ~40 % humidity) on glass substrates at different microgel concentrations (0.001-1 wt%).

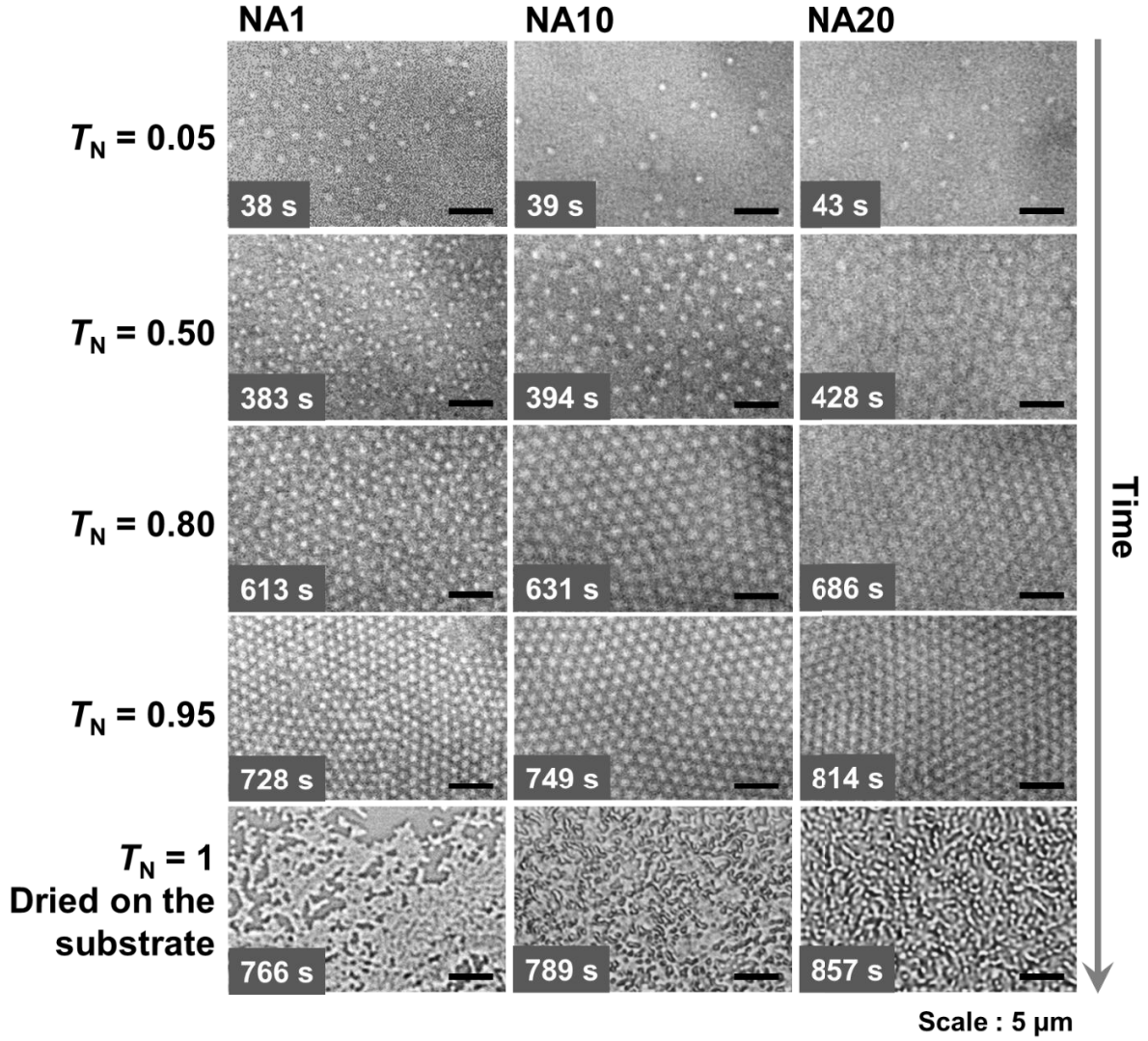

Figure S5. Optical microscope images of NA1, NA10, and NA20 microgels at the air/water interface of each droplet as a function of T_N. The droplets were dried at room temperature (~25 °C, ~40 % humidity) at 0.005 wt% on glass substrates.

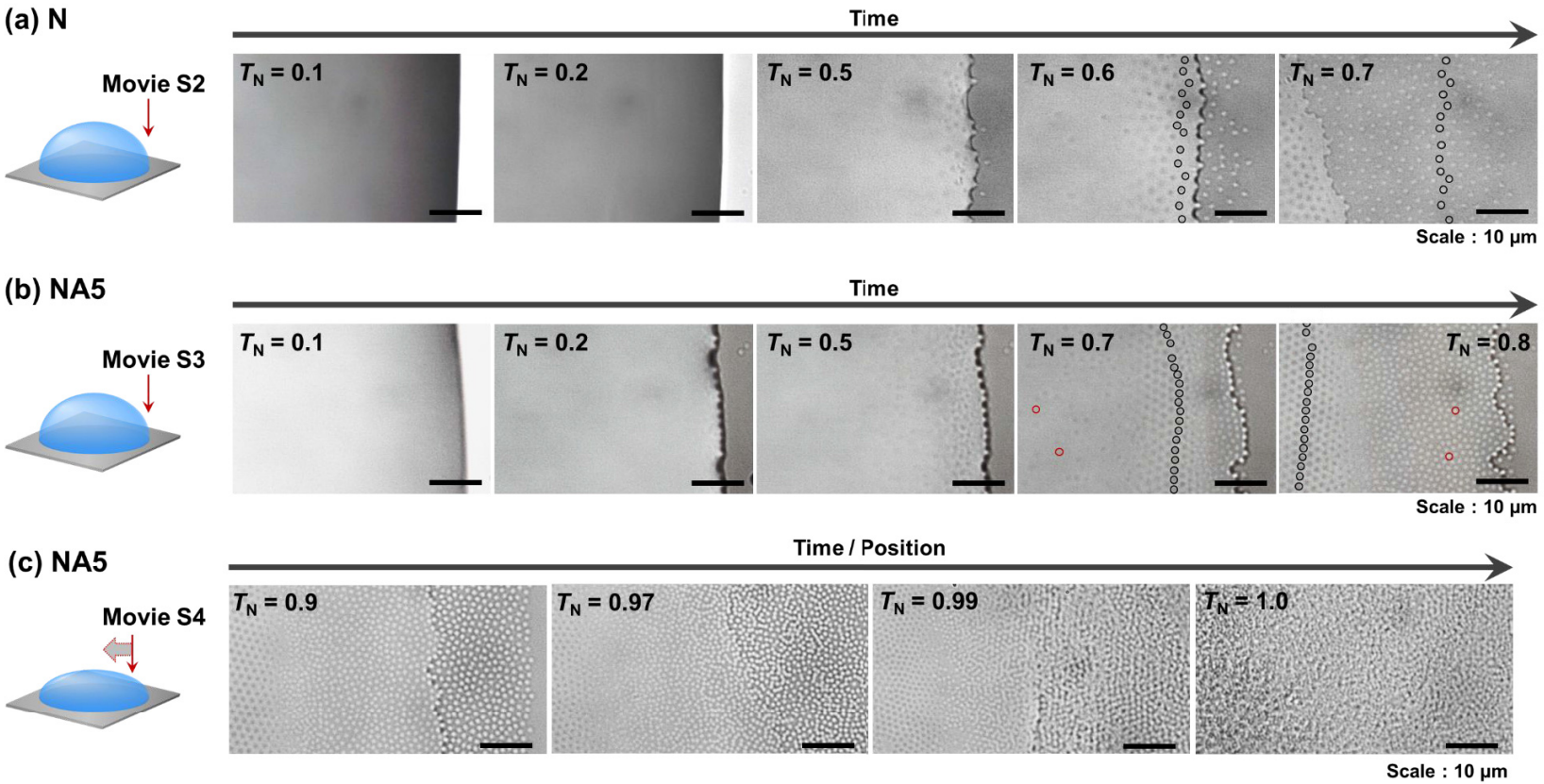

Figure S6. The drying process of dispersions including N or NA5 microgels was observed (a: N, **Movie S2**) (b: NA5, **Movie S3**) at the edge without moving the observation position and (c: NA5, **Movie S4**) from the edge to the center with moving the observation position of the droplet during the evaporation. The droplet of the 1 μL NA5 microgel dispersion was dried at room temperature (~25 °C, ~30 % humidity) at 0.005 wt% on the glass substrate. Marked microgels indicate the position of the particles before and after the passage of time.

Table S1. For the N and NA5 microgels, self-diffusion coefficients were calculated from the MSD plots at T_N = 0.25, 0.55, 0.70, and 0.85.

Microgel	T_N	Slope ($\mu m^2 s^{-1}$)	R^2	D ($\mu m^2 s^{-1}$)
N	0.25	0.300	0.8793	0.0750
	0.55	0.415	0.8186	0.104
	0.70	0.112	0.9987	0.0279
	0.85	0.0535	0.9281	0.0134
NA5	0.25	6.03	0.9525	1.51
	0.55	1.78	0.9913	0.445
	0.70	0.887	0.9852	0.222
	0.85	0.213	0.9701	0.0532

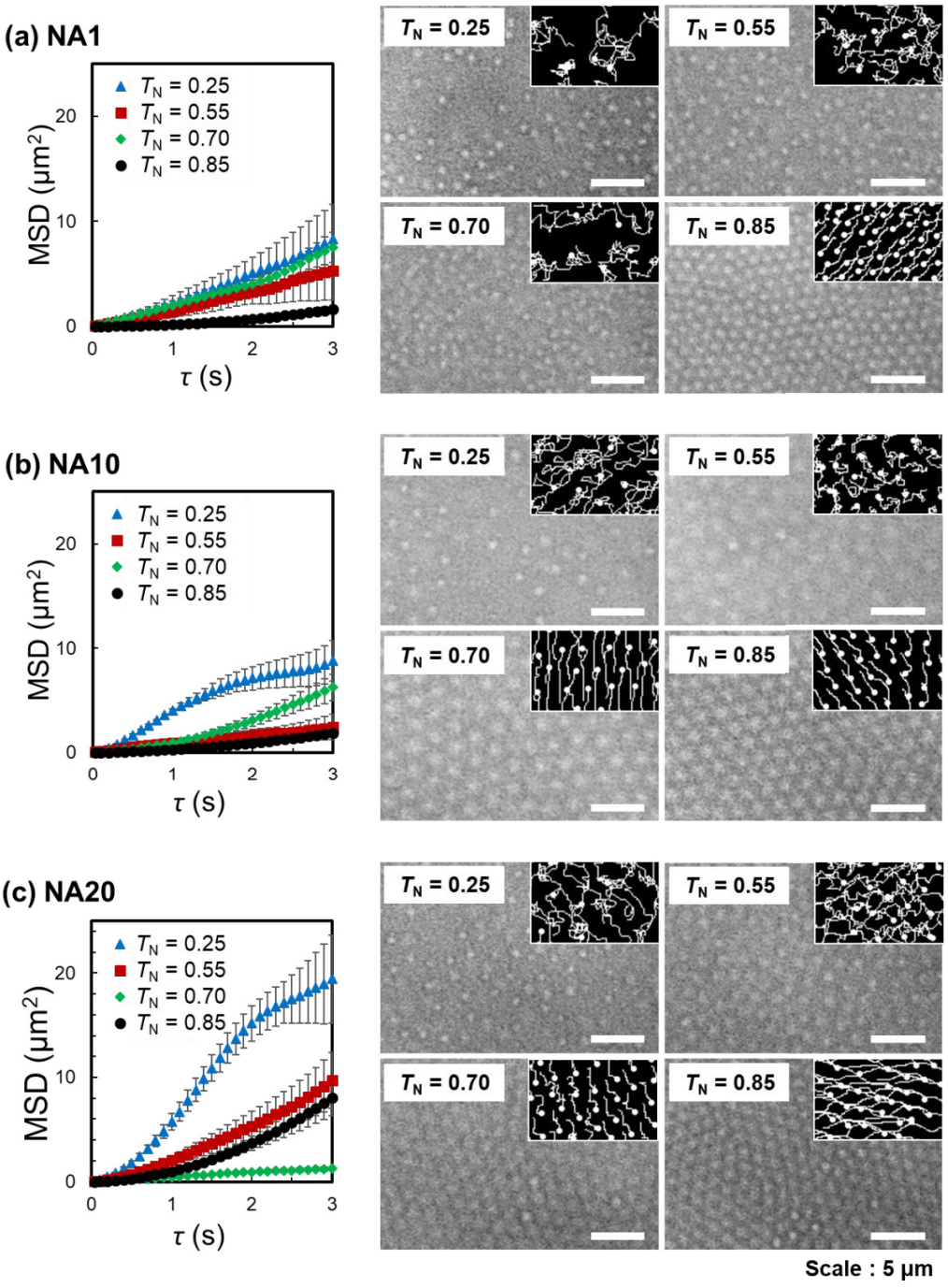

Figure S7. Particle-trajectory images and MSD plots of (a) NA1, (b) NA10, and (c) NA20 microgels adsorbed at the air/water interface of the sessile droplets at T_N = 0.25, 0.55, 0.70, and 0.85.

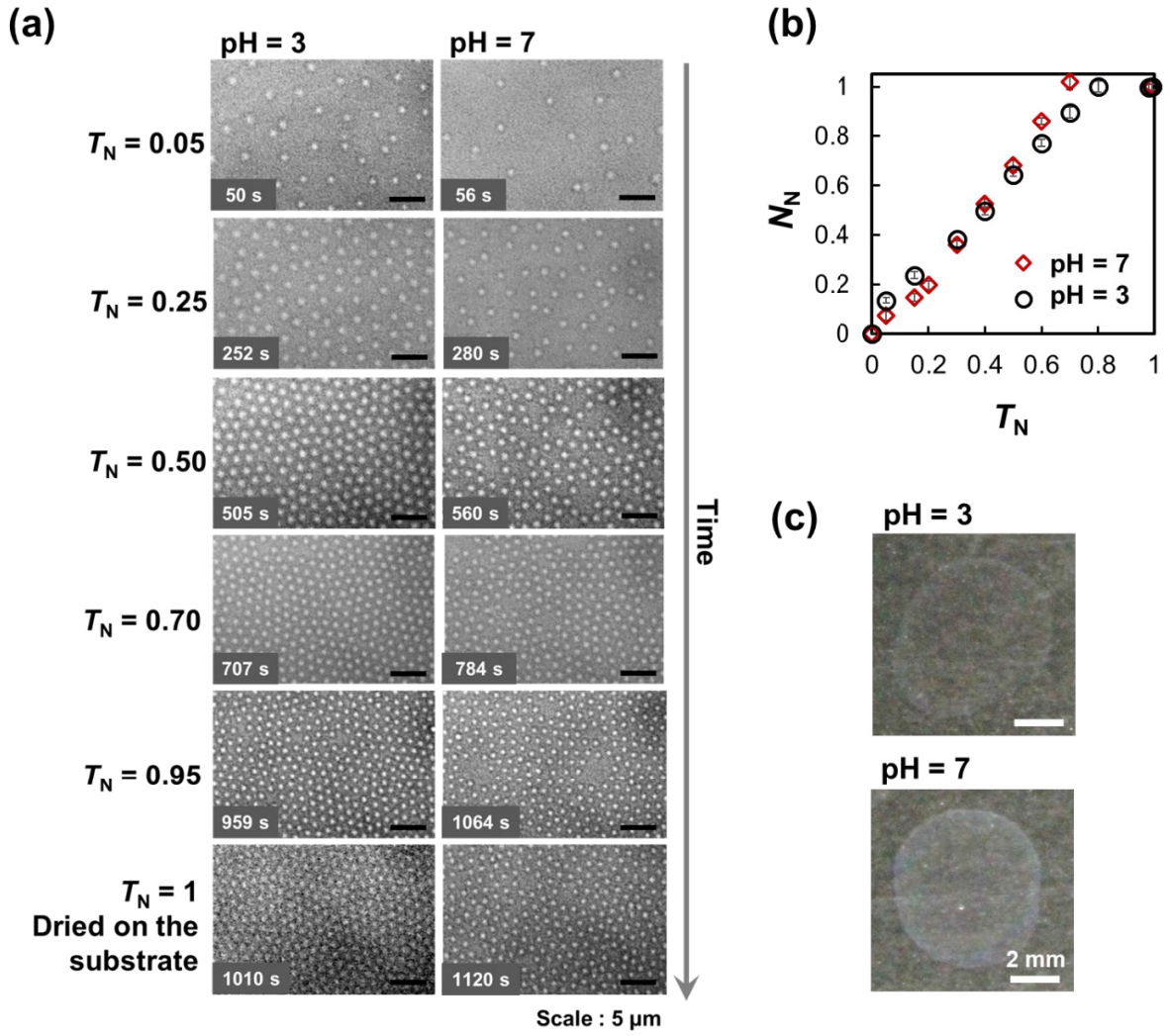

Figure S8. (a) Optical microscopy images of NA5 microgels at the air/water interface as a function of T_N. (b) Normalized adsorbed amount, N_N, for each charged microgel as a function of T_N. (c) Photographs of thin films of microgel dispersions after drying on glass substrate. The droplet was dried at room temperature (~25 °C; ~60 % humidity) at 0.005 wt% at pH = 3 or pH = 7. McIlvaine buffers, composed of 50 mM disodium hydrogen phosphate and 25 mM citric acid, were used.

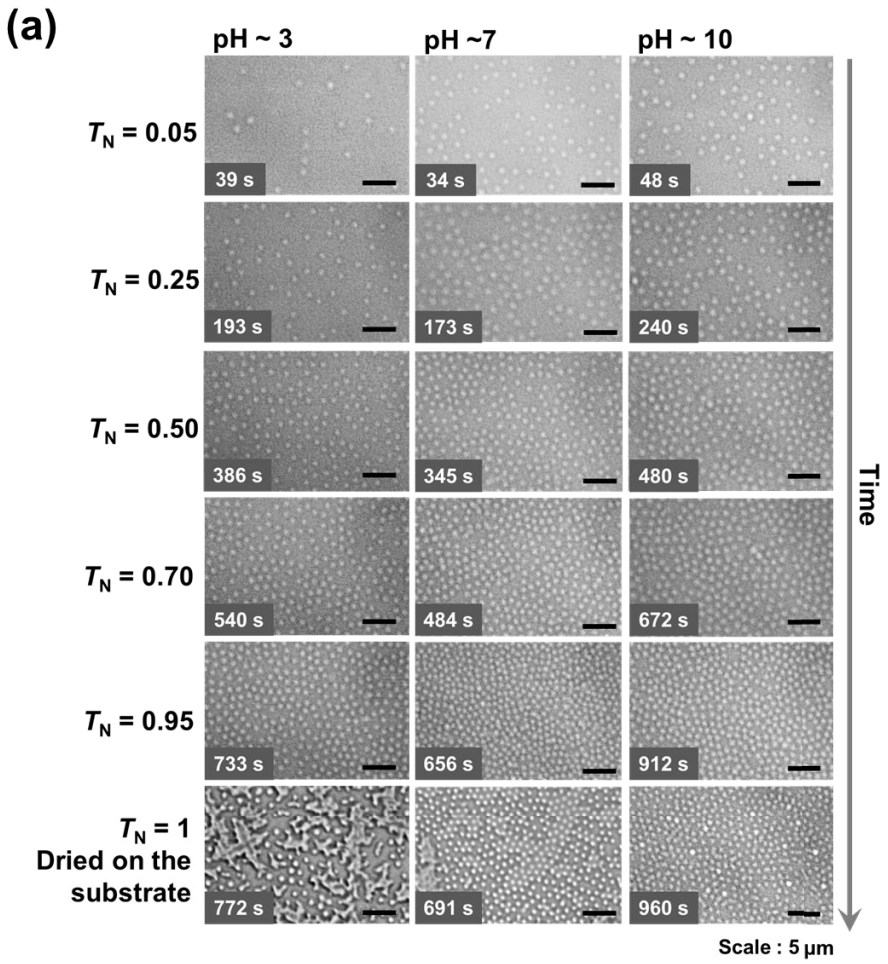

Figure S9. (a) Optical microscopy images of NA5 microgels at the air/water interface as a function of T_N. (b) Normalized adsorbed amount, N_N, for each charged microgel as a function of T_N. The droplet was dried at room temperature (~25 °C; ~60 % humidity) at 0.005 wt% at pH ~ 3, pH ~7, and pH ~ 10 in 10 mM simple electrolytes (HCl, NaOH, and NaCl).

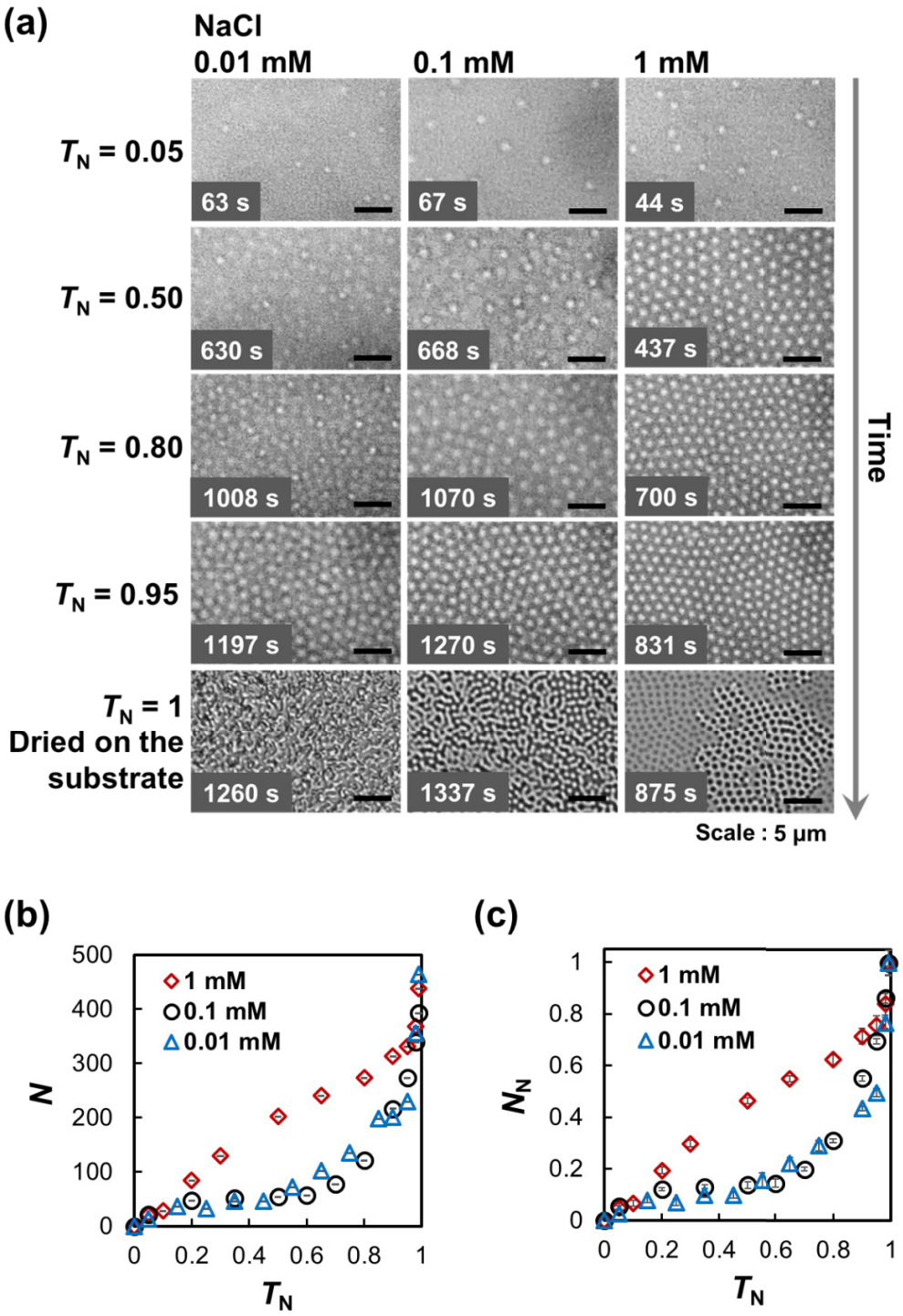

Figure S10. Impact of the ionic strength in NA5 microgel dispersions on the adsorption behavior at the air/water interface. (a) Optical microscopy images of NA5 microgels at the air/water interface of each droplet as a function of T_N at [NaCl] = 0.01, 0.1 and 1 mM. The adsorbed amount of (b) N and (c) N_N for each charged microgel as a function of T_N. The droplets were dried at room temperature (~25 °C, ~60 % humidity) at 0.005 wt% on glass substrates.

Table S2. Self-diffusion coefficients for NA5 microgels, caluculated from the MSD plots at T_N = 0.25, 0.55, 0.70 and 0.85 at different NaCl concentrations.

NaCl (mM)	T_N	Slope (μm^2 s^{-1})	R^2	D (μm^2 s^{-1})
0.01	0.25	1.50	0.9905	0.376
	0.55	1.13	0.9786	0.284
	0.70	0.742	0.8994	0.185
	0.85	0.652	0.8620	0.163
0.1	0.25	1.31	0.9569	0.327
	0.55	1.16	0.9867	0.290
	0.70	0.851	0.9483	0.213
	0.85	0.163	0.9333	0.0407
1	0.25	0.299	0.5679	0.0749
	0.55	0.0160	0.9817	0.00400
	0.70	0.0403	0.9289	0.0101
	0.85	0.142	0.9088	0.0355

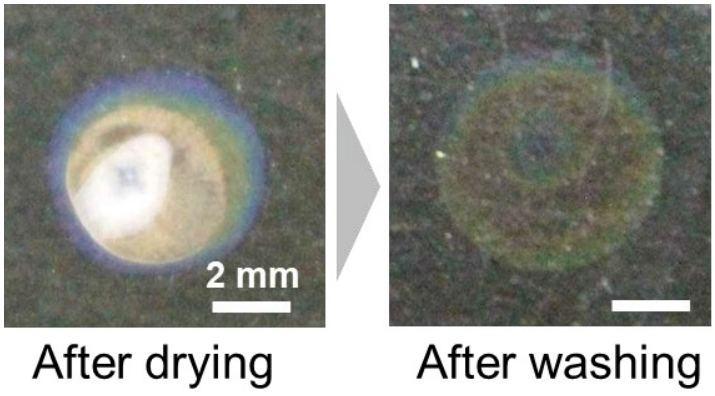

Figure S11. Photographs of the dried structures of the dispersion of NA5 microgels charge-screened at [NaCl] = 1 mM before and after washing with pure water.

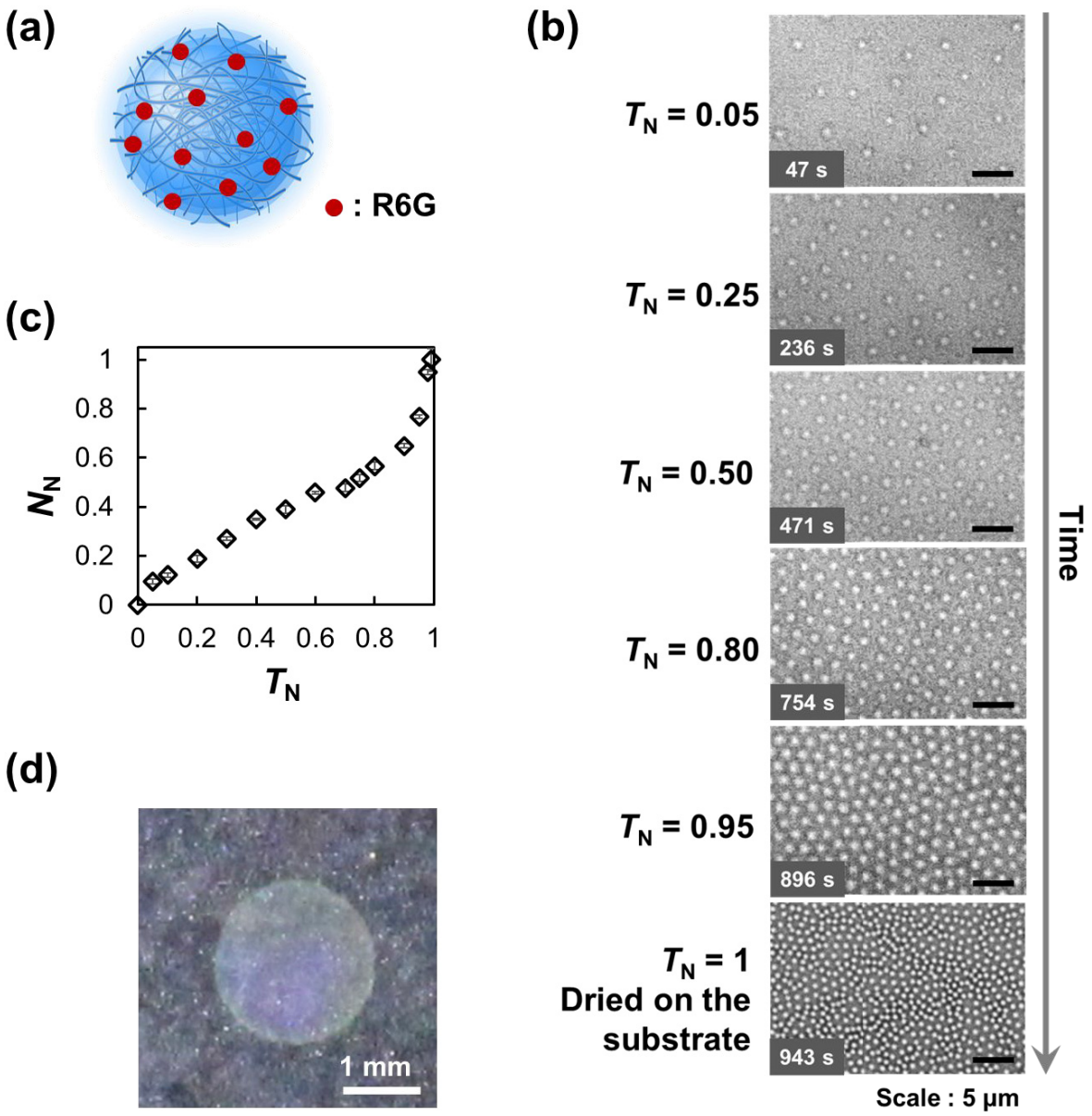

Figure S12. (a) Schematic illustration of the microgels in the presence of the cationic dye R6G. (b) Optical microscopy images of NA10 microgels in the presence of R6G at the air/water interface of the sessile droplet on glass substrates as a function of T_N. (c) Normalized adsorbed amount, N_N, for each charged microgel as a function of T_N. (d) Photographs of a thin film of microgel dispersions on glass substrates after drying. The droplets were dried at room temperature (~25 °C, ~60 % humidity) at 0.005 wt%. It should be noted here that the excess of R6G was removed by purifying via two cycles of centrifugation/redispersion in water after adding a sufficient amount of R6G (commensurate to the amount of carboxy groups) to these microgels.

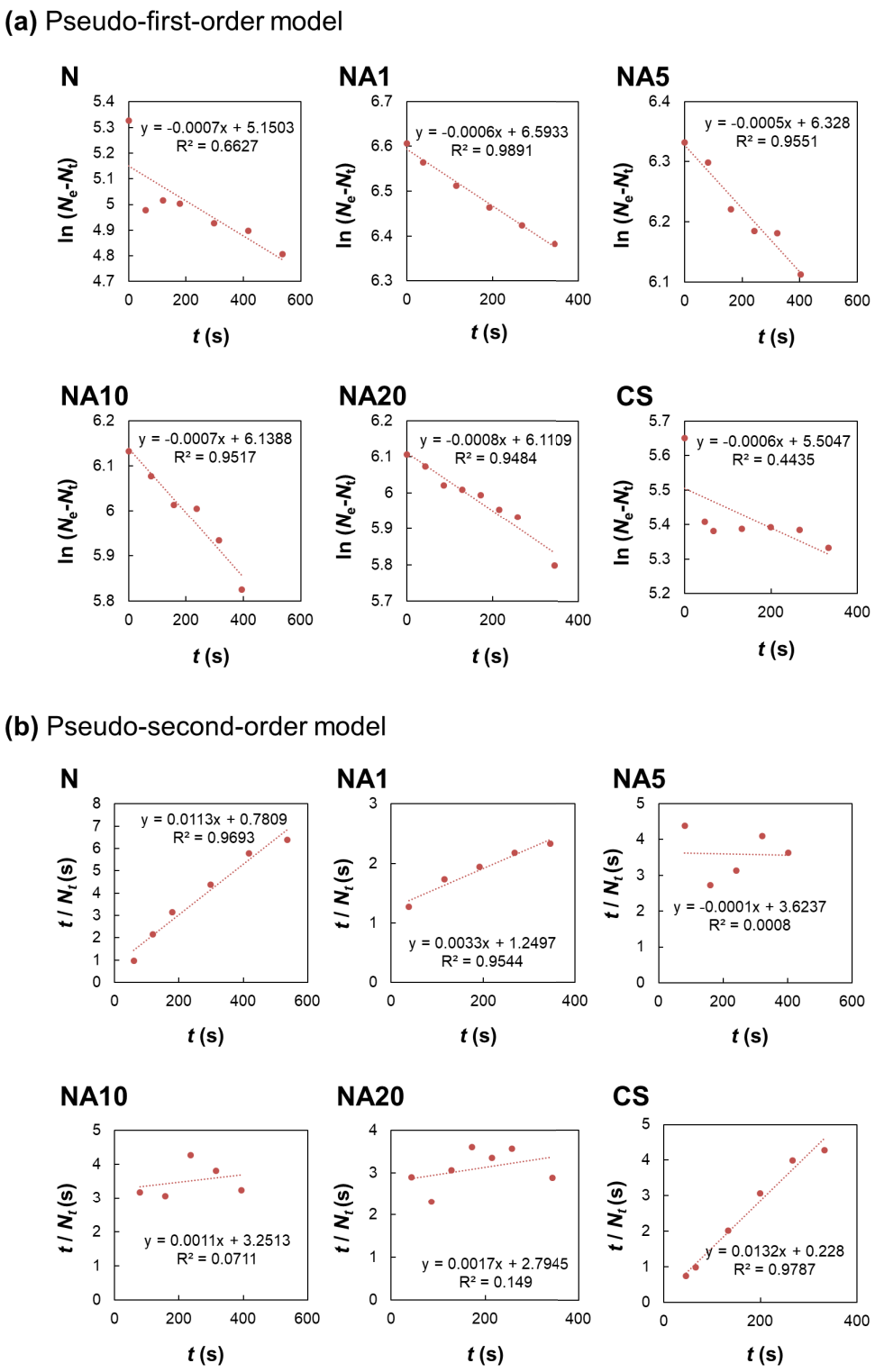

Figure S13. Adsorption kinetics for N, NA1, NA5, NA10, NA20, and CS microgels at the air/water interface at T_N 0~0.5 with (a) the pseudo-first-order model, and (b) the pseudo-second-order model.

Movie S1. Drying processes of a sessile droplet of a N microgel dispersion (1 μL) as a function of the normalized time, T_N, covering the entire droplet and the edge of the droplet. The droplet was dried at room temperature (~25 °C, ~30 % humidity) at 0.1 wt%. The speed of the movies is 16x.

Movie S2. Drying processes of a sessile droplet of a N microgel dispersion (1 μL) as a function of the normalized time, T_N, at the edge of the droplet during the evaporating. The droplet was dried at room temperature (~25 °C, ~30 % humidity) at 0.003 wt% on the glass substrate. The speed of the movie is 4x.

Movie S3 and **S4**. Drying processes of a sessile droplet of a NA5 microgel dispersion (1 μL) as a function of normalized time, T_N, at the edge of the droplet without moving the observation position, and from the edge of the droplet to the center of the droplet with moving the observation position of the droplet during the evaporating. The droplet was dried at room temperature (~25 °C, ~30 % humidity) at 0.005 wt% on the glass substrate. The speed of the movies is 4x and 0.5x, respectively.

Movie S5 and **S6**. Moment when the N and NA5 microgels adsorb at the air/water interface (T_N = ~0.7). The tracked time-trajectory of each microgel represents 6 s (30 frame s^{-1}).

iii. Publications / Presentations

List of Publications

1. Haruka Minato, Masaki Murai, Takumi Watanabe, Shusuke Matsui, Masaya Takizawa, Takuma Kureha*, Daisuke Suzuki*:
   "The Deformation of Hydrogel Microspheres at the Air/Water Interface"
   Chemical Communications, 54 (8), 932-935 (2018).
   DOI: 10.1039/C7CC09603H

2. Haruka Minato, Masaya Takizawa, Seina Hiroshige, Daisuke Suzuki*:
   "Effect of Charge Groups Immobilized in Hydrogel Microspheres during the Evaporation of Aqueous Sessile Droplets"
   Langmuir, 35 (32), 10412-10423 (2019).
   DOI: 10.1021/acs.langmuir.9b01933

Other Publications

1. Masaya Takizawa, Yuka Sazuka, Koji Horigome, Yuki Sakurai, Shusuke Matsui, Haruka Minato, Takuma Kureha, Daisuke Suzuki*:
   "Self-organization of Soft Hydrogel Microspheres during the Evaporation of Aqueous Droplets"
   Langmuir, 34 (15), 4515−4525 (2018).
   DOI: 10.1021/acs.langmuir.8b00230

2. Haruhiko Ishii, Takatsune Narumi*, Daisuke Suzuki, Haruka Minato, Kenji Urayama, Akiomi Ushida, Taisuke Sato:
   "Evaluation of deformation characteristics of micron-size hydrogel particles with strain recovery processes"
   Journal of the Society of Rheology, Japan, 46 (5), 227-231 (2018).
   DOI: 10.1678/rheology.46.227

3. Shun Oura, Takumi Watanabe, Haruka Minato, Daisuke Suzuki*:
   "Impact of Particle Softness on Segregation of Binary Colloidal Suspensions Flowing in Microchannel"
   KOBUNSHI RONBUNSHU, 76 (3), 226-233 (2019).
   DOI: 10.1295/koron.2019-0003

4. Takuma Kureha, Haruka Minato, Daisuke Suzuki, Kenji Urayama and Mitsuhiro Shibayama*:
   "Concentration Dependence of Dynamics for Microgel Suspension Investigated by Dynamic Light Scattering"
   Soft Matter, 15 (27), 5390-5399 (2019).
   DOI: 10.1039/C9SM01030K

5. Shusuke Matsui, Kensuke Hosho, Haruka Minato, Takayuki Uchihashi*, Daisuke Suzuki*:
"Protein Uptake into Individual Hydrogel Microspheres Visualized by High-Speed Atomic Force Microscopy"
Chemical Communications, 55 (68), 10064-10067 (2019).
DOI: 10.1039/C9CC05116C

Reviews

1. 湊遥香、鈴木大介*:
「やわらかいハイドロゲル微粒子の界面挙動」
ケミカルエンジニヤリング　2019 年 1 月号　Vol.51、p27-31 (2019).

Oral Presentation (International conference)

1. ○Haruka Minato, Daisuke Suzuki:
"Preparation of Anisotropic Microgels via Heteroaggregation at the Water-Oil Interface of Emulsions"
Textile Summit 2016 and Postgraduate Student Conference (Hung Hom, Hong Kong) June 29th (2016) Oral (O-20)

2. ○Haruka Minato, Daisuke Suzuki:
"Development of Micron-sized Hydrogel Particles by Precipitation Polymerization in Water"
Textile Summit 2017 (North Carolina, America) March 21th (2017)

3. ○Haruka Minato, Masaya Takizawa, Daisuke Suzuki:
"Adsorption Behavior of Microgels at the Air/Water"
Textile Summit 2018 (Nagano, Japan) September 22th (2018) Oral (O-20)

4. ○Haruka Minato, Yuka Sazuka, Masaya Takizawa, Kenshiro Honda, Daisuke Suzuki:
"Self-assembly of Deformable Soft Hydrogel Microspheres at the Air/water Interface"
ACS Fall 2019 National Meeting & Expo (San Diego, America) August 27th (2019) Oral (COLL 459)

5. ○Haruka Minato, Daisuke Suzuki:
"Effect of Charge in Hydrogel Microspheres on Self-Assembly at the Air/Water Interface"
Okinawa Colloid 2019 (Okinawa, Japan) November 8th (2019) Oral (5D11)

Oral Presentation (National conference)

1. ○湊遥香、渡邊拓巳、鈴木大介:
「温度制御／フィード沈殿重合法による巨大ハイドロゲル微粒子の創製と界面におけるゲル微粒子の変形挙動の評価」
第 29 回高分子ゲル研究討論会、東京工業大学、東京、1 月 11 日(2018)、口頭(3)

2. ○湊遥香、滝沢優哉、渡邊拓巳、鈴木大介:
「気水界面における変形を可視化するための巨大ハイドロゲル微粒子の合成」
第 67 回高分子学会年次大会、名古屋国際会議場、愛知、5 月 24 日(2018)、口頭(2C10)

3. ○湊遥香、滝沢優哉、鈴木大介:
「高分子電解質ゲル微粒子の薄膜形成」
第 20 回高分子ミクロスフェア討論会、岡山大学、岡山、11 月 15 日(2018)
口頭(2-09A)

4. ○Haruka Minato, Daisuke Suzuki:
"Self-organization of Charged Hydrogel Microspheres"
1st G'L'owing Polymer Symposium in KANTO、早稲田大学、東京、12 月 15 日(2018)、
口頭 (C18)

5. ○湊遥香、滝沢優哉、広重聖奈、鈴木大介:
「気水表面において織り成す高分子電解質ゲル微粒子の特異な自己組織化挙動」
第 68 回高分子討論会、福井大学、福井、10 月 25 日(2019)、口頭(1J10)

6. ○Haruka Minato, Masaki Murai, Takumi Watanabe, Shusuke Matsui, Masaya Takizawa, Takuma Kureha, Daisuke Suzuki:
"Adsorption and Deformation Behaviors of Hydrogel Microspheres at the Air/Water Interface"
第 68 回高分子討論会、福井大学、福井、10 月 27 日(2019)、口頭(3ESA11)

7. ○湊遥香、鈴木大介:
「ゲル微粒子分散液の乾燥に伴う自己組織化」
第 50 回中部化学関係学協会支部連合秋季大会、信州大学松本キャンパス、長野
11 月 9 日(2019)、口頭(1E12)

8. ○湊遥香、滝沢優哉、広重聖奈、鈴木大介:
「気水界面における高分子電解質ゲル微粒子がみせる自己組織化挙動」
第 29 回 日本 MRS 年次大会、横浜情報文化センター、神奈川、11 月 29 日(2019)
口頭(O-O29-004)

Patents

1. 鈴木大介、湊遥香、大浦舜:
「ゲル微粒子の製造方法」
特願 2017-093570、出願日 5 月 10 日 (2017)
※ゲル微粒子の製造方法(特願 2016-180109)の権利を拡張し再出願
特開 2018-048298、公開日 3 月 29 日 (2018)

2. 秋山佳丈、鈴木大介、湊遥香:
「ゲル微粒子による 3 次元造形」
特願 2018-059892、出願日 3 月 27 日 (2018)
特開 2019-171605、公開日 10 月 10 日 (2019)

iv. Acknowledgment

First of all, I would like to express my sincere gratitude to my supervisor Professor Dr. Daisuke Suzuki (Shinshu University) for all the continuous support, patience, motivation and encouragement during my research. His advice on my research as well as on my career have been invaluable.

I would also like to thank Prof. Dr. Hideaki Morikawa (Shinshu Univ.), Prof. Dr. Yoshitake Akiyama (Shinshu Univ.), Prof. Dr. Mizuo Maeda (Shinshu Univ.), Prof. Dr. Yasuo Gotoh (Shinshu Univ.), Prof. Dr. Michinari Kohri (Chiba Univ.), Prof. Dr. Matthias Karg (Heinrich Heine Univ.), Emeritus Prof. Dr. Haruma Kawaguchi (Keio Univ.), Prof. Dr. Mitsuhiro Shibayama (Univ. of Tokyo), and Prof. Dr. Kenji Urayama (Kyoto Institute of Technology Univ.) for insightful comments, suggestions and discussions.

I gratefully acknowledge the funding received from the Shinshu University Advanced Leading Graduate Program from the Japanese Ministry of Education, Culture, Sports, Science, and Technology. I am also thankful for all the supports of the program.

I am also grateful to the Suzuki laboratory members for their continuous friendship and support. I gained a lot from them through their friendly relations and their comments, suggestions, and discussions at various points of my research. I wish their continued success.

Last but not least, I would like to thank my family: my parents, Yoshihide, Yukiko, and my sisters, Yuka, Chiho, for all their love, support and encouragement they provided.

Haruka Minato

湊　遥香